Winter 2011

Evaluating the material properties of building derived aggregate using laboratory testing methods

Noah S. Chinburg
University of New Hampshire, Durham

EVALUATING THE MATERIAL PROPERTIES OF BUILDING DERIVED AGGREGATE USING LABORATORY TESTING METHODS

BY

NOAH S. CHINBURG

B.S. Civil Engineering, University of Hampshire, 2010

THESIS

Submitted to the University of New Hampshire

In Partial Fulfillment of

The Requirements for the Degree of

Master of Science

In

Civil Engineering

December, 2011

This thesis has been examined and approved.

Thesis Director, Jeffrey S. Melton
Affiliate Faculty, Civil Engineering

Jean Benoît
Professor, Civil Engineering

Jo Sias Daniel
Associate Professor, Civil Engineering

12/1/2011
Date

Table of Contents

LIST OF TABLES

LIST OF FIGURES

ABSTRACT

EVALUATING THE MATERIAL PROPERTIES OF BUILDING DERIVED AGGREGATE USING LABORATORY TESTING METHODS

by

Noah Chinburg

University of New Hampshire. December, 2011

Construction and demolition (C&D) waste makes up a significant portion of landfill waste every year. Building derived aggregate (BDA), is the inert component of C&D waste accounting for approximately 50% of C&D waste by weight. Because BDA is inert, it has the potential for use as a highway construction material. However, due to its variability, it has not been used on a large scale for highway construction, particularly as a result of concerns about the effects of brick under various loading and environmental conditions. Because of this the New Hampshire Department of Transportation has limited the amount of brick in crushed material to 5% by weight of total aggregate.

This research evaluated the affects of varying amounts of brick in BDA based on stiffness, bearing capacity, durability, and abrasion resistance. The test methods used to evaluate these properties were Repeat Load Triaxial, California Bearing Ratio, freeze-thaw, and Micro-Deval, respectively. Results were compared with accepted standards to determine if a limit should be placed on brick content in BDA. The results of this testing suggest that brick content has little to no effect on performance in proportions up to 20%. However, due to the national variability of C&D waste, the results from this research can only be considered valid for the Northeast.

CHAPTER 1

INTRODUCTION

1.1 Problem Statement

With landfill space constantly decreasing, natural aggregate becoming increasingly scarce, and a growing sustainability movement across the United States, interest has grown in the use of recycled materials for highway construction. The focus of this research is to determine the suitability of building derived aggregate (BDA) as a base or base and subbase material in highways. BDA comes from waste produced during the construction or demolition of structures, and generally is composed of varying amounts of concrete, brick, and recycled asphalt pavement (RAP). Previous research using California Bearing Ratio and Resilient Modulus tests suggest that BDA is suitable for use as a highway base and subbase (Clark, 2010). However, the tests were run over a relatively short time frame using loading conditions that may not represent traffic loads typically experienced by highway base and subbase. The tests were also run on BDA that was primarily concrete, and its exact composition was not recorded. Currently little is known about the effects of brick and RAP have on the performance of BDA as a base and subbase and the general performance of BDA over long term cyclic loading. This research used different material test methods such as California Bearing Ratio, Resilient Modulus, Micro-Deval wearing, and freeze-thaw degradation to determine the performance of BDA with

varying percentages of brick and RAP. The results were compared against accepted performance standards to determine if there should be limits on the amount of brick and RAP in BDA used for highway base and subbase.

1.1.1 Flexible Pavement

Pavement design can be broken down into two categories: rigid pavement design and flexible pavement design. Since flexible pavement is the primary type of highway construction in New Hampshire, this research focused on the flexible pavement system. Generally flexible pavement consists of asphalt concrete, granular base, and granular subbase, which all rests upon the existing bearing layer, or subgrade, as shown in Figure 1.

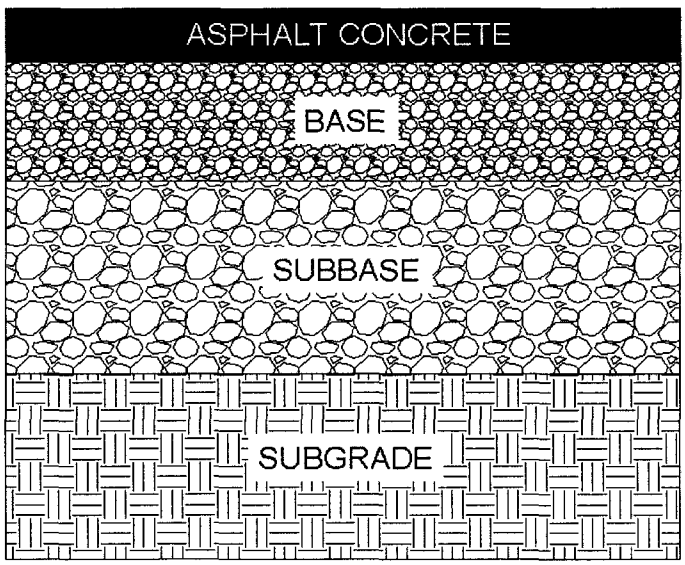

Figure 1: Flexible Pavement System

Flexible pavement design recommends the thickness of each layer be based on the anticipated traffic load, the quality of material in each layer, and the quality of the subgrade. The parameter that generally controls the quality of each layer is the resilient modulus (M_R), which is a measure of material stiffness. For

typical highways, greater pavement thickness means a higher M_R; which decreases strain and deformation, meaning less load related distresses such as cracking and rutting. Since M_R is a difficult parameter to obtain for unbound materials, the California Bearing Ratio, a bearing capacity test, is traditionally used to evaluate unbound materials for flexible pavement design. The California Bearing Ratio, M_R, abrasion resistance, and durability were examined in this research.

1.1.2 Aggregate Materials

Natural aggregates make up the vast majority of materials that are used for base and subbase layers in highway construction. With the constant need for new roads and rehabilitation of existing roads, there is a high demand for natural aggregates. The problem is that high quality natural aggregates suitable for use in highway construction are a finite resource, so other materials must be utilized in order to keep up with the current pace of construction. BDA could be a promising alternative material. However there are concerns about long-term performance due to the variability of the material and its performance under varying conditions, which are discussed in detail in Chapter 2.

1.1.3 Material Characterization

Building derived aggregate is composed of different amounts of concrete, brick, and RAP; however the majority (approximately 90%) of BDA is concrete. Once crushed the material is a mix of hardened Portland cement and aggregate particles. Brick is made out of mineral clays and shales mixed with sand. Once mixed the material is formed and fired for weather resistance. Crushed brick is a

mix of fire-hardened pieces and softer core pieces which behave much more like the clay from which they were derived. RAP from BDA is typically recovered from parking lots, driveways and other non-highway sources. RAP is composed of aggregate coated with asphalt binder. Before BDA is processed by crushing, the components vary in size from 6 to 12 or more inches in diameter.

Research has shown that crushed concrete for base and subbase tends to be stiffer than natural aggregate (Clark 2010, DeRocchi 2008), however little is known about how the performance of crushed concrete is affected once brick and RAP are mixed in. In order to determine these effects, the concrete, brick, and RAP were separated and then blended at known quantities. Since BDA is primarily composed of concrete, increasing quantities of brick and RAP were blended using concrete as the original material. Any blend referred to having no brick or RAP in this research is composed of 100% concrete. Thus, this research explored the effects of brick and RAP on the performance of recycled concrete aggregate.

1.2 Thesis Objectives

The primary goal of this research is to analyze the effects brick and RAP have on crushed concrete when used as base and subbase for highway construction; with an emphasis on performance under long term cyclic loading. Long term loading, for this research, is defined as exceeding the number of load cycles specified by AASHTO T-307; which is the accepted method for resilient modulus testing of highway base and subbase materials. This is done by performing Repeat Load Triaxial, California Bearing Ratio, Micro-Deval wearing,

and freeze-thaw tests. The results from the California Bearing Ratio, Micro-Deval, and freeze-thaw tests were compared with results from 100% crushed concrete to determine the effects of each BDA component on performance. The stiffness parameter obtained from the Repeat Load Triaxial Test is then input into the Mechanistic Empirical Pavement Design Guide to evaluate rutting performance.

1.2.1 Materials

During this research two different materials were tested. The first material was crushed stone used by the New Hampshire Department of Transportation (NHDOT). This was the same stone used by Clark (2010), and was used as the control. The second material was crushed BDA obtained from the Environmental Resource Return Corporation (ERRCO) in Epping, NH. The BDA was separated into its individual components and tested to examine the effects of different brick and RAP contents on properties.

1.2.2 Methods

The test methods used for this research were selected to evaluate base and subbase properties related to performance. Although stiffness is the primary factor influencing pavement performance, other factors such as degree of saturation, freeze-thaw degradation, and wearing due to handling and placement can also have significant negative effects on the material. The four test methods selected were:

- Lab California Bearing Ratio (Saturated and Unsaturated)
- Lab Resilient Modulus (Saturated and Unsaturated)

- Micro-Deval Wearing Test (Saturated and Unsaturated)
- Freeze-Thaw Test

All components of BDA and crushed stone were run through all tests with some exceptions. Freeze-thaw and Micro-Deval testing was not conducted on crushed stone because it was only used as a control for stiffness measurements. Freeze-thaw and Micro-Deval testing was not conducted on RAP because the primary concern for wearing and freeze-thaw resistance was for brick and crushed concrete. Five replicate tests were performed for each sample in attempts to provide comparable results. Each specimen was individually blended so comparisons could be made between different blends.

CHAPTER 2

LITERATURE REVIEW

2.1 Background

2.1.1 C&D Debris

Over the past several decades existing landfill capacity has been decreasing, and new landfills are becoming increasingly difficult to permit, design, and build. This, along with reducing availability of natural aggregate, has prompted research on recycling construction and demolition (C&D) debris for an end use outside of a landfill. Any waste resulting from new construction, renovation, or demolition is considered C&D debris. C&D debris typically includes materials such as concrete, wood, brick, glass, metals, asphalt pavement, asphalt shingles, and plastic. C&D waste makes up a significant portion of the solid waste stream; according to the EPA, 36% of residential waste and 50% of commercial waste consisted of C&D debris in the state of Massachusetts in 2002. In 2006, the northeast United States, which includes Connecticut, Maine, Massachusetts, New Hampshire, New Jersey, New York, Rhode Island, and Vermont; generated over 12 million tons of C&D debris, only 10% of which found an end use outside of a landfill (Northeast Waste Management Officials Association, 2009). Metals made up the only significant portion of the recycled material, with approximately 53% of total estimated

generation recovered. This leaves all the other materials and 47% of the metals that make up C&D debris occupying valuable landfill space.

2.1.2 Building Derived Aggregate

BDA is defined as any portion of the C&D waste stream that is non-organic, non-plastic, and non-metal. BDA is composed primarily of concrete, brick, and recycled asphalt pavement (RAP). Figure 2 shows a breakdown of the C&D waste stream: 45% of which is concrete, 5% brick. RAP in particular was not addressed in this study, and was likely combined with concrete when all the material was quantified.

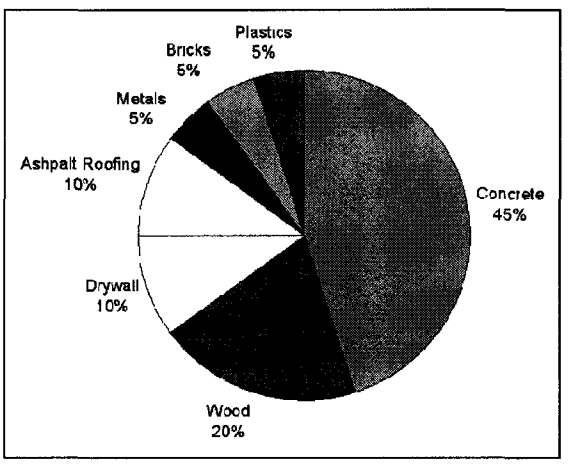

Figure 2: 2003 National C&D Waste Average (Environmental Protection and Economic Development, 2003)

Asphalt pavement and roofing also make up a significant portion of the C&D waste stream. There may be some quantity of asphalt roofing in BDA, but when asphalt is mentioned in the context of BDA, recycled asphalt pavement is being referred to. Figure 3 shows the components of BDA as they are found at processing facilities.

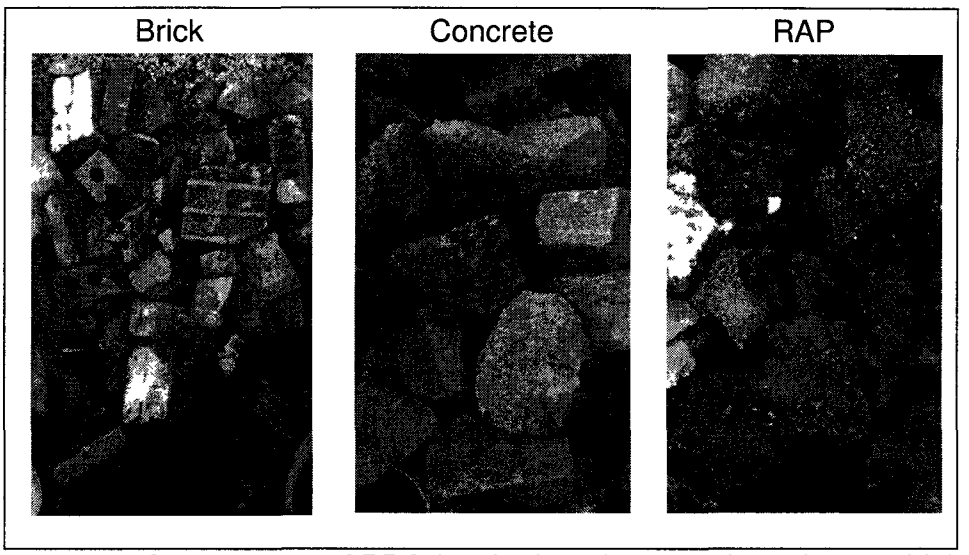

Figure 3: Components of BDA (each photo is approximately 18" wide)

2.2 Recycling Building Derived Aggregate for Roadway Construction

Due to concerns about variability of unsorted BDA, it is not common practice to use building derived aggregate for roadway construction. However, recycled concrete aggregate has been successfully applied as a base and subbase throughout the majority of the United States (FHWA, 2004). Another common practice is the use of RAP in reclaimed stabilized base, which is a method of roadway rehabilitation. It must be noted that the RAP that is used for reclaimed stabilized base is directly recycled on site so it never becomes part of the C&D waste stream; however its success as a construction material shows promise for its performance as a component of BDA.

The variability of BDA has been the major obstacle in using it for highway construction. There is a high degree of variability in each individual component due to multiple unknown sources, which leads to a high degree of variability

when evaluating the BDA blend. The following sections will discuss the benefits and concerns of each component of BDA.

2.2.1 Recycled Concrete Aggregate

Recycled concrete aggregate (RCA) can come from many sources, including columns, retaining walls, sidewalks, and residential hand mix concrete. The multitude of sources leads to a high degree of variability in material properties, but the assumption is that when crushed and mixed the concrete properties will be relatively homogeneous. Concrete is composed of portland cement paste and aggregate, and when crushed some residual portland cement powder is released, which has benefits and drawbacks. The benefit is that when the portland cement reacts with water, hydration products are created that stiffen the material, which is desirable for highway applications. The drawback is the runoff can have a high pH, which could raise environmental concerns in certain areas. As mentioned before, recycled concrete aggregate has been successfully used for roadway construction, often with more favorable material properties than natural crushed stone. The issue that arises with BDA is when the concrete is blended with other materials that may not interact well or just perform poorly.

2.2.2 Recycled Asphalt Pavement

The RAP typically found in BDA comes from driveways and parking lots adjacent to demolition projects. RAP from roads is typically milled and recycled in hot mix asphalt pavement or mixed into reclaimed stabilized base. Since driveways and parking lots typically do not have the same level of QC/QA as roadway construction, it can be expected that RAP in BDA will have less

consistent properties. That being said, RAP is still fundamentally the same: aggregate particles coated in asphalt binder. The primary factor affecting the performance of RAP as a base and subbase is the asphalt binder, since the aggregate particles are essentially the same as traditional base and subbase material.

Asphalt binder is a temperature dependent viscoelastic material, meaning its strength and stiffness changes with temperature and loading rate. The viscoelastic nature of asphalt binder makes it susceptible to creep effects, which poses long term permanent deformation concerns, particularly when blends contain large percentages of RAP (Cosentino, 2003). The asphalt binder may also be susceptible to temperature, as its strength decreases with temperature; so its performance may be affected in warmer climates. A benefit of viscoelastic material is that it strain hardens, so it has the potential to stiffen under repetitive loading. Research has shown an increase in stiffness with the increase of RAP in base and subbase blends (Structural Numbers for Reclaimed Asphalt Pavement Base and Subbase Course Mixes, 1999). One other characteristic of asphalt binder is that it is hydrophobic; this can lead to unpredictable moisture density relationships due to the binder coating limiting absorption of the aggregate particles.

Some research has already been done on the effects of RAP content on blends of crushed stone and concrete. Results have suggested that increasing the RAP content leads to an increase in resilient modulus (Lee, et al., 2001). However, this research was done with relatively high RAP contents (40-100%).

Since RAP does not make up a significant portion of the C&D waste stream, it is unlikely that RAP contents this high will ever be observed. In order to test blends of BDA that best characterize the C&D waste stream, this research will focus on the effects of lower (10-20%) RAP contents.

2.2.3 Brick

Bricks are one of the oldest building materials known to man, and have been in use in various forms around the world for millennia. The manufacture of brick has stayed essentially the same throughout time. First a mixture of 50-75% sand and 25-50% clay is blended with water until it is moldable, then it is placed in a form, and fired for weather resistance (Bengtsson, et al., 1988). The "firing" of the clay uses a large amount of heat to produce a glass like skin around the brick, which protects the less weather resistant material on the inside. During construction bricks are bonded using mortar, which is a blend of Portland cement, water, and sand. Upon demolition, all of these materials get introduced into the C&D waste stream in some form.

Since bricks have been use for thousands of years all over the world, each culture has slightly different methods of manufacturing bricks, mixing the mortar, and assembling the bricks into a structure. For example, if Irish and Italian bricklayers were working across the street from each other in Boston in the 1800's. Each bricklayer would have their own preference as to which clay deposits their brick came from, what proportions their mortar was mixed to, and how much mortar to use in each joint; so two brick buildings on the same street could have very different material properties. This provides some interesting

insight as to why bricks in particular have a much higher degree of variability than other components of BDA.

Most bricks that are found in BDA have been manufactured within the past few hundred years, but significant advances in manufacturing processes in those years lead to a high degree of variability in brick properties. Current brick manufacturing has been optimized to fire bricks so that each brick comes out with the same properties as the next. Historically this is not the case. Unlike modern continuous kilns, historic kilns had lower firing temperatures and usually relied on a central heat source. This resulted in inconsistent firing, which caused the brick properties to vary from over fired and brittle to under fired and soft. Due to the varying temperatures within a kiln, historic bricks generally have three distinct zones of hardness within their cross section, shown in Figure 4 (Coates, 2008). This is compared to the relatively homogeneous cross section of contemporary brick, shown in Figure 5.

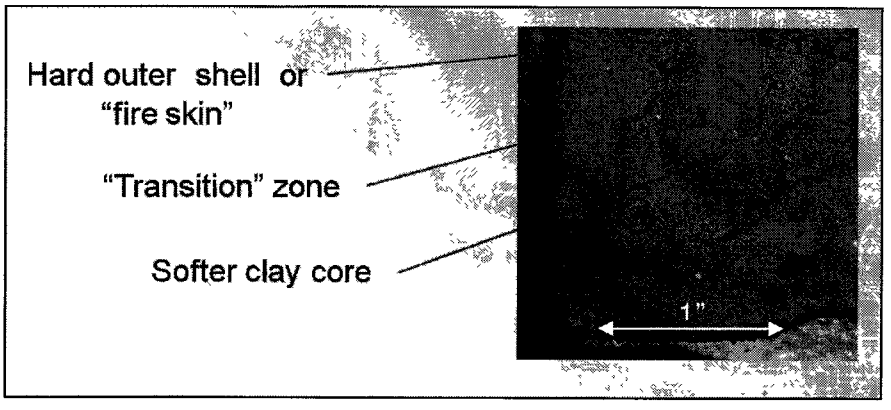

Figure 4: Historic Brick Cross Section

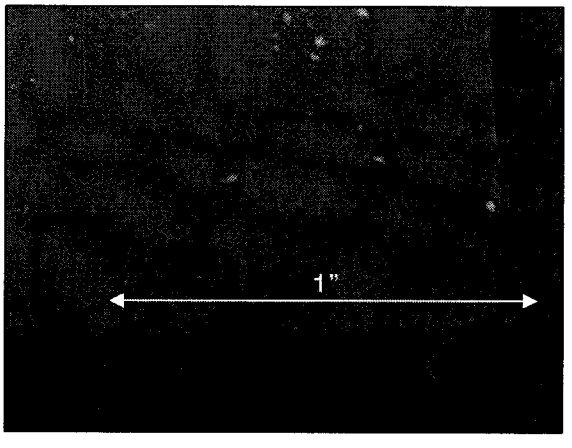

Figure 5: Contemporary Brick Cross Section

The concern of this heterogeneous cross section with BDA is that once crushed, all layers are exposed to the elements. Brick quality deteriorates once water has penetrated the fire skin, which in turn leads to many other problems. Saturated brick becomes more susceptible to freeze-thaw cycles; additionally, if the mortar used was non-hydraulic it can be leached away, leaving only sand. Another phenomenon is cryptoflorescence, which is the growth of crystals below the brick surface caused by salts. The pressures caused by this growth can lead the brick surface to deteriorate (Coates, 2008). Another consideration is that the

raw material used to make brick is mostly clay, which is unsuitable as a base and subbase for any application.

Figure 6: Spalling Caused by Cryptoflorescence (Guadagni, 2003)

As mentioned previously, there are many well founded concerns about the suitability of BDA for highway construction. The irregular properties of each component are compounded when using unsorted BDA, since the composition of any given sample varies widely. In order to best evaluate BDA for use in highway construction, samples with controlled composition were tested using several different laboratory methods in attempts to predict performance in the field.

2.3 California Bearing Ratio

The California Bearing Ratio (CBR) is a bearing capacity test that is widely used to evaluate the strength of geotechnical materials. The test is relatively inexpensive and repeatable, and as a result, there is a wide variety of data is available for a wide range of geotechnical materials. The CBR has been most popular in the evaluation of geotechnical materials for highways and airports in

the past several decades. It is a strength based test that compares the strength of the material being tested at a specified deformation to a reference material at the same deformation using a ratio as shown in Equation 1.

$$CBR(\%) = \frac{\sigma_1 \text{ @ } (\Delta=0.1\ in)}{\sigma_n \text{ @ } (\Delta=0.1in)} \qquad \text{(Equation 1)}$$

σ_1= the stress required to penetrate soil specimen 0.1"

σ_n= the stress required to penetrate the standard specimen 0.1"

For example, a high quality crushed stone will have a CBR of 100%, and soft clay would have a CBR of 3%. Typical CBR values for a range of soil types are shown in Table 1.As a side note, for design purposes any material that has a CBR of greater than 100%is generally designed as having a CBR of 100%.

Table 1: Typical CBR Values (Aj McCormack & Son, 1997)

Soil Type	CBR (%)
Clay	3
Silty Clay	5
Sandy Clay	7
Poorly Graded Sand	20
Well Graded Sand	40
Well Graded Sandy Gravel	60

2.3.1 Current Practices and Uses

DOT's throughout the country routinely use the CBR to evaluate geotechnical materials due to its relative simplicity and low cost. The CBR can be performed either in the field or in the laboratory as long as field conditions are accurately represented. Only laboratory testing was conducted for this research.

2.3.2 Testing Standards

Two standards exist for the CBR: AASHTO T 193-99 and ASTM D 1883-07. The same general procedure was followed for both standards, and can be used interchangeably. First, the specimen was compacted at optimum moisture content into a six inch diameter steel mold. Once compacted a 10 pound surcharge was placed on top of the material. At this point the material was tested as is or soaked for 96 hours. The soaking allows for full saturation of the material. Both saturated and unsaturated samples were tested for this research. Once the specimen was ready to be tested it is placed into a load frame where a three square inch piston was driven in at a constant rate of 0.05 inches per minute.

2.3.3 Suitability of CBR for Evaluating Material for Highway Construction

The CBR is an acceptable method for evaluating geotechnical materials for highway construction. However, experience has shown that traffic loading is more likely to cause a material to fail from fatigue than bearing capacity. The problem is that the CBR does a great job measuring bearing capacity of a material; but does not measure stiffness, the material property that determines resistance to fatigue failure. The resilient modulus triaxial (RMT) test is the standard method to directly measure the Resilient Modulus (M_R), a measure of material stiffness.

2.4 Material Stiffness

Material strength is defined as the resistance of a material to failure. So a "strong" material will resist large loads. To determine the strength of a material, it is subjected to increasing stresses and the resulting deformations are recorded. Figure 7 shows a typical stress-strain curve for a linear elastic material. In the curve the material begins to yield at (σ_{ys}, ε_{yp}), reaches its ultimate strength at (σ_{uts}, ε_u), and ultimately reaches failure at ε_f. The linear portion between the origin and the yield point is the elastic region, and the portion between the yield point and the ultimate strength is the plastic region.

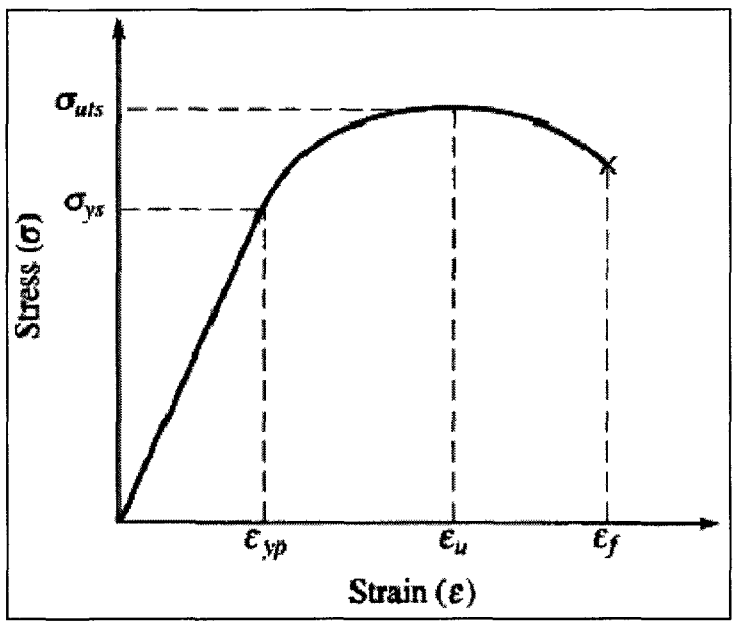

Figure 7: Typical Stress Strain Curve (Clark, 2010)

Soils typically behave in a non linear fashion, so a stress strain curve for soils will have an ill-defined or non-existent linear region. Also soils generally do not have the abrupt failure typical of many other engineering materials, instead the stress-strain curve trends downward after failure as shown in Figure 8.

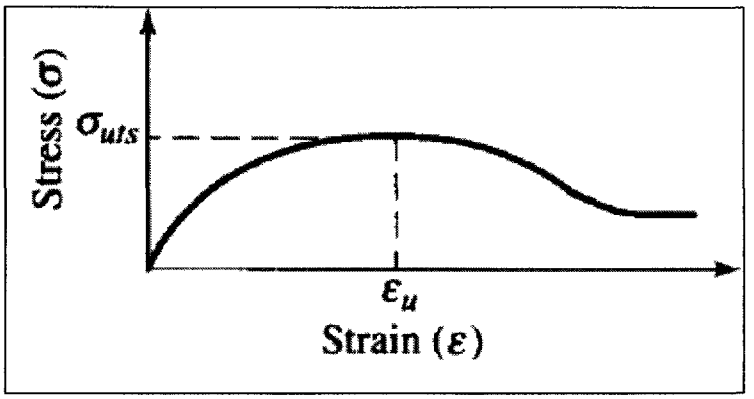

Figure 8: Stress Strain Curve for Soil (Clark, 2010)

Although material strength is an important property, material stiffness is more important when dealing with highway base and subbase. Material strength is a property defined by its resistance to failure, while material stiffness is the relationship between stress and strain; so a stiff material will have greater resistance to permanent deformation. This is an important concept because highways typically are not subjected to large loads that would result in bearing capacity failure. Instead they are subjected to smaller repeated loads; which makes them susceptible to fatigue failure. To evaluate the stiffness of a soil, either the tangent modulus or secant modulus is used. The tangent modulus for any given point is determined by drawing a line tangent to the curve at that point. The secant modulus for any point is determined by drawing a line from the point to the origin. Finding the slope of either of these lines will yield their respective modulus. Figure 9 shows an example of how to determine the tangent modulus and secant modulus.

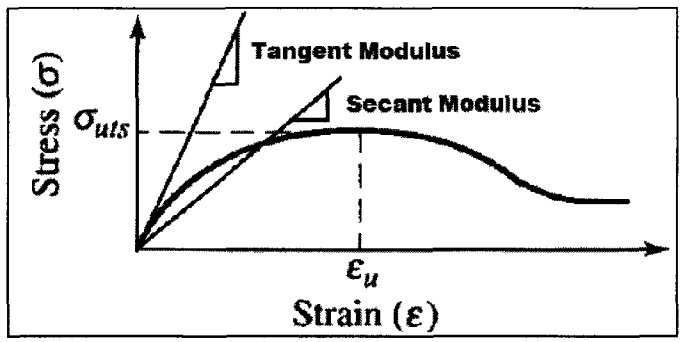

Figure 9: Determining the Tangent and Secant Modulus (Clark, 2010)

2.4.1 The Triaxial Test

The triaxial test is a common method used to produce a stress strain curve for soils. This test is particularly useful because it can be run using a wide variety of materials and stress combinations. The test is performed by applying stresses along all three axes of the material to simulate in-situ conditions. Figure 10 shows the triaxial test stress configuration; σ_1 simulates the axial stress on the specimen, σ_2 and σ_3 are equal and simulate the confining stress on the cylinder. σ_1 is broken down into two parts: σ_3 and σ_d. σ_3 is the normal overburden stress and is equal to the confining pressure, and σ_d is the deviator stress, which is the load that the soil is anticipated to support in the field. In order to get an idea of the "stress state" that a material is in, a parameter called the bulk stress is used. The bulk stress is defined by θ, as shown in Equation 2.

$$\theta = \sigma_1 + \sigma_2 + \sigma_3 \qquad \text{(Equation 2)}$$

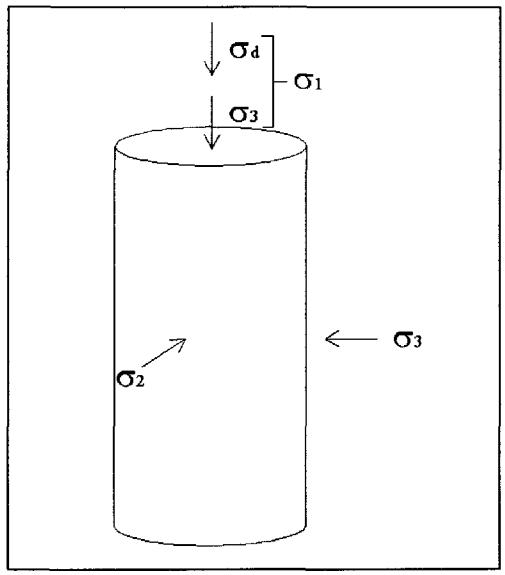

Figure 10: Triaxial Test Stress Configuration

The specimen is prepared by compacting the material inside of a mold with a latex liner. Once the desired compaction has been achieved the mold is removed, leaving a freestanding soil specimen enclosed in the latex liner. The specimen is then placed in a chamber with a load piston similar to the one shown in Figure 11. The piston transmits the axial load and the chamber is either filled with pressurized air or water to simulate the confining pressure. Once the stresses are applied, instrumentation is connected to different parts of the test apparatus or specimen and data is recorded throughout the test.

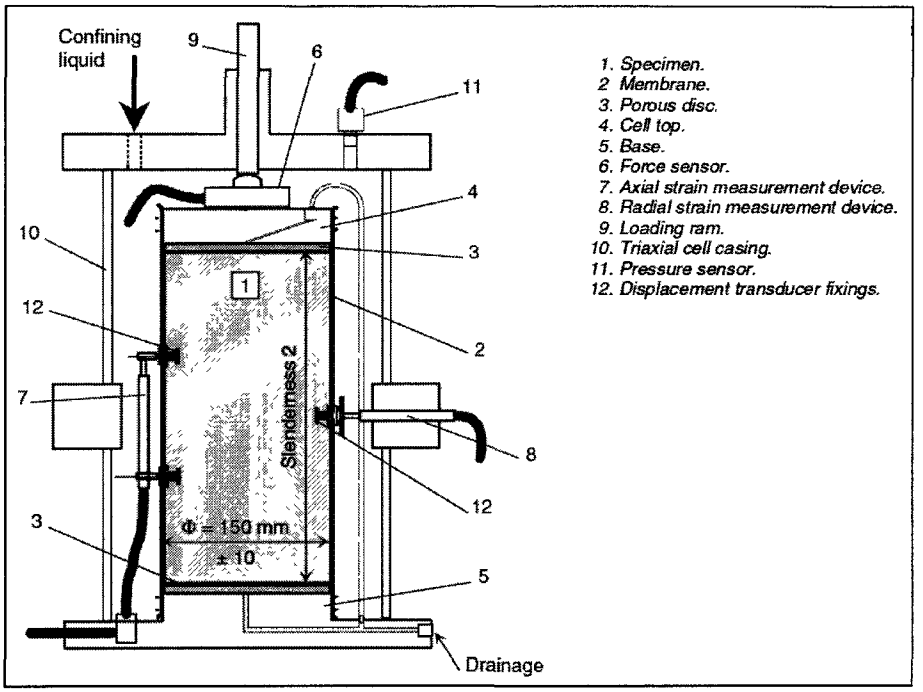

Figure 11: Diagram of Triaxial Apparatus (Gidel, et al., 2001)

2.4.2 Deviator Stress

When performing a triaxial test for highway construction materials, the deviator stress simulates traffic passing over the specimen. Traffic loading is different from loads experienced in many other geotechnical applications because it is dynamic. Since the majority of roadway sections will experience moving traffic loads the deviator stress must change over time, creating a dynamic load pulse. This dynamic load pulse is best represented by a haversine wave form, which is described in Equation 3. A graphical representation of the haversine wave is shown in Figure 12.

$$\frac{1-\cos(x)}{2} \qquad \text{(Equation 3)}$$

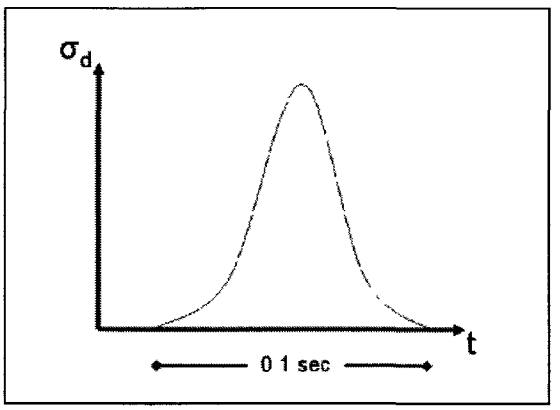

Figure 12: Dynamic Load Pulse Haversine Wave Form (Clark, 2010)

2.4.3 Resilient Strain

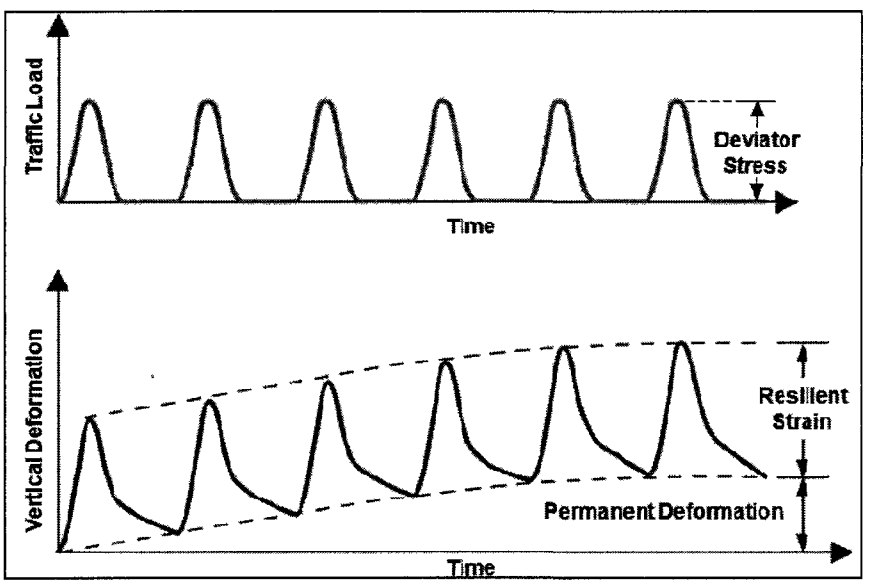

Figure 13: Resilient Strain vs. Permanent Strain (DeRocchi, 2008)

When the deviator stress is applied it creates strains within the specimen. The resulting strain can be broken down into two parts: permanent strain and resilient strain. Permanent strain is irreversible, and resilient strain is recoverable. Figure 13 shows the strain response to repeated deviator stresses. As the deviator stresses progress with time, total strain increases. For every

application of deviator stress there is a portion of the total strain that is recoverable and another portion that is permanent. The resilient strain, when compared to the permanent deformation, is an indicator of material stiffness. The resilient strain and deviator stress are used to measure the stiffness of the material being tested.

2.4.4 The Resilient Modulus

Highway base and subbase typically experience repeated stresses that are significantly less than the bearing capacity of the material; suggesting that pavement will not fail due to bearing capacity, but to fatigue failure. In 1993 the AASHTO pavement design guide recommended the use of the Resilient Modulus (M_R) (Puppala, 2008). As discussed earlier the M_R is a measure of material stiffness, an indicator of resistance to fatigue stresses. Unfortunately the M_R of a material can be quite difficult to obtain.

The M_R is a measure of stress versus strain. In the case of traffic loading the M_R is defined as the ratio of the deviator stress to the resilient strain as shown in Equation 4.

$$M_R = \frac{\sigma_d}{\varepsilon_r} \qquad \text{(Equation 4)}$$

M_R = Resilient Modulus (force per unit area)

σ_d = Deviator Stress (force per unit area)

ε_r = Resilient Strain (unitless)

The resilient modulus can be obtained using many different correlations. However, the only way to directly obtain the M_R is by using the repeat load triaxial

test. There are also several other equations based on empirical correlations where the M_R can be estimated from other test results.

2.5 Repeat Load Triaxial Test

A common method for simulating traffic loads on base and base and subbase material is the repeat load triaxial (RLT) test. The RLT test uses the same configuration as the triaxial test discussed in the previous chapter. The operator defines the confining stress, deviator stress, and number of loading cycles depending on the desired load simulation. The RLT test used to determine the resilient modulus accepted by AASHTO is the Resilient Modulus Triaxial test as defined by AASHTO T-307.

2.5.1 AASHTO T-307

AASHTO T-307 is a repeat load triaxial test designed specifically to simulate traffic loading, and is currently the accepted procedure for determining resilient modulus values in the United States. The load frame must be capable to withstand loads greater than 10,000 pounds and contain a specimen that is six inches in diameter and twelve inches tall. Additionally, the triaxial cell must be able to deliver a haversine load pulse. The confining fluid may be either water or air, depending on the desired confining pressure.

Once the specimen is prepared and the confining pressure has been set, the procedure begins with a conditioning sequence, which subjects the specimen to 500-1000 haversine deviator cycles to seat the loading platen. The conditioning sequence eliminates any deformations that may occur due to

misalignment of the platen. In order to simulate traffic loading the deviator stress is applied over a period of 0.1 seconds, and followed by a 0.9 second rest, then repeated. This loading sequence is intended to simulate the stresses produced by a tire passing over an in-situ soil specimen at highway speed. The 0.9 second rest period is intended to allow the specimen to fully rebound from loading so a resilient strain value can be measured.

Once the conditioning sequence is completed, the specimen is subjected to 15 different loading sequences. Each sequence has a different deviator stress and confining pressure, which can be summarized as the bulk stress. The procedure begins with the lowest bulk stress and then increases until the highest bulk stress is reached on the 15^{th} sequence. Each sequence consists of 100 load pulses delivered in the same fashion as the conditioning sequence. The M_R for each particular bulk stress is determined using the last 5 load pulses. This is done under the assumption that the specimen has experienced the majority of its plastic deformation in cycle 0-95, and will mostly be behaving elastically during cycles 95-100. AASHTO T-307 may be conducted on either base of base and subbase material, but due to general differences in stress distributions for each layer based on pavement layer thicknesses, they each have their own loading sequences, as shown in Table 2 and Table **3.**

Table 2: AASTHO T-307 Loading Sequence for Subgrade Materials

Sequence Number	Confining Pressure (kPa)	Maximum Axial Stress (kPa)	Cyclic Stress (kPa)	Constant Stress (kPa)	Load Cycles (#)
(0) Condition	41.4	27.6	24.8	2.8	500-1000
1	41.4	13.8	12.4	1.4	100
2	41.4	27.6	24.8	2.8	100
3	41.4	41.4	37.3	4.1	100
4	41.4	55.2	49.7	5.5	100
5	41.4	68.9	62.0	6.9	100
6	27.6	13.8	12.4	1.4	100
7	27.6	27.6	24.8	2.8	100
8	27.6	41.4	37.3	4.1	100
9	27.6	55.2	49.7	5.5	100
10	27.6	68.9	62.0	6.9	100
11	13.8	13.8	12.4	1.4	100
12	13.8	27.6	24.8	2.8	100
13	13.8	41.4	37.3	4.1	100
14	13.8	55.2	49.7	5.5	100
15	13.8	68.9	62.0	6.9	100

Table 3: AASHTO T-307 Loading Sequence for Base/Subbase Materials

Sequence Number	Confining Pressure (kPa)	Maximum Axial Stress (kPa)	Cyclic Stress (kPa)	Constant Stress (kPa)	Load Cycles (#)
(0) Condition	103.4	103.4	93.1	10.3	500-1000
1	20.7	13.8	12.4	2.1	100
2	20.7	27.6	24.8	4.1	100
3	20.7	41.4	37.3	6.2	100
4	34.5	55.2	49.7	3.5	100
5	34.5	68.9	62.0	6.9	100
6	34.5	13.8	12.4	10.3	100
7	68.9	27.6	24.8	6.9	100
8	68.9	41.4	37.3	13.8	100
9	68.9	55.2	49.7	20.7	100
10	103.4	68.9	62.0	6.9	100
11	103.4	13.8	12.4	10.3	100
12	103.4	27.6	24.8	20.7	100
13	137.9	41.4	37.3	10.3	100
14	137.9	55.2	49.7	13.8	100
15	137.9	68.9	62.0	27.6	100

2.5.2 Issues with AASHTO T-307

Since the M_R is a key input property for the mechanistic-empirical pavement design guide the Transportation Research Board States that "Inaccurate determination of the resilient modulus of the unbound materials in the

pavement structure will contribute to erroneous predictions of overall pavement response and pavement performance" (NCHRP, 2004). The major issue is accurately determining the M_R of the unbound base. The two primary factors that affect the M_R value, outside the properties of the material itself, are the bulk stress and the number of loading cycles. With coarse grained materials like highway base and subbase, the M_R value increases as the bulk stress increases. This relationship in shown in Figure 14, which shows the results of several resilient modulus tests performed at constant confining pressure (CCP) and variable confining pressure (VCP).

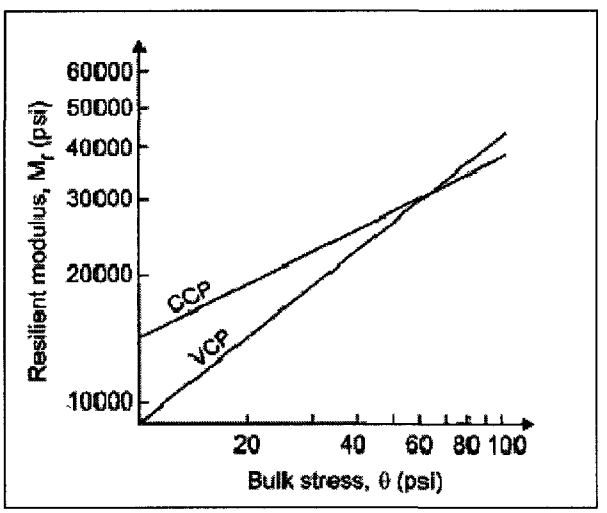

Figure 14: Resilient Modulus vs. Bulk Stress (Lekarp, et al., 2000)

The data shown in Figure 14 highlights the importance of accurately modeling in-situ stresses for base and subbase materials. Because the resilient modulus increases exponentially with bulk stress; over-estimating bulk stress can lead to predicted resilient modulus values much greater than observed under in-situ conditions. T-307 attempts to address this by subjecting the specimen to several different bulk stresses which are intended to cover a wide range of in-situ

conditions. However, these bulk stresses vary widely, and may not realistically model bulk stresses resulting from traffic loads. Additionally, each bulk stress from T-307 is only applied for 100 cycles, which is far less than any road will experience and may not represent in-situ material behavior over time.

2.5.3 The Summary Resilient Modulus

Investigation on bulk stresses experienced by base and subbase based on traffic data and has come up with a value that represents a conservative maximum bulk stress (Witczak, 2003). Based on recommendations from NCHRP Project 1-28A, "Harmonized Test Methods for Laboratory Determination of Resilient Modulus for Flexible Pavement Design," the bulk stress for unbound base and subbase materials should be 208 kPa. This is defined as the summary resilient modulus (SRM). The SRM captures the bulk stress that is produced by the majority of traffic on highways in the United States. Figure 15 shows the SRM plotted as a solid line against the bulk stress from each sequence of T-307.

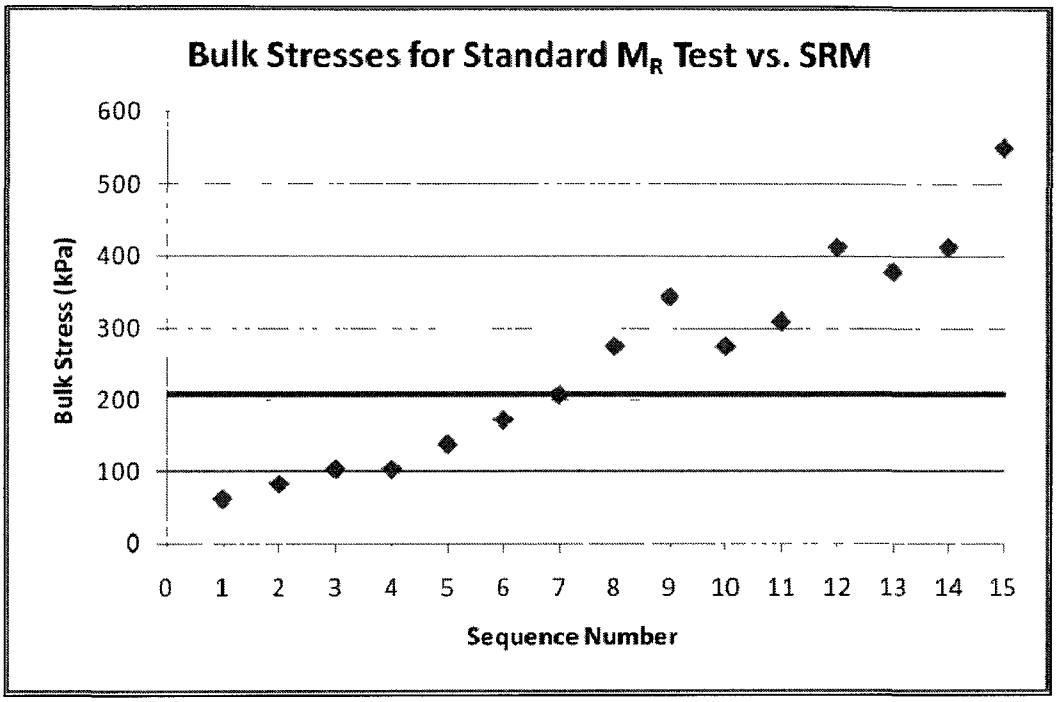

Figure 15: Comparison of SRM Bulk Stresses to AASHTO T-307 Bulk Stresses

As shown in Figure 15, the SRM is only closely represented in sequence 7 of T-307. This means only 100 cycles out 2500 provide a representative load, with the other 14 either underestimating or overestimating. With only 100 cycles of realistic loading it is likely that T-307 is not providing a representative model from which to obtain a reasonable value for M_R. Additionally, since the SRM test is performed at a constant bulk stress, it allows for better comparison of different materials since it is based on one traffic load. Since there is only one traffic load throughout the duration of the test, there is no uncertainty from the possibility of material properties changing between loading sequences.

Another consideration is material behavior under long term cyclical loading. It is very likely that most soils will not exhibit in-situ properties after only 2500 cycles of loading. This goes back to predicting a representative M_R, if in-

situ conditions are not accurately modeled, then unrepresentative values of M_R will be obtained. Research has been done using long term cyclical loading of base and subbase materials. In the paper titled "Practical Approach for Designing Pavement Structures with Recycled Road Materials" (Ebrahimi, et al., 2010) discussed the results of tests on samples of road surface gravel and RAP. Each specimen was subjected 10,000 load cycles at the SRM bulk stress of 208 kPa. The data showed a degree of strain hardening in both the road surface gravel and the RAP, meaning the M_R had a positive correlation with increasing load cycles. Based on this data it is likely that other base and subbase materials will behave in the same way. The question is, when does the M_R stop increasing, and when it stops does it decrease or remain constant?

2.5.4 BDA and the Summary Resilient Modulus

As mentioned before, there is short term data on BDA which came from AASHTO T-307 resilient modulus testing (Clark 2010, DeRocchi 2008). However, in order to obtain representative long term M_R values, a different approach is needed. The idea of this research is that combining long term cyclical loading at a constant bulk stress of 208 kPa will result in more representative M_R values. Previous testing showed a trend of increasing M_R all the way until the last cycle (Ebrahimi, et al., 2010), in order to try and determine if or when the M_R begins to decrease, the BDA will be run through 50,000 cycles. Ideally this test method will yield results that can help determine a representative M_R for different blends of BDA.

2.6 Correlations Between Stiffness and CBR

As mentioned earlier, the CBR does not represent the failure of unbound highway construction materials, which typically fail due to lack of stiffness. Since the CBR is a simple and repeatable test, several correlations have been attempted. Data collected during the use of the 1993 AASHTO design has determined that the correlation proposed by Powell et al. (1984) to be the most applicable for comparing M_R to CBR (Clark, 2010).

$$M_R(\text{psi}) = 2554 \times \text{CBR}^{0.64} \text{ (Powell et al. 1984)} \qquad \text{(Equation 5)}$$

AASHTO has determined that the correlation proposed by Powell et al. is the most applicable; however research done by Mr. Corey Clark and Mr. Mark DeRocchi has challenged their accuracy. The research done by Clark determined the M_R of sand, crushed stone, and BDA. The research done by Derocchi determined the MR of crushed stone from several locations and BDA. Both used the relationship set forth by Powell et al. to predict M_R values, and as shown in Figure 16 and Figure **17**, both resulted in very poor correlations.

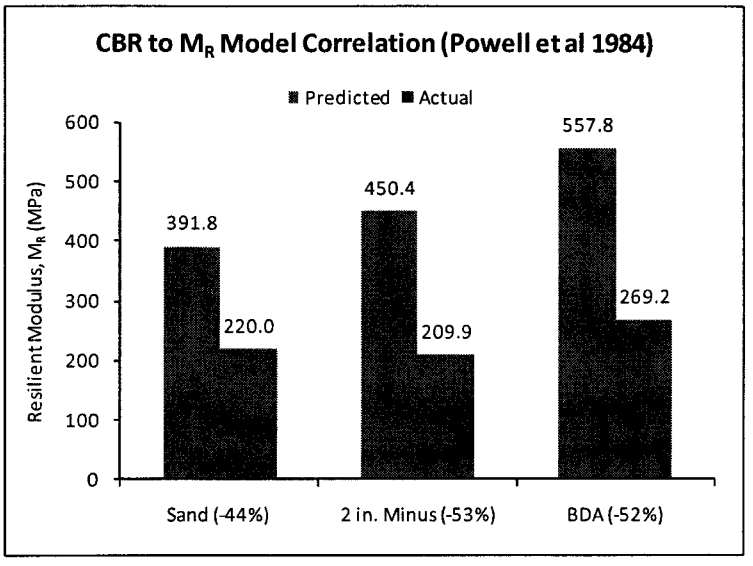

Figure 16: CBR to M_R Model Prediction vs. M_R Results (Clark, 2010)

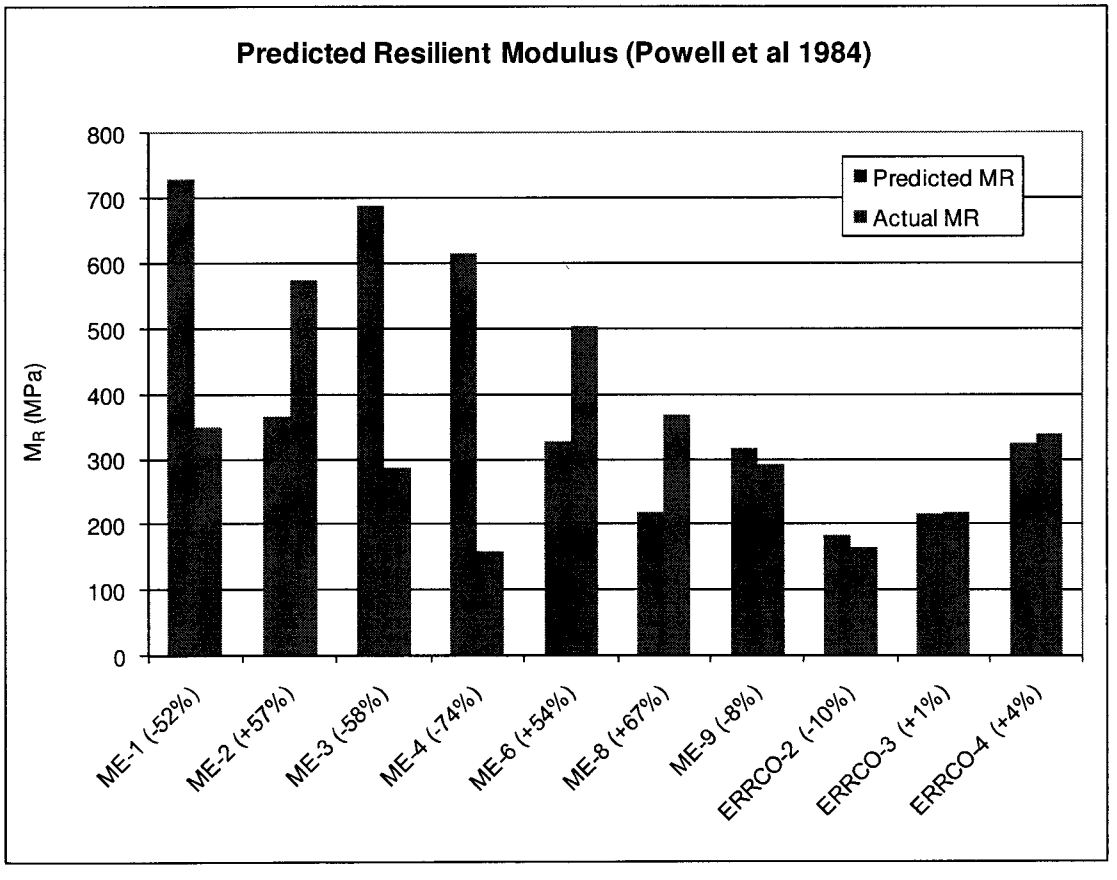

Figure 17: CBR to M_R Model Prediction vs. M_R Results (DeRocchi, 2008)

There are several possible reasons for the poor correlations. AASHTO T-193 states that "Past practice has shown that CBR materials having substantial percentages of particles retained on the 4.75 mm (No.4) sieve are more variable than for finer materials. Consequently, more trials may be required for those materials to establish a reliable CBR." Because highway base and subbase is a granular material, trying to obtain an accurate CBR is difficult, much less trying to establish a correlation using that data.

Another issue is that the CBR test requires that all material retained on the 3/4" not be used in the sample. AASHTO T-193 requires that the material retained on the 3/4" sieve be removed and replaced by an equal mass of material passing the 3/4" sieve and retained on the 4.75 mm (No.4) sieve. The specification states that although the procedure for modifying the material is not ideal due to the strength differences between the original and modified material, experience has shown that the results are acceptable. As mentioned before, the CBR is "capped" at 100%, so if a material has a CBR of 200% it is still considered an excellent material and reported as 100%; so the material modification should have little effect. However the modification required by AASHTO T-193 changes the gradation that would be used in an RMT test, so even if the same material is being tested, its gradation may cause it to respond differently.

2.7 The Mechanistic-Empirical Pavement Design Guide

Throughout the past several decades AASHTO has published many pavement design guides to assist engineers in designing roadways. Throughout

this time, these pavement design guides relied on empirical equations derived from an extensive road test conducted by AASHTO in 1958 (DeRocchi, 2008). In 1996 the Transportation Research Board (TRB) started project 1-37A with a goal of developing a pavement design guide that used a mechanistic-empirical approach. The contract for project 1-37A was awarded to Applied Research Associates Incorporated (ARA) in 1998, who, in coordination with Arizona State University (ASU) published the first draft of the MEPDG in 2004 (DeRocchi, 2008). Since then several updated versions have been released. The version used for this research was Version 1.100, with a "last build" date of August 31, 2009.

2.7.1 The MEPDG Model

The MEPDG takes all inputs for roadway design, mechanistic and empirical, and combines them into a software package that allows the designer to precisely control every aspect of roadway design.

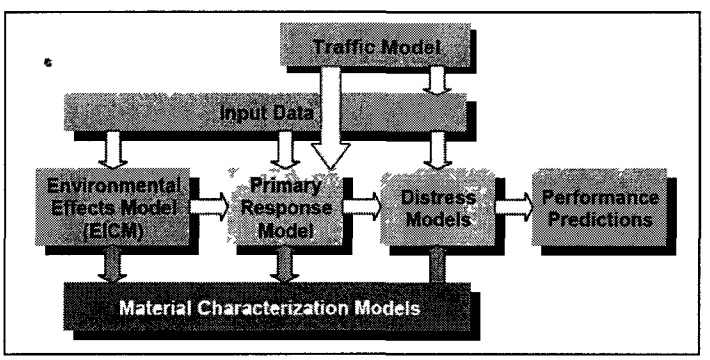

Figure 18: Diagram of the MEPDG Model

This research is primarily concerned with the material characterization models. The MEPDG develops the material characterization models by separating each material into a separate layer to simulate the composition of a roadway cross

section, much like what is shown in Figure 1. It then takes each layer and uses material properties that are either determined in the lab or in the field and runs it through the model shown in Figure 18 to determine pavement performance. The MEPDG allows the user to specify either a flexible or rigid pavement system. The input screen for the flexible pavement system used in this research is shown in Figure 19.

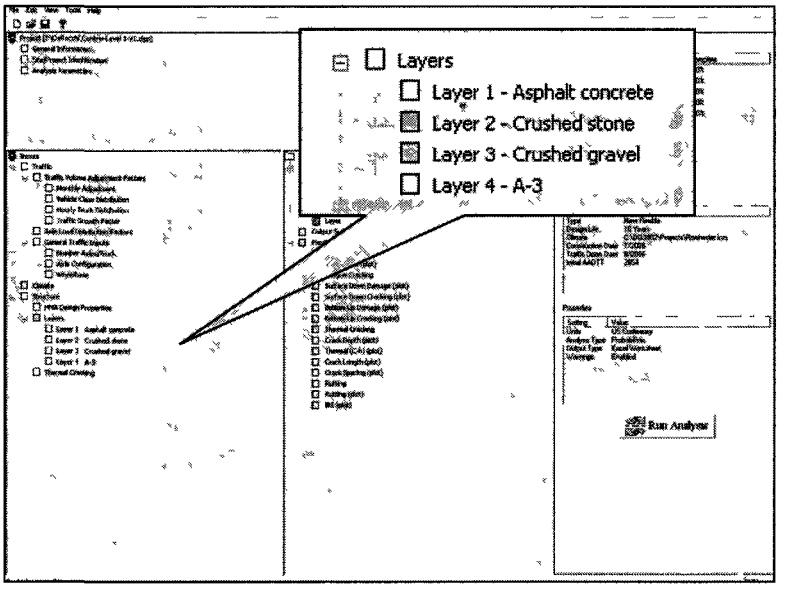

Figure 19: MEPDG Input Screen

With the flexible pavement system, the first layer is always specified as hot mix asphalt (HMA). Below the HMA layer the user has the option to add multiple layers with different properties based on the pavement design. The MEPDG allows the user to specify what type of layer (base, base and subbase, subgrade), the material the layer will be constructed with (crushed stone, sand, etc), and the material properties based on many commonly used field and laboratory testing methods.

2.7.2 MEPDG Results

Once all design values have been input to the MEPDG model, the program runs an analysis on the pavement performance over the design life. Once the analysis is complete the results are exported as a Microsoft Excel file. The user can then determine the effects of the design on a wide variety of performance criteria including: surface down cracking, thermal cracking, crack depth, crack length, rutting, international roughness index (IRI), among many others. This data is reported for each month of the roads design life so the user can get detailed information about pavement distress throughout the design life of the roadway.

2.8 Abrasion and Durability

Angularity and gradation of base and subbase materials are two important characteristics that affect pavement performance. Aggregate angularity provides the interlocking action that crushed stone depends on for its strength. The gradation of a soil is what determines many properties, including density, strength, stiffness, and drainage characteristics. Geotechnical materials are handled many times between their source and final destination, which puts them in conditions that can have negative effects on the gradation and angularity. Abrasion resistance is defined as the ability of a surface to resist being worn away when rubbed with another object. Durability is defined as the ability to resist wear and tear or decay. In a geotechnical context, abrasion resistance in the ability to maintain angularity, and durability is the ability to maintain the design gradation. These properties must be evaluated in order to determine an

aggregate's suitability for use as a base and subbase. Two tests were used to evaluate abrasion and durability: the Micro-Deval Wearing test for abrasion resistance, and freeze-thaw testing for durability.

2.8.1 The Micro-Deval Wearing Test

The New Hampshire Department of Transportation (NHDOT) specifies that any aggregate base course material shall not exceed 50% wear as determined by AASHTO T-96, the Los Angeles Abrasion test. Currently the Los Angeles Abrasion test is the most common method of evaluating durability, with 41 DOTs incorporating it into their material evaluation process. The Micro-Deval test is second, with 20 DOTs using it for testing. When comparing the two tests, research has shown that the Micro-Deval provides the most conservative results, meaning it tends to yield the highest percent losses (Cuelho, et al., 2008). It was decided that despite the L.A. Abrasion test being the NHDOT's method of evaluating abrasion resistance, the Micro-Deval test would be used for this research. This is because the variable properties of each component of BDA can potentially lead to significant issues with abrasion resistance, so it should be evaluated using the most aggressive test to simulate the worst field conditions.

The Micro-Deval Wearing test is a steel ball mill test. A specimen of consisting of 1.5 kg of aggregate organized into pre-determined sizes, 2 Liters of water, and 5 kg of 5mm steel charge is placed in a steel drum, shown in Figure 20, and rotated at 100 rpm for 2 hours.

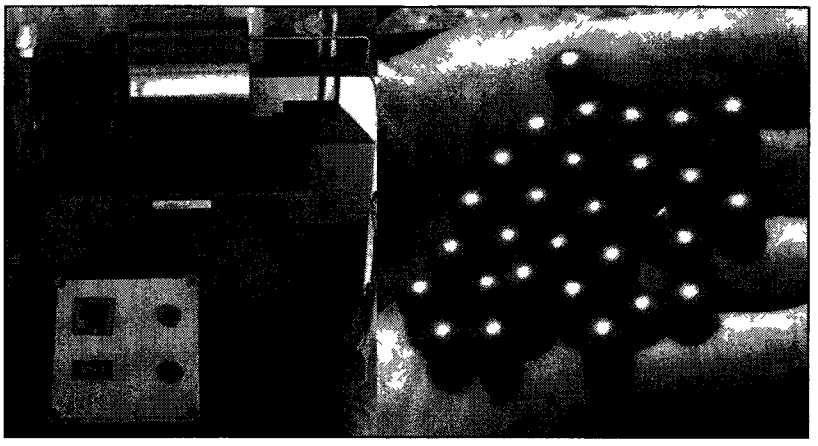

Figure 20: Micro-Deval Mill and 5mm Steel Charge

The aggregate is then washed, dried, and sieved to determine percent loss. AASHTO requires that the material be saturated for 24 hours prior to running the test. However, for the purpose of determining the effect of saturation on the base and subbase material, this test was run in both saturated and unsaturated conditions.

2.8.2 Freeze-Thaw Testing

Roadways in the Northeast typically get particularly severe exposure to freeze-thaw cycles. Frost generally penetrates down approximately four feet in New England depending on the location, putting the majority of base and subbase materials within the depth of frost. Water expands approximately 9% when it freezes, so when it is absorbed in a soil particle, significant stresses can accumulate. Annual exposure to freezing and thawing subjects the base and subbase material to tensile stresses which can quickly degrade a material not suited for that type of exposure. Degradation leads to rutting and other types of roadway failures.

The durability of a material is what determines its resistance degradation as a result of cyclical stresses, so DOTs in states where freeze-thaw conditions are a concern use laboratory freeze-thaw testing to evaluate the durability of highway construction materials. The NHDOT does not specify any particular test for evaluating durability, so for this research AASHTO Designation T-103-91 was used. To simulate the most damaging conditions, the samples were tested in a fully immersed state. This research only tested coarse fractions of aggregate for durability.

2.9 Summary

Pavement design has progressively evolved from design based on experience to design using complex computer modeling programs and laboratory testing techniques. Computer models need reliable parameters to accurately predict pavement performance. In order to obtain reliable parameters field conditions must be accurately simulated. It is the goal of this research to simulate field conditions using the summary resilient modulus loading conditions, with the result of providing the most representative M_R parameters for different blends of BDA.

As landfill space and virgin aggregate become scarce, use of BDA outside of landfill disposal needs to be explored. BDA has the potential to be an excellent geotechnical material, but its variable properties and lack of performance data make engineers hesitant to use it in place of conventional material. To address this, performance characteristics need to be established

based on composition. This research will evaluate BDA using the most common methods of determining aggregate quality.

CHAPTER 3

MATERIALS AND METHODS

3.1 Introduction

Federal, state, and county agencies own 67% of the roads in the United States (Kane, 2006), so the materials and methods in this research were selected to match the current materials and methods in use by these agencies today. All tests were conducted according to established AASHTO standards, and all material was matched to gradations accepted by the NHDOT. Evaluating BDA using NHDOT standards ensures that it will be held to the same standards as traditional highway construction material, without receiving preferential treatment because of its potential to benefit other sectors.

3.2 NHDOT Spaulding Turnpike Expansion Materials

For the past several years the NHDOT has been rehabilitating and constructing new lanes on New Hampshire Route 16 between Exits 11 and 16 in Rochester. Previous research done by Clark (2010) used fine crushed stone (NHDOT Item 304.4) from the project as a control for tests on BDA. The gradation for all BDA samples were prepared to match the gradation of fine crushed stone from the Route 16 project to allow for direct comparison of results.

The gradation curve for fine crushed stone is shown in Figure 21. More complete details of the aggregate collection are given in Clark (2010).

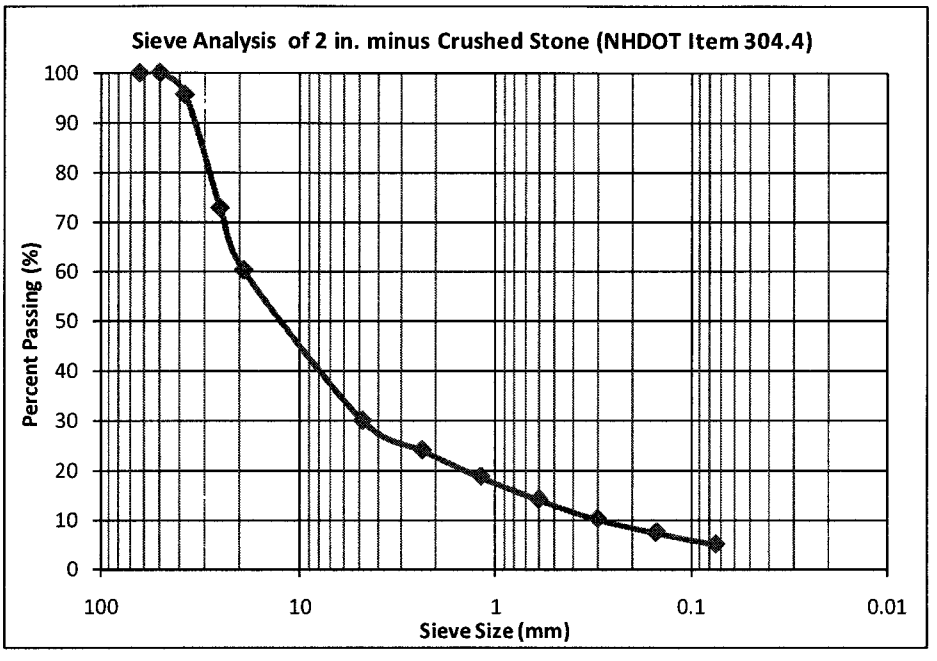

Figure 21: Fine Crushed Stone Gradation Curve

3.3 ERRCO Construction and Demolition Debris

The first step in this research was to find a source of construction and demolition (C&D) debris from which to obtain BDA. There are several facilities that process C&D debris in New Hampshire. The previous research by Clark (2010) and DeRocchi (2008) was done on BDA selected from Environmental Resource Return Corporation (ERRCO) of Epping, NH due to its proximity both to the University and the Spaulding turnpike project.

ERRCO receives the majority of its material from demolition contractors, and the remainder comes from construction contractors. The C&D debris that

comes into ERRCO comes from many sources throughout New England, so its composition reflects building materials commonly used in the region. The C&D debris at ERRCO contain a large portion of concrete and masonry; followed by smaller proportions of bricks, various types of wood, drywall, RAP, metals, plastics and asphalt shingles. To sort out all this material, ERRCO uses various types of magnets and float tanks to separate out comingled materials.

3.3.1 Material Selection

Once the C&D debris is separated it is stockpiled in the yard for further processing. There is no way to separate the individual components of BDA so all of the brick, asphalt, concrete, and other masonry is all combined into one pile, shown in Figure 22.

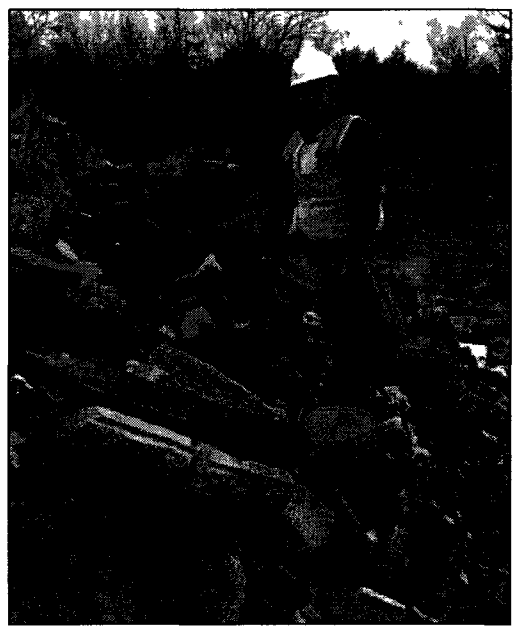

Figure 22: BDA Stockpile at ERRCO

All of the material used for this research was hand selected from the BDA stockpiles and organized into fractions of brick, concrete, and RAP. Organizing it

in this fashion ensured that the various blends in the lab could be precisely prepared.

3.3.2 BDA Preparation for Laboratory Testing

The BDA from the ERRCO stockpile was generally between 6 and 12 inches in diameter, with some pieces much larger. To produce a sample that matched the fine crushed stone used by the NHDOT, it was crushed down to the appropriate size. The Civil Engineering Department does not have a crusher capable of handling 12 inch diameter material, so the first step was to crush it down to a diameter of approximately 4 inches using a sledge hammer. At this point it was small enough for the Department's largest jaw crusher. In order to maximize production of specific gradations needed for each sample, three different sized crushers were used.

The coarse material (retained on the No. 4 sieve) was handled by the Civil Engineering Department's two jaw crushers, shown in Figure **23**. Both jaw crushers operate by an electric motor which spins a flywheel, which causes two jaw plates to oscillate towards one another. The material (concrete, brick, stone, etc.) is passed between the plates and crushed as they oscillate. The larger crusher was very useful for reducing the 4 inch diameter material; however it broke it down to a 2 inch minus gradation with a significant amount of material retained on the one inch sieve. This is a result of the crusher jaws being worn down and a limited range of adjustment. Because all specimens needed to be prepared using material passing the 3/4" sieve, another smaller jaw crusher was used. This crusher, shown in on the right in

Figure **23**, had a wider range of movement in the jaws, which helped to produce more of any particular gradation needed at the time. Unfortunately both jaw crushers failed to produce an adequate amount of fine material, particularly material that passed the No. 100 sieve. In order to address this, surplus fine material was run through the plate mill shown in Figure 24. This mill operates by spinning a plate with tapered radial cut grooves at a distance of approximately 1/8" from another plate that has a feed chute located in the center. It operates by placing the aggregate through the feed chute in the static plate, which runs into the spinning plate and travels down the radial grooves. The aggregate is crushed as it travels down the decreasing groove cross section. The use of these three crushers helped to reduce material waste and optimize production of sieve sizes required to match the NHDOT gradation.

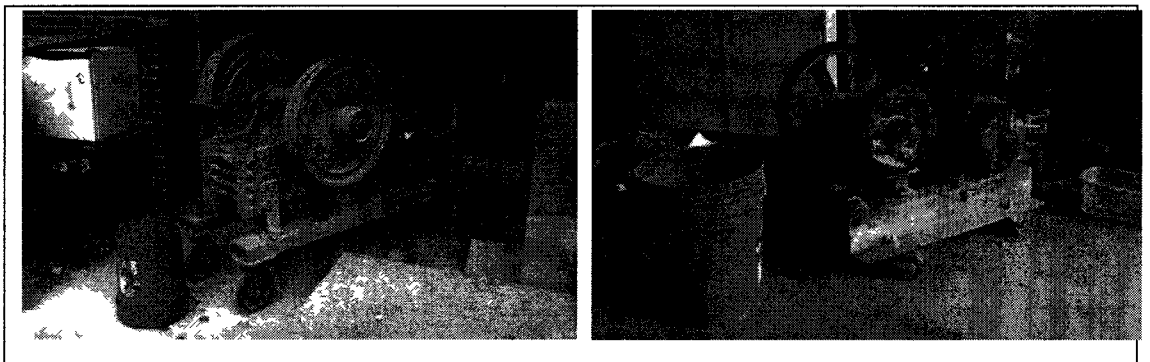

Large Crusher Smaller Crusher

Figure 23: Large and Small Crushers Used to Prepare Coarse BDA

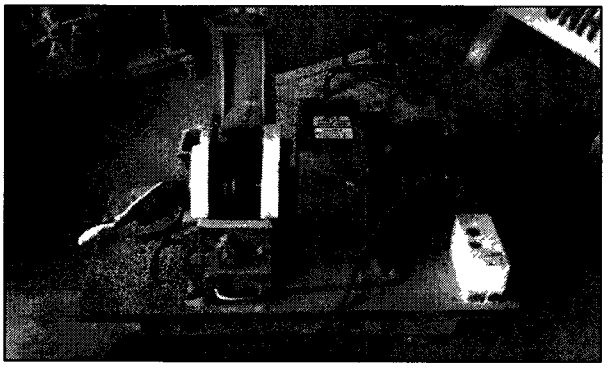

Figure 24: Plate Mill Used to Prepare Fine BDA

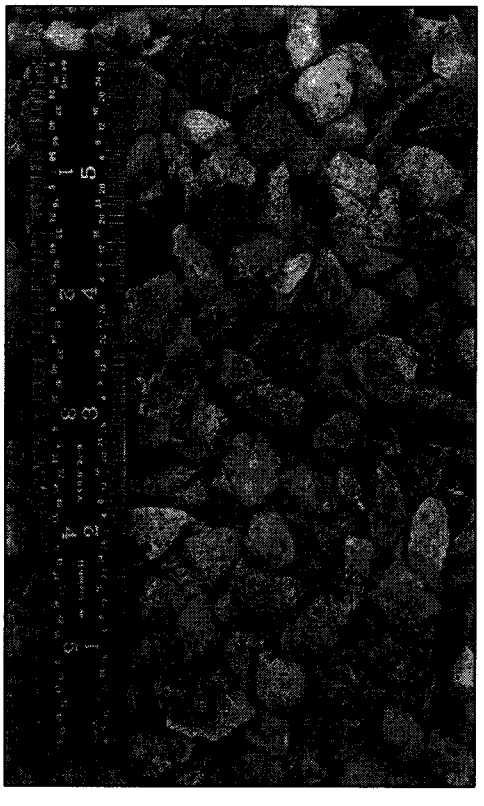

Figure 25: Processed BDA

3.3.3 Sample Mixtures

Because the goal of this research is to determine the effects of different components of BDA on overall performance, samples were prepared with increasing quantities of brick or RAP. Each blend was mixed to the same

proportions throughout the gradation. Once samples of each component were tested and material properties established, the blends shown in Table 4 were tested to best determine the effects of each component on BDA. Note that for Resilient Modulus testing, RAP was only tested at 10% and 20%.

Table 4: BDA Blends Used for Testing

	Percentage of Brick or RAP in Crushed Concrete Blend								
	0	5	10	15	20	30	50	70	100
CBR (AASHTO T-193)	X	X	X	X	X		X		X
Resilient Modulus (*Modified* AASHTO T-307)	X		X		X	X	X	X	X
Micro-Deval (AASHTO T-327)	X		X						X
Freeze-Thaw (AASHTO T-103)	X								X
Standard Proctor (AASHTO T-99)	X								X

Concrete accounts for the majority of the material in BDA. Because of this more blends were run at lower brick and RAP contents so more data could be obtained in a range that better represents the composition of BDA coming out of a C&D waste processing facility. The freeze-thaw and Micro-Deval were not run on RAP because the brick and concrete components of BDA were the primary concern for these properties.

3.3.4 Specimen Compaction

In order to ensure reproducible data, all CBR and Repeat Load Triaxial (RLT) specimens were compacted using the same method using the Bosch

11623 impact hammer shown in Figure 26. This hammer was outfitted with a 6 inch diameter compaction head which was selected to fit inside the 6 inch CBR and RLT molds.

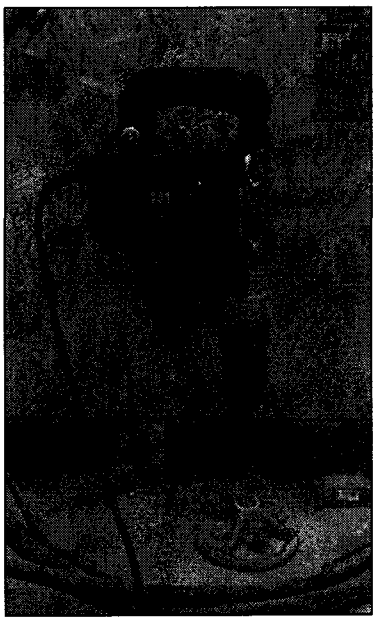

Figure 26: Bosch 11263 Impact Hammer Used for Compaction

The impact hammer is more desirable for coarse specimens because it delivers a much greater energy than standard or modified proctor methods, which simulates field vibratory compaction more effectively. The impact hammer vibrates to deliver energy to the specimen, simulating compaction in the field. This delivers the energy necessary for the coarse material to reorganize into a denser configuration. All specimens were compacted to the greatest density possible. To achieve this, the material was mixed to optimum water content, placed in one inch lifts, and compacted for approximately 20 seconds per lift. The material was placed in one inch lifts in order to achieve uniform density throughout the specimen. This method has been previously validated by DeRocchi (2008).

3.4 Material Characterization

The next step after material preparation was to characterize each material using non-structural testing. The following methods do not describe performance under loading. However, they do indicate optimum performance ranges based on density, as well as susceptibility to environmental effects, which can have long term effects on structural performance. All tests were run on 5 different specimens to balance time spent testing and data quality.

3.4.1 Standard Proctor Testing (AASHTO T-99)

Since the energy delivered from the impact hammer cannot be accurately measured, a relationship between densities obtained using the impact hammer and standard densities needed to be established. In order to do this, densities were determined using the Standard Proctor Test (AASHTO T99). The standard proctor test uses a compaction mold similar to the CBR mold, in the case of this research, the CBR mold was used. The material is blended at optimum water content and placed in three equal lifts; each compacted with 25 blows from a 5.5 pound hammer dropped from 12 inches. The mold extension collar was then removed and the excess material was struck off. The mold and material was then weighed, using this weight, the weight of the mold, the volume of the mold, and the water content of the material, the dry density could be calculated. These tests were run on blends of 100% concrete, brick, asphalt, and crushed stone.

3.4.2 Micro-Deval Testing (AASHTO T-327)

As described in Chapter 2, the Micro-Deval test is a steel ball mill test that was done in both saturated and unsaturated conditions for this research. Before

the sample was prepared the aggregate needed to be thoroughly washed and oven dried to a constant mass to remove smaller particles that could throw off results. Since the gradation for the resilient modulus and the CBR had a maximum nominal aggregate size of 3/4", the specimen was prepared according to section 8.2 of ASTM D6928, shown in Table 5.

Table 5: Micro-Deval Specimen Composition

Aggregate Size*	**Mass (g)**
P3/4" R5/8"	375
P5/8" R1/2"	375
P1/2" R3/8"	750
Total	1500±5

* P=Passing, R=Retained

The specimen was then prepared and placed into the mill with the steel charge. If a saturated specimen was to be tested it was left to soak for a minimum of one hour. The specimen was then placed in the mill and rotated at 100 rpm for two hours.

Upon the completion of the test the contents of the mill were carefully poured over a No. 4 sieve nested in a No. 16 sieve. The aggregate and steel charge were then thoroughly washed until all material passing the No. 16 sieve was removed. At this point the steel charge was removed using a hand-held magnet, taking care not to remove aggregate pieces. Once all of the charge was removed the aggregate retained on the No. 4 and No. 16 sieves was emptied into a dish and oven dried to a constant temperature. Once fully dry the aggregate was weighed to determine percent loss.

3.4.3 Freeze-thaw Testing (AASHTO T-103)

The NHDOT states that "materials that break up when alternately frozen and thawed shall not be used for aggregate base course" (NHDOT, 2010). It does not specify the number of cycles, particle size, or method of testing. Because of this lack of specificity, AASHTO T-103: Soundness of Aggregates by Freezing and Thawing was selected as the standard to follow. T-103 has three procedures that can be followed: total immersion in water, partial immersion in water, and partial immersion in alcohol/water solution. Since this research is attempting to simulate performance under "worst-case" in-situ conditions, the total immersion procedure was used. Since no specific number of freeze-thaw cycles was outlined by the NHDOT, T-103 was consulted. T-103 suggests that a minimum of 50 freeze-thaw cycles be run for the total immersion procedure. In light of this, it was decided that 50 cycles be used for this research, however due to time constraints and limited freezer capacity only 44 cycles were completed. In terms of particle size, T-103 outlines 5 different fractions that may be used depending on the gradation of the material, ranging from fine to coarse. The majority of the gradation used for this research is coarse, a sample of coarse material was selected. The sample composition is shown in Table 6.

Table 6: Sample Used for Freeze-Thaw Testing

Fraction	Particle Size	Mass (grams)
A 1 ½" to ¾"	1 ½" to 1"	1000±50
	1" to ¾"	500±30
	Total	1500±50

In preparation for testing, all material was thoroughly washed to remove any fine particles, then oven dried to constant mass. Then 5 specimens were prepared and soaked for 24 hours. Once the specimens were done soaking they were stacked in a chest freezer. Sturdy wooden rods were stacked in between each tray to ensure even cooling throughout the specimen. The trays were then left until they had frozen solid. At this point the trays were removed for thawing. The material was thawed in the lab sinks. This test is for fully submerged aggregate, so the specimens had to remain in water at all times. The trays were placed in the sink and a sponge was inserted into the drain to reduce flow. At this point the trays were fully submerged in room temperature water. When the trays were fully submerged the faucet was adjusted until steady state flow was achieved. The setup for thawing the aggregate is shown in Figure 27.

Figure 27: Thawing Aggregate Specimens

When thawed the specimens were stacked in the freezer in the same fashion described earlier. This process was repeated until 41 freeze-thaw cycles were completed.

Once the freeze-thaw cycles were finished each specimen was drained and oven dried to constant mass. Then each specimen was sieved over the 5/8" sieve to determine percent loss. Upon completion of the test, the material was disposed of.

3.5 California Bearing Ratio Testing

CBR testing was done in addition to RLT testing. This helped establish bearing capacity values for each component of BDA. Although the CBR is not the most effective method for evaluating performance of highway construction materials, the vast amount of CBR data available makes it a useful test to run for comparison purposes. CBR testing was done according to AASHTO T-198. In order to balance the number of tests with available time, 5 tests were run on each blend to ensure representative CBR values. AASHTO T-198 permits the CBR to be taken at 0.1 or 0.2 inches of deformation. When possible, all CBR values were taken at 0.2 inches of deformation, however some specimens did not reach 0.2 inches before the load cell reached capacity. When this happened the CBR was taken at 0.1 inches. If a specimen did not reach 0.1 inches of deformation before the load cell reached capacity, a new specimen was prepared and the test was rerun.

3.5.1 CBR Loadframe and System Setup

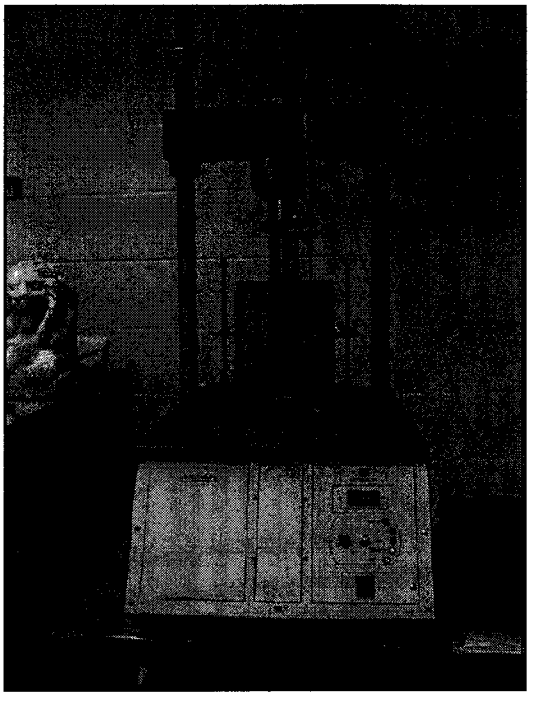

Figure 28: California Bearing Ratio Specimen in Loadframe

The CBR loadframe and specimen is shown in Figure 28, and consists of a 10,000 pound loadframe, a platen that is actuated from the base, and a piston mounted on a 10,000 pound load cell. A LVDT mounted to the piston measured the displacement of the specimen relative to the loadframe. The CBR was run directly from the controls on the loadframe, with no computer controlled input. Load and deformation data are collected using the GCTS Computer Aided Testing Software (CATS), which has a California Bearing Ratio test file. This test file produces a curve comparing load and deformation from which the CBR could be obtained.

The standard CBR mold as required by AASHTO T-198 has a diameter of 6 inches and a volume of 0.075 cubic feet. Due to the diameter of the mold, the

gradation of the sample needed to be limited to particles less than 3/4" in diameter. Unlike the RLT specimen the material greater than 3/4" is not scalped off. For the CBR the material greater than 3/4" needs to be scalped, weighed, and replaced by an equal mass of material passing the 3/4" sieve and retained on the No. 4 sieve. Once the mass is reintroduced in smaller fractions, the material is then blended in preparation for CBR testing.

All specimens were mixed individually at optimum moisture content. In order to obtain densities the mold was weighed prior to compaction so the material mass could be determined from weighing the prepared specimen. The CBR mold components and dimensions are shown in Figure 29.

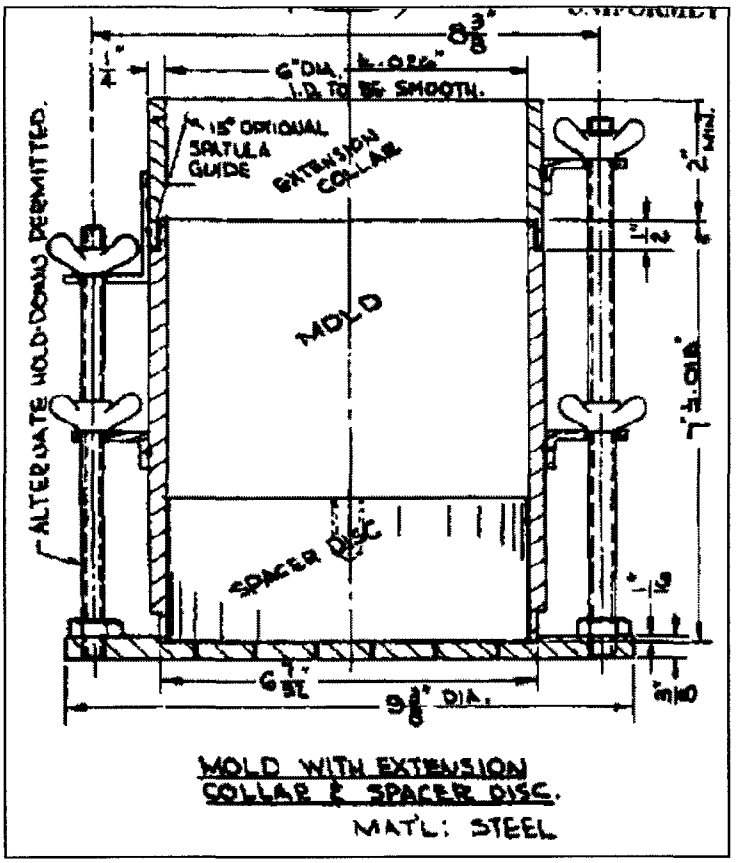

Figure 29: Diagram of CBR Mold with Extension Collar and Spacer Disk (ASTM, 2007)

The specimen is prepared by compacting one inch lifts on top of the spacer disk until the material is fully compacted above the joint where the extension collar and mold meet. At this point the extension collar is removed, excess material is struck off, the mold is inverted and the spacer disk is removed. The intent of this is to provide a flat, well compacted surface on which to drive the loading piston. One problem encountered upon inversion was the loss of material at the base of the inverted specimen; this caused a loss in uniformity, making it unsuitable for testing. This happened frequently because the CBR gradation has a high percentage of coarse material that is easily disturbed when struck off. To

address this fine material was placed in the voids created by striking off the specimen and compacted for approximately five seconds to create a flat surface. This surface helped retain material upon inversion so the specimen could be tested. This method of compaction was performed on all specimens to ensure consistent compaction of all materials.

3.5.2 Performing the CBR Test

When the specimen was fully prepared its mass was recorded so density could be determined. Before the specimen was ready for testing a 10 pound surcharge was placed on top of the material. This surcharge helps simulate the stresses on a material at depth by applying an overburden stress. At this point if an unsaturated test was desired the specimen would be placed in the CBR loadframe. If a saturated specimen was desired the specimen was fully submerged in a tank of water for 96 hours. After 96 hours it was removed, drained, and placed in the CBR loadframe.

Once in the loadframe, the CBR loading piston was leveled and the specimen was raised until 10 pounds of force was acting on it. This provides a seating stress and prevents any loose particles resting on the top from affecting the data. The LVDT and CBR load cell were then zeroed in CATS. All instruments were then zeroed and the test was started by raising the platen at a constant deformation rate of 0.05 inches per minute. This was continued until the load cell reached capacity or a deformation of 0.4 inches was reached. Upon completion of the test the specimen was removed from the loadframe and discarded.

3.5.3 Determining the CBR

The CBR is determined by comparing stresses at given deformations to a reference material based on a typical soil stress-strain curve, like the one shown in Figure 8. This can usually be done directly from the stress-strain curve obtained from the test results, however sometimes corrections need to be made for inconsistencies. Occasionally surface irregularities would cause the beginning of the curve to be non-linear, and other times the first 0.1" or so would be in a concave upward shape, as shown in Figure 30. Because the CBR is based on the assumption of linear elastic behavior in the beginning of the soil load-deformation curve, these inconsistencies needed to be corrected. This was done by drawing a line through the linear portion of the curve to the intersection with the x-axis and recording the deformation at the intersection. The curve was then shifted in the negative x direction using the deformation value from the linear approximation. This shift resulted in a linear portion of the soil load-deformation curve extending from the origin, shown in Figure 30.

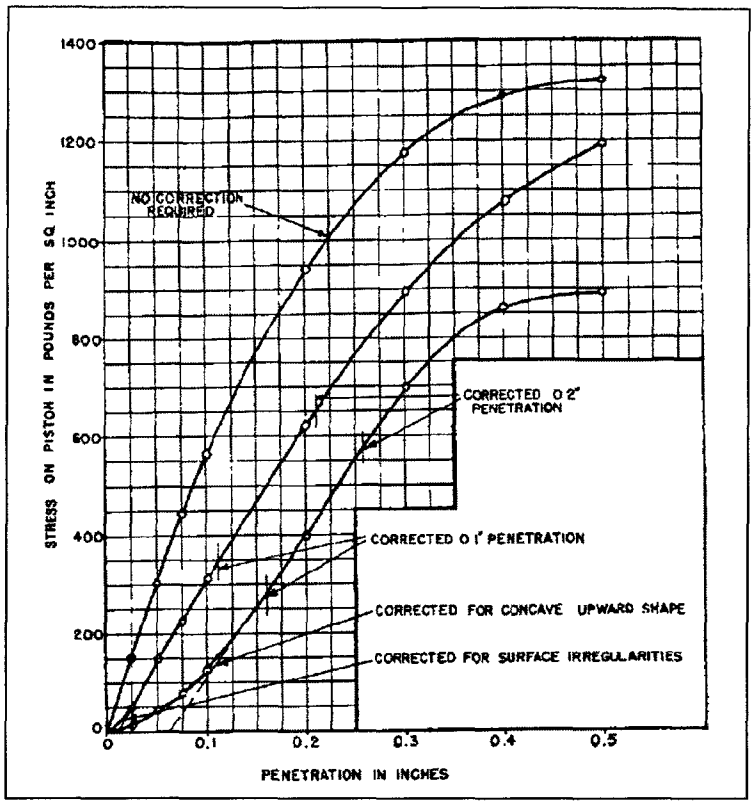

Figure 30: Correction of CBR Curve (ASTM, 2007)

Once the corrected curve was determined, the stresses corresponding to 0.1 inches and 0.2 inches were obtained. These stresses were compared to the standard CBR stresses from Equation 1:

$$\Delta = 0.1 \text{ in: } \sigma_n = 1000 \text{ psi}$$

$$\Delta = 0.2 \text{ in: } \sigma_n = 1500 \text{ psi}$$

The CBR obtained using Equation 1 and the standard stresses were compared to other data to evaluate the quality of the material. AASHTO and ASTM recommend the ratio be used for a deformation of 0.2 inches. However, if the CBR for a deformation of 0.1 inches is determined to be higher, then that value may be used for that particular material.

3.6 Repeat Load Triaxial Testing (AASHTO T-307, Modified)

Due to the goals of this research, it was decided that AASHTO T-307 not be used because of its unrealistic bulk stresses and short testing period. A modified procedure of AASHTO T-307 was developed. This procedure used a constant Summary Resilient Modulus bulk stress of θ = 208 kPa for 50,000 load cycles. Using this modified procedure allows more effective analysis of material behavior over time by keeping the bulk stress at a constant, theoretically maximum load. This test was done on different blends of BDA in order to obtain resilient modulus values. The resilient modulus values can be entered into the MEPDG to model rutting performance. Five tests were run on each individual blend. More tests would be desirable in order to obtain more representative values and eliminate outliers; however this was not practical due to the amount of time the RLT test takes to run.

3.6.1 GCTS Loadframe and System Setup

The triaxial setup used in this research is configured to run several different triaxial tests. The triaxial setup is manufactured by GCTS Testing Systems of Tempe, Arizona, and is shown in Figure 31. The GCTS Triaxial Testing System is outfitted to handle specimens up to six inches in diameter and is capable of repeated loading. The system includes a 50,000 pound load frame, a hydraulic actuator for loading, two external LVDTs to measure displacement, and a control tower to regulate air and water pressure.

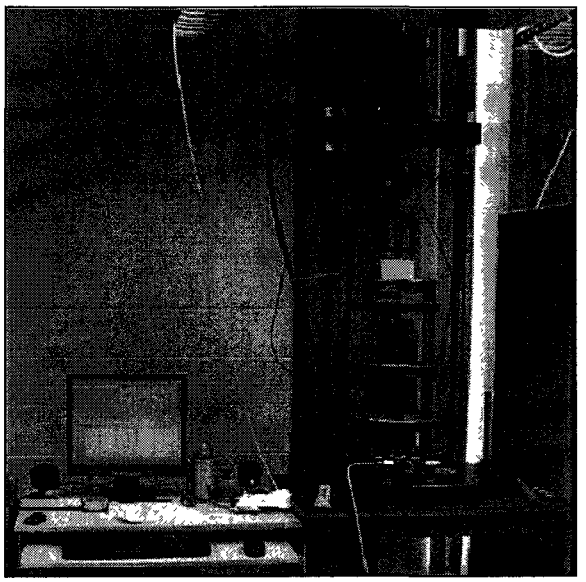

Figure 31: GCTS Triaxial Testing System

The external hardware is run by a computer based software system from GCTS called CATS. This software controls the hydraulic actuator and the control tower that regulates air and water pressure. It also receives feedback from the load cell, LVDT's, and servos. Figure 32 shows a screenshot of the CATS software during RLT testing. The software also enables the operator to run tests automated or user controlled. The automated function ensures that the confining pressure, deviator stresses, and load cycles are controlled so the test is run and stopped as desired by the operator. This is particularly useful for the long term SRM tests, which take over 13 hours to complete.

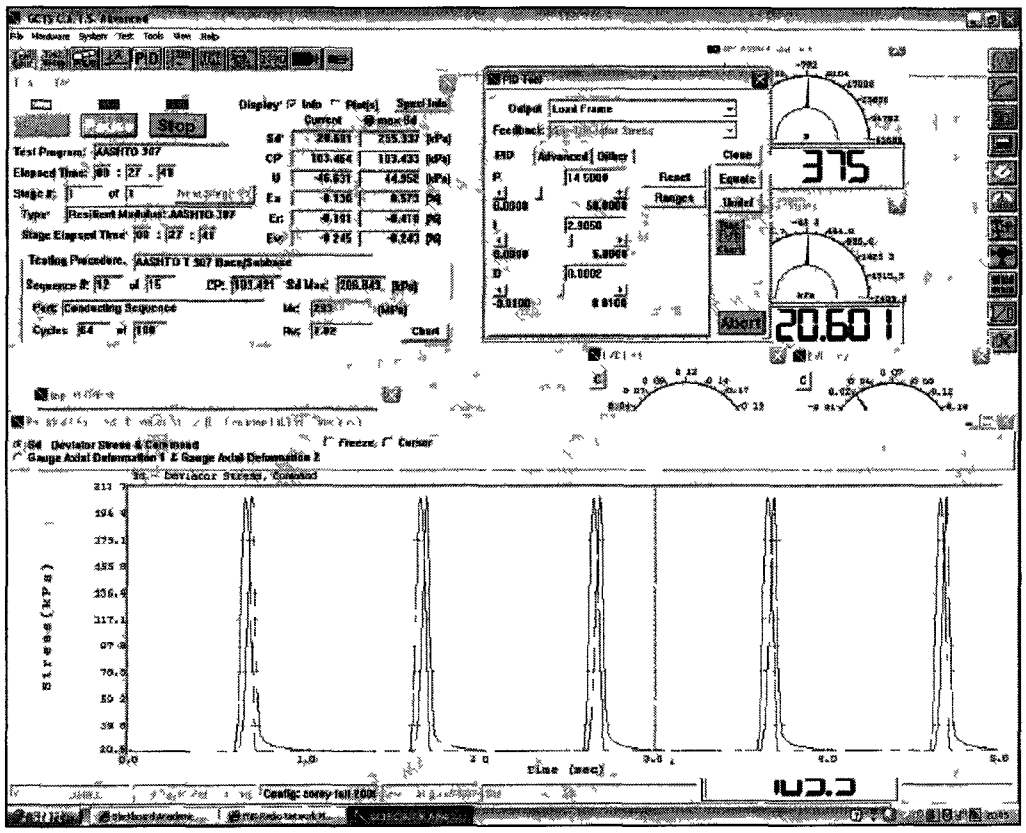

Figure 32: Screenshot of CATS Software Running an RLT Test

One feature that is essential to the successful operation of a triaxial test is the proportional, integral, derivative (PID) function. The function ensures that parameters such as cell pressure, load pulse intensity, and load pulse duration remain at the values defined within the CATS software. The PID function uses the same principle as cruise control in a car. Cruise control works by reading the speedometer at a certain frequency and the dynamically adjusting the accelerator to maintain a constant speed. The PID function in CATS uses the feedback from the deviator stress and cell pressure to control the conditions around the soil specimen. The only time that the operator may run into PID problems is with the load impulse duration and intensity. The screen shot shown

in Figure 33 shows incorrect command and feedback for deviator stress; compared with the normally functioning command and feedback shown in Figure 34. Note the blue line in both figures is the command, and the black line is system feedback. Incorrect PID values have resulted in extreme stresses, occasionally resulting in specimen failure.

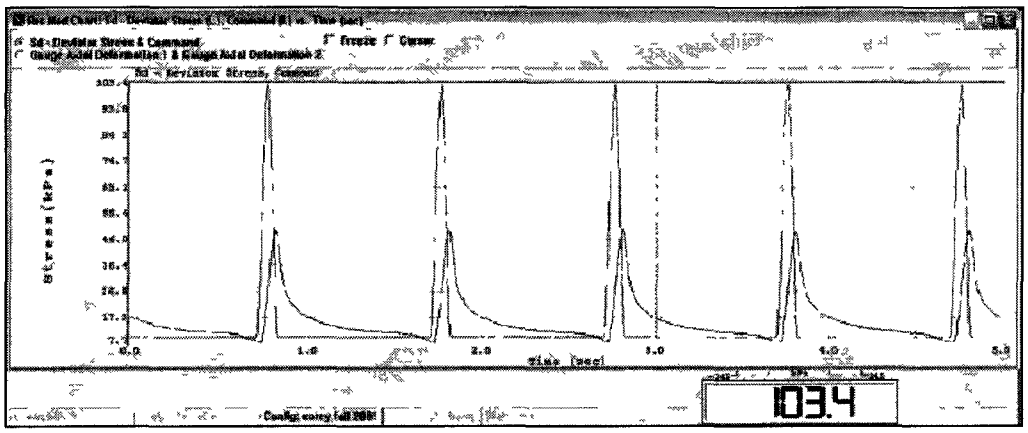

Figure 33: Poor Command and Feedback Due to Incorrect PID Inputs

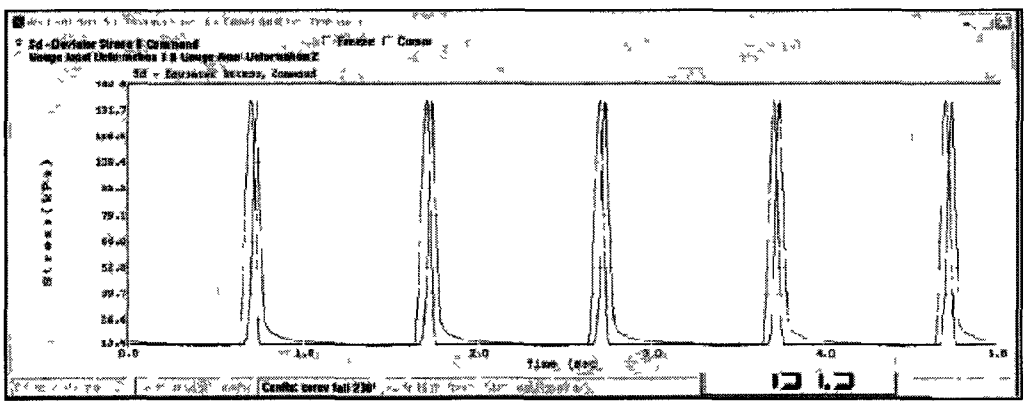

Figure 34: Acceptable Command and Feedback Due to Correct PID Inputs

All PID settings can be found in the configuration file provided by GCTS. A hard copy is located in Appendix F, should any problems be encountered with command matching feedback, the PID configuration file should be referenced. It should be noted that the PID function does not need to be adjusted during

normal operation, and setting values other than what is found in the configuration file can lead to poor results or specimen failure.

3.6.2 Specimen Size

The size of the specimen used for testing is dictated by the size of the aggregate in the sample. Since there is no standard for the RLT testing in this research, the specimen size from AASHTO T-307 was used. AASHTO T-307 requires that base and subbase be prepared in 150 mm (6 inch) diameter molds. All specimens were prepared to a height between 310 and 330 mm (12-13 inches), which satisfies the AASHTO standard requiring the specimen's height to be at least twice the diameter.

3.6.3 Specimen Preparation

As mentioned before, there is no standard to the RLT testing in this research, so all specimen preparation was performed as outlined by AASHTO T-307. AASHTO limits the maximum particle size to $1/5^{th}$ of the mold diameter to ensure that oversized particles do not cause the material to behave differently in the lab than in the field. This can have a significant effect on the gradation used for testing, particularly for base and subbase, which can have a maximum particle size of 6 inches or greater. All of the material in this research used the NHDOT 2" minus gradation with all material greater than 3/4" diameter removed. Although the maximum allowable particle size for the specimen mold diameter is 1.2 inches, the maximum size was reduced to 3/4" because the crusher used for material preparation tended to produce particles 3/4" or less in diameter.

All specimens were prepared at optimum moisture content in order to achieve the highest densities possible. T-307 permits the use of either a drop hammer or vibratory tool for compaction. The vibratory method was selected because it allows for quicker specimen preparation and can achieve higher densities. It also more effectively simulates vibratory field compaction. Prior to compaction all material was mixed with water according to the amount of each component in the blend and its respective optimum moisture content. Once mixed the material was placed in one inch lifts and compacted for approximately 20 seconds per lift.

Due to the angularity of crushed stone and sand, holes inevitably formed in the latex membrane. A typical puncture is shown in Figure 35. These holes can have adverse effects on test results because they prevent the specimen from being fully isolated during testing, causing issues with pore pressures and intrusion of air, particularly with saturated specimens. In order to address this issue, the specimen was wrapped in cling wrap so the entire surface was covered with at least two layers. The fully prepared specimen is shown in Figure 36.

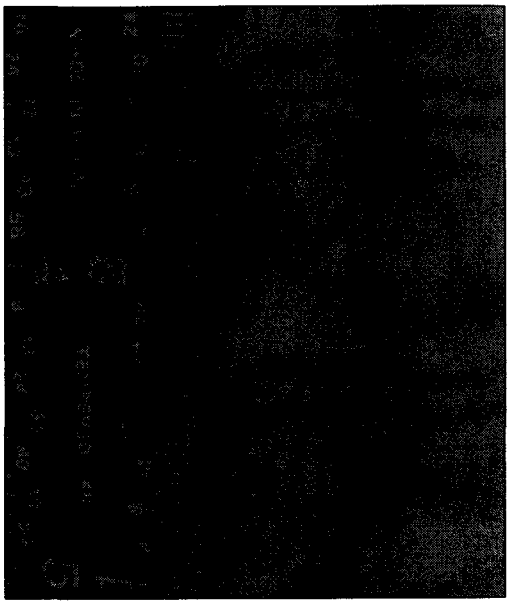

Figure 35: Hole in Membrane Caused by Aggregate

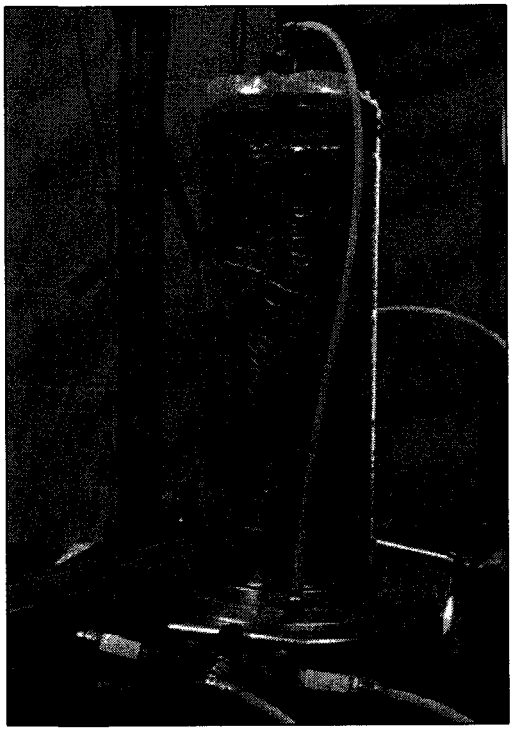

Figure 36: Fully Prepared RLT Specimen

The mass of the specimen was determined by weighing the material prior to compaction and then weighing the remaining material after compaction. The volume of the specimen was determined by measuring the height of the specimen and assuming the 6 inch diameter was constant throughout its length. This was verified by measuring the circumference of several specimens at one-inch intervals across their entire length and back calculating the diameter. Although this method is not the most accurate due to voids created along the outside of the specimen by larger particles, however it is the most practical given the test setup.

3.6.4 Customizing CATS for Summary Resilient Modulus Testing

Before this research was conducted, CATS had a pre-programmed test file configured to run resilient modulus testing according to AASHTO T-307. As discussed previously, the summary resilient modulus is much different than AASHTO T-307, particularly because of the large number of loading cycles. In order to get the program to fit the needs of this research, a meeting was arranged with GCTS. During their visit all of the LVDT's were calibrated and they used a proof ring to calibrate the load cells for both the triaxial and CBR systems.

Once the calibrating was done a custom testing file needed to be produced to run the SRM test. Ideally data points should be recorded for each loading cycle; however this is not possible because the data collection device does not have sufficient capacity to handle the size of the data file. The solution was to modify the AASHTO T-307 file to run 50,000 loading cycles and collect as much data as possible. To do this a copy of the AASHTO T-307 file was made

and renamed. After this the triaxial program was accessed. A screenshot of the triaxial program is shown in Figure 37. In this window the number of cycles for pre-conditioning and per deviator stress can be defined. From this window the operator can edit the user defined testing procedure. This will direct the operator to the resilient modulus testing sequence window, shown in Figure 38.

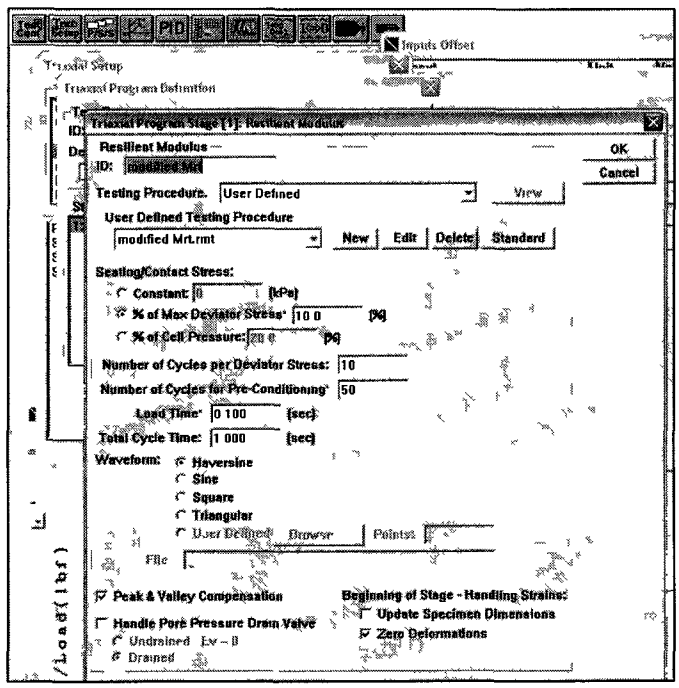

Figure 37: Accessing the Triaxial Program

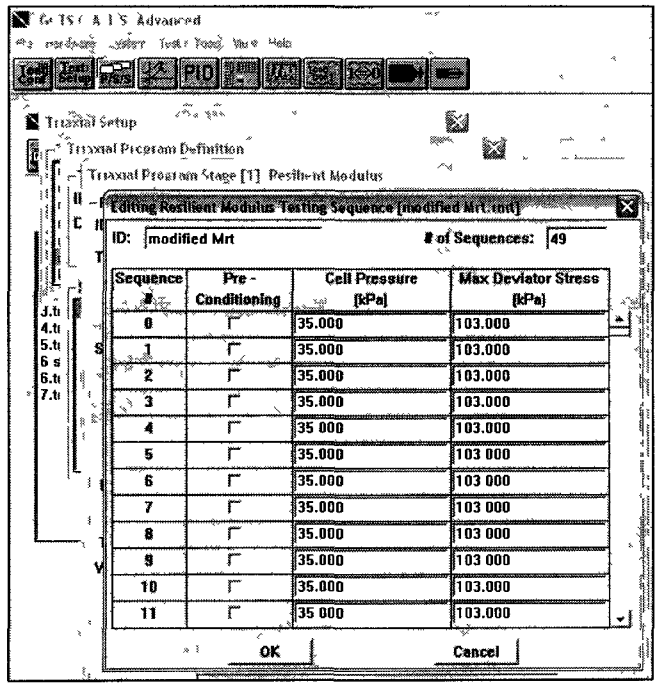

Figure 38: Screenshot of Editing the Resilient Modulus Testing Sequence

In this window the number of sequences, cell pressure, and deviator stresses can be defined. CATS allows a maximum of 50 sequences, it must be noted that sequence 0 counts as a loading sequence, so 49 is the maximum value that can be input in the upper right corner. Once in the resilient modulus testing sequence window, a cell pressure of 35 kPa and a maximum deviator stress of 103 kPa (corresponding to a bulk stress of 208 kPa) must be input for each individual sequence. When the sequence is fully defined the number of sequences per cycle in the previous window needs to be set to 1,000. This results in a test that will deliver 50,000 load pulses with constant deviator and confining stresses. The data is collected in a similar fashion as AASHTO T-307, with the last five data points of each sequence recorded. This yields a data file that reports five data points per 1,000 loading cycles, so resilient modulus data is

collected at even intervals throughout the duration of test. This allows the operator to determine changes in material behavior over long term loading.

3.6.5 Conducting Repeat Load Triaxial Testing

When the specimen was fully prepared it was enclosed in the triaxial cell and placed in the load frame. The fully assembled triaxial setup is shown in Figure 39.

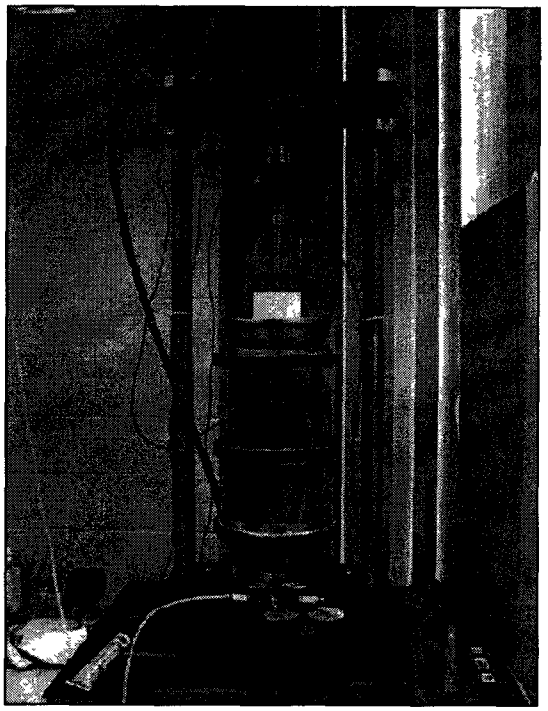

Figure 39: Specimen in GCTS Loadframe Ready for Testing

Once the specimen was ready for testing, the LVDT's were adjusted to allow for maximum range of motion during testing. Then a confining pressure of 35 kPa was applied according to the summary resilient modulus. At this point, if a saturated specimen was desired a line from a reservoir stored above the test setup was connected so water would flow into the base and out the top of the

specimen. The inflow and outflow was recorded until steady-state flow was observed. At this point the specimen could be considered fully saturated and the remainder of test preparation could be carried out. Once the confining pressure was stabilized a seating deviator stress of 5 kPa was applied. This sequence was followed because the confining pressure has a significant effect on a soil's stress response; so the confining pressure must be applied before any axial loads to avoid improper loading conditions. Once the deviator stress and confining pressure were applied, the LVDT's were zeroed in CATS and the test was initiated. During the test the operator watched the feedback to ensure the test was running as expected. Once it was determined that the test was properly running, the operator could leave and allow the automatic function in CATS to finish the test.

Occasionally equipment malfunctions occurred during testing. The most common cause of a system malfunction was related to the LVDTs. The triaxial setup uses two LVDTs mounted on a bracket attached to the loading piston, shown in Figure 40.

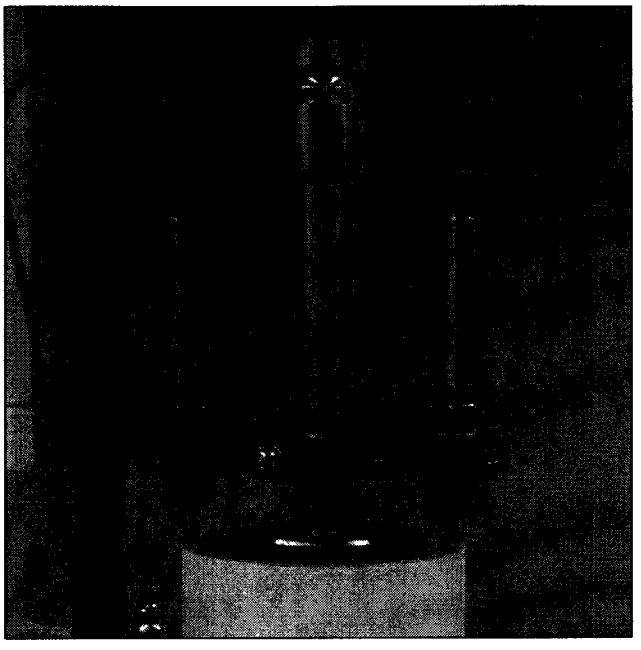

Figure 40: LVDT Bracket Mounted to Loading Piston

In order to ensure accurate deformation readings, CATS measures a parameter called the Rv value. The Rv value is an indicator of the relative difference between the two LVDT readings. Anything that is out of level in the loading mechanism can affect the Rv value, this includes the LVDT bracket, the upper loading platen, and the contact points for the LVDTs. If the Rv value exceeded 1.3, the test was paused, often for a long time since most tests were run overnight when there was no one present in the lab. Due to the properties of recycled concrete, these pauses without loading allowed it to stiffen considerably, so when the test was resumed in the morning a jump in M_R uncharacteristic of other results was observed. When this happened the test was re-run to stay in accordance with the rest of the data.

3.7 Simulating Material Performance Using the MEPDG

Once the SRM data was collected, it was input into the MEPDG to simulate the effects it would have on pavement performance. As discussed in Chapter 2, the MEPDG uses factors such as traffic volume, axial loading patterns, climate, hot mix asphalt properties, base and subbase properties, and subgrade properties to analyze pavement distress throughout the design life of a road.

The MEPDG requires multiple levels of input, many of which are outside the scope of this research. Because of this a base model was used to ensure that conditions and construction methods typical of this region accurately represented. This model was obtained from research done by DeRocchi (2008). The base model provided used measured data from a section of I-393 in Chichester, NH; which was a part of the research by Daniel (2008) on the use of RAP in HMA. This base model originally used NCHRP climatic data from Rochester, NH. However since DeRocchi's research has been completed, a newer version of the MEPDG had been released, which required updated climatic data files. The location remained the same for the new data files; however they are different than ones used in previous research, which may affect comparability of results. The only variable in this base model was the base layer, which was modeled as crushed stone with M_R inputs from laboratory results. All other inputs remained constant; allowing for base and subbase stiffness values to be isolated so the effects of brick content of the performance of BDA are more apparent.

A screenshot of the base model input screen is shown in Figure 41. The MEPDG uses red, green, or yellow boxes to indicate whether or not the model is ready to run a simulation. Red indicates that no data has been entered or the data is outside of acceptable values. Green shows that the parameter is ready to run the simulation. Yellow indicates that there is acceptable data, but it has not been checked for the simulation that is about to be run. The simulation will be allowed to proceed with green and yellow indicators. As shown in Figure 41, the majority of the inputs shown on the left hand side of the screen are yellow. This is because they are part of the base model provided and are intended to remain constant, so they were not checked or changed for each simulation. The only green boxes on the input screen are the layer inputs and the climate data, which needed to be loaded for each simulation.

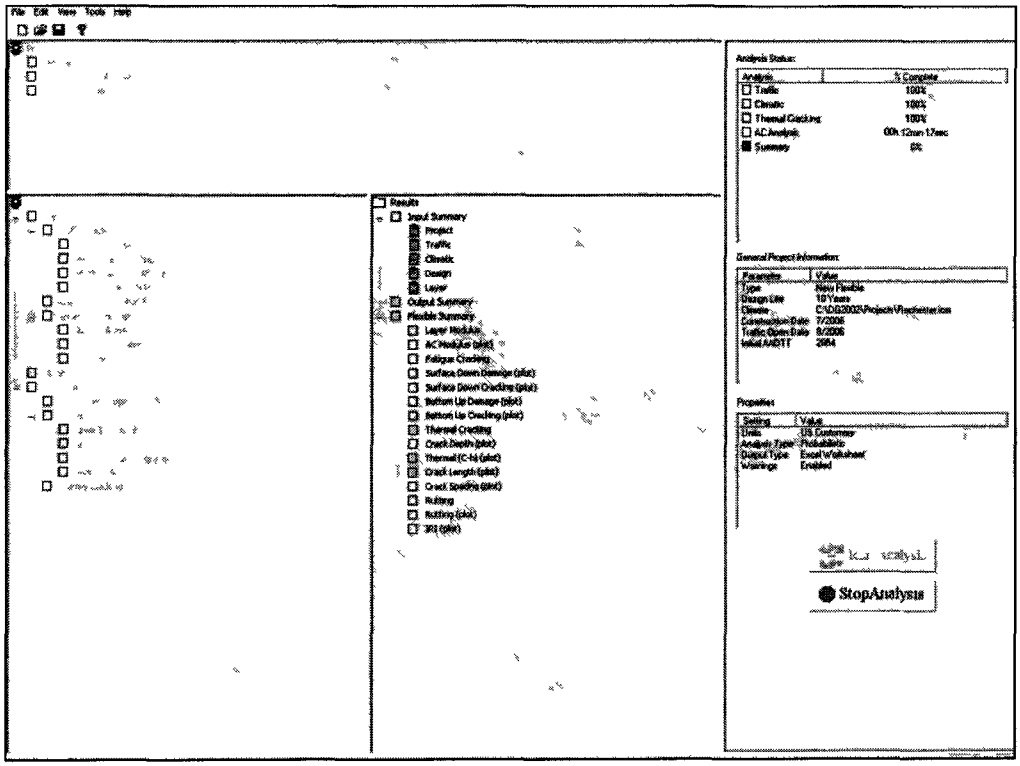

Figure 41: MEPDG Input Screen

The only variable for each model was the base and base and subbase M_R.

A screenshot of the pavement structure input screen is shown in Figure 42.

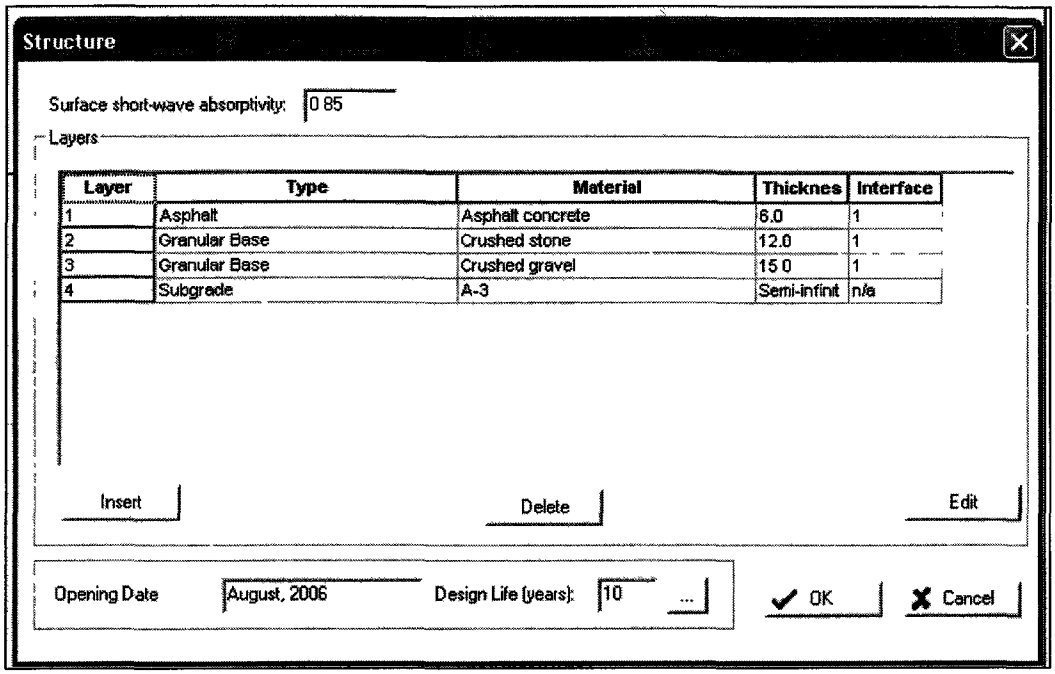

Figure 42: MEPDG Pavement Structure Input Screen for Base Model

The base model specified four layers: one asphalt, two granular bases, and the subgrade or existing soil. In order to amplify the effects of BDA brick content with respect to rutting performance, both granular base layers were modeled with the same M_R, effectively creating one 27" thick granular base layer. Once the laboratory M_R results were input, the model was run.

Upon completing the simulation, the MEPDG produced an output file that displayed each pavement distress result in both graphic and tabular form. An example graph of rutting output from this research is shown in Figure 43. This shows the total rutting and the contribution from each individual layer compared to the rutting design limit. This research reported the total rutting for comparison of BDA blends. This was used because the total rutting determines whether or not the pavement passes performance standards. The provided base model was

based on a 10 year design life. All rutting values were reported at the end of the tenth year of the roadway simulation.

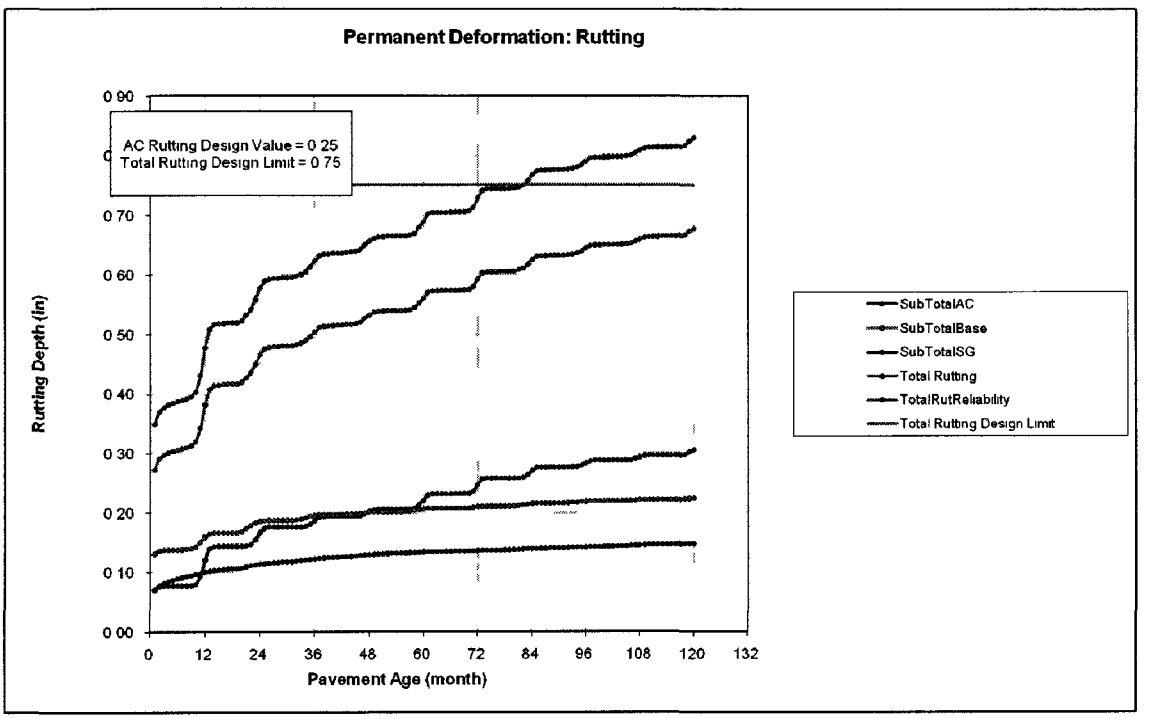

Figure 43: MEPDG Rutting Output

3.8 Data Collection and Post Processing

For this research data was collected after each test was completed. The data for each specimen was interpreted as required by each standard and results were obtained. Once the results were obtained statistical analysis was performed in order to establish relationships between different blends of BDA and performance standards while taking into account the variability and number of tests performed.

3.8.1 Linear Regression Analysis and Hypothesis Testing

Once data has been collected for any research, it must be analyzed to determine whether or not a relationship between the variables exists. In the case of this research, the variables were brick content in BDA blends and performance standards, specifically CBR, M_R, and rut depth. This relationship is determined using hypothesis testing.

When two variables are plotted against each other, a scatter plot is created. In order to establish a relationship with the data, a best fit line is drawn. This should describe the behavior of the data, but with all data there is a degree of variability which casts doubt on how well best fit line actually describes the relationship. This is where hypothesis testing comes in. Linear regression analysis describes the best fit line shown in Equation 6.

$$y = \beta_0 + \beta_1 x \qquad \text{(Equation 6)}$$

Whereβ_0 is the intercept andβ_1 is the slope of the line. Hypothesis testing determines how well the best fit line describes the data by starting with two hypotheses:

$$H_0: \beta_1 = 0$$

$$H_1: \beta_1 \neq 0$$

"Failure to reject H_0: $\beta_1 = 0$ is equivalent to concluding that there is no linear relationship between x and y" (Montgomery, 1994).Examples of both outcomes of hypothesis testing are shown in Figure 44 and Figure 45.

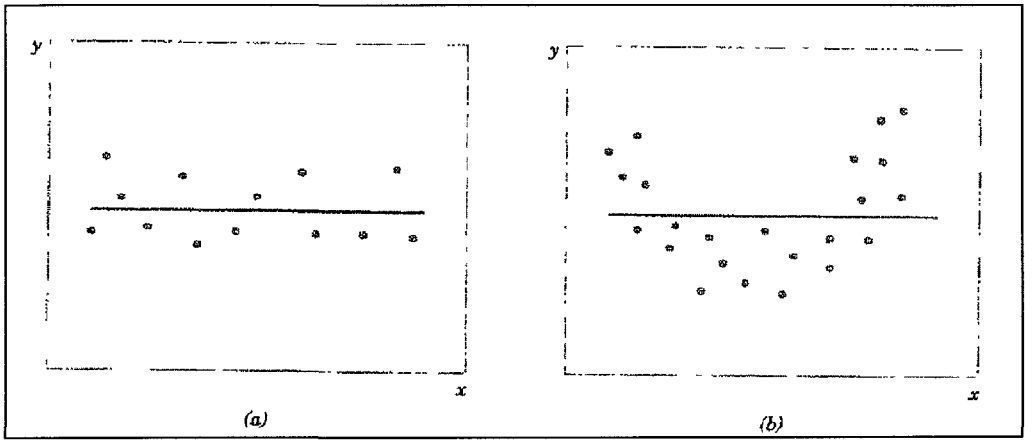

Figure 44: H_0: $\beta_1 = 0$ is Not Rejected (Montgomery, 1994)

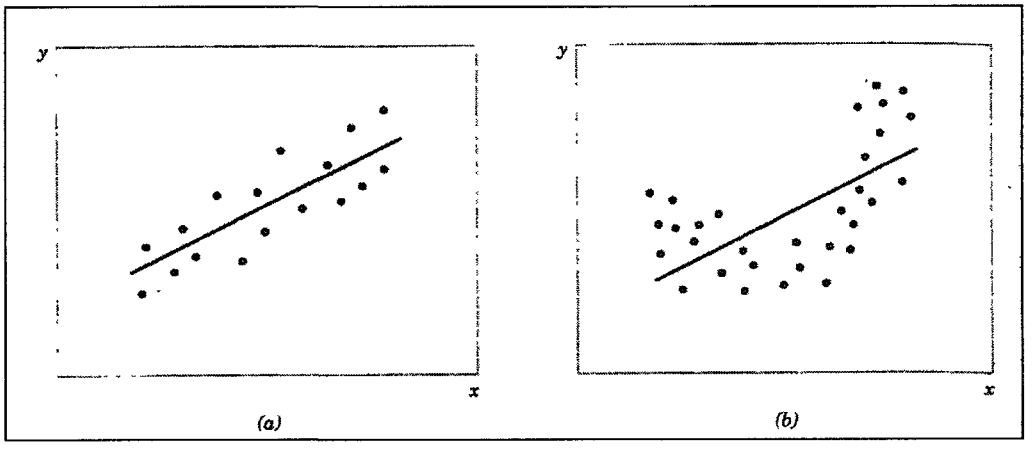

Figure 45: H_0: $\beta_1 = 0$ is Rejected (Montgomery, 1994)

As can be seen in Figure 44, there is no relationship between the data, so the null hypothesis, H_0, is accepted. On the other hand when the data shows a relationship the null hypothesis is rejected, as shown in Figure 45. Statistically speaking, rejecting the null hypothesis makes a stronger statement than accepting it because it establishes that there is a relationship between the data, so most hypothesis tests are set up so that the null hypothesis is zero for the purpose of establishing a stronger relationship between the variables being analyzed.

In order to determine at what point the hypothesis should be accepted or rejected; an acceptable confidence level must be established. A confidence level is a measure of how often a set of results are predicted to fall within a given range. For example if a null hypothesis for β_1 is made, a 95% confidence level would mean that 95% of the time the slope would fall within a specified range. As the confidence level decreases the range of values increases. In statistics, the confidence level is described as:

$$\text{Confidence Interval} = 1 - \alpha \qquad \text{(Equation 7)}$$

Where α is the significance level of the test. When the desired confidence level is established, α can be obtained. To determine whether or not to reject the null hypothesis, the α value must be compared to a parameter call the P-value. The P-value describes how well the data fits the linear fit, and was determined using a Microsoft Excel statistical analysis package. The reason the P-value is important is because it establishes the smallest α value where the null hypothesis can be rejected. Once the P-value is obtained it can be determined if the data shows a relationship and at what confidence level.

3.8.2 Establishing Confidence Limits about the Regression Line

When it has been proven that there is a relationship with the data, the accuracy of the best fit line must be determined. This accuracy is determined by analyzing the degree of "scatter" about the regression line. Since linear regression is the only method used in this research; there are two variables

associated with the best fit line, the slope (β_1), and intercept (β_0) from Equation 6. There is a degree of error associated with each variable which is related to how well that regression line fits the data. Standard statistical methods use the errors from the slope and the intercept to determine a confidence interval about the regression line. The particular method used for this research can be found in Chapter 9 of *Applied Probability and Statistics for Engineers*, by Montgomery and Runger (1994).

3.9 Summary

All of this research was completed according to standardized procedures. The laboratory testing was done to replicate testing done by a state DOT or hired firm. All laboratory testing conditions were set to simulate field conditions. All materials used in this research were selected and blended at random to minimize bias as much as possible. The materials used in this research were blended to match the gradation used by the NHDOT as closely as possible.

The Summary Resilient Modulus was performed using a bulk stress recommended by *Laboratory Determination of Resilient Modulus for Flexible Pavement Design* (NCHRP, 2004). To produce results comparable to previous resilient modulus testing done at the University of New Hampshire, specimens were prepared with the same tools and techniques used by Corey Clark (2010). The material used for specimen preparation was modified slightly from the NHDOT gradation in order to adhere to particle diameter limits set by mold size. This modification would be done by any other agency testing the material, so the reproducibility of this research will not be affected.

CBR testing was performed according to AASHTO T-198. Both saturated and unsaturated samples were tested. Material modification also had to be performed; however this would be done by any agency, so reproducibility will not be affected. The ratio reported for each material was reported as permitted by AASHTO T-198, however it should be noted that not all ratios were taken at the same displacement due to limitations of the testing equipment.

Abrasion and durability testing were both performed according to their respective specifications. No material modification was required.

Most results from this research had a high standard deviation. This is very common with geotechnical materials. Generally conducting more tests will help achieve more reliable results, however this is costly and time consuming. The number of tests conducted on each sample was determined to balance practicality and reliability of data. Statistical analysis was performed on all test data in order to determine the accuracy based on the sample size and distribution of results.

The purpose of this research was to determine if unsorted BDA is a suitable material for use as a base and subbase in highway construction; and if deemed unsuitable, what specific components have the greatest effect on performance. This research only explores the structural properties of BDA; any recommendations made are based on that. Before BDA is considered for use in highway construction, environmental effects should also be considered.

CHAPTER 4

RESULTS AND DISCUSSION

4.1 Introduction

The following sections present the results of the research described in the previous chapters. Summaries for each individual test are presented first, followed by linear regression data. All results summaries show the average result of five tests for each blend in order to display the properties of each material. Individual results for each test are presented in the appendix.

4.2 Moisture-Density Properties

The moisture density properties were evaluated in conditions that closely represented the testing conditions. The material was compacted into CBR molds using a Bosch 11623 impact hammer with a 6 inch diameter compaction head and prepared in a similar fashion to how the CBR specimens were prepared. Once a sufficient number of data points were collected they were plotted in Microsoft Excel. If it was determined that more data points were necessary to obtain a more representative moisture density relationship, then more tests were

run at the necessary water contents. The moisture density curves are shown in

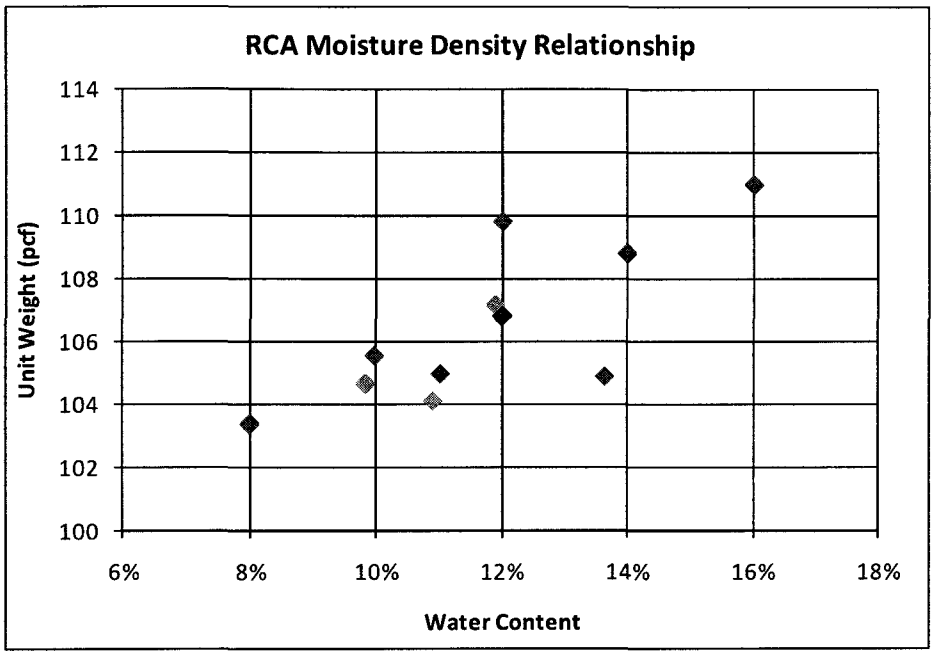

Figure 46 through Figure **48**.

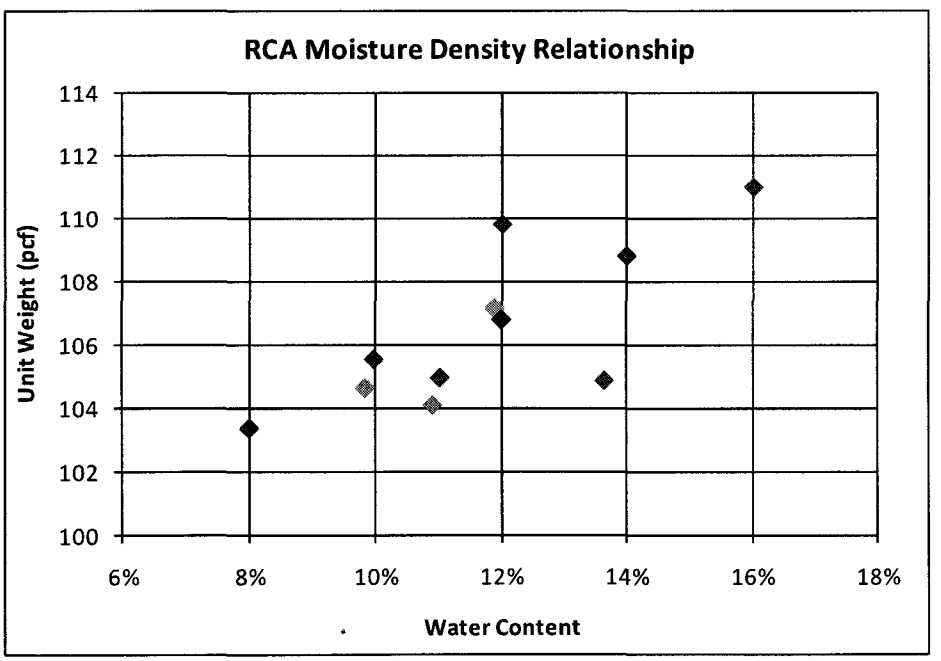

Figure 46: Concrete Moisture Density Curves

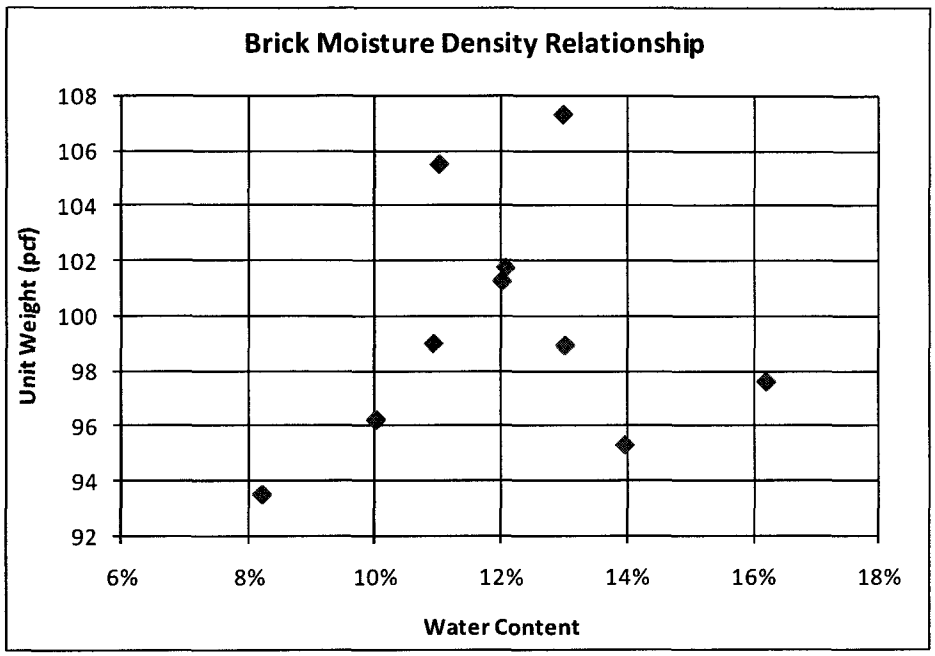

Figure 47: Brick Moisture Density Curves

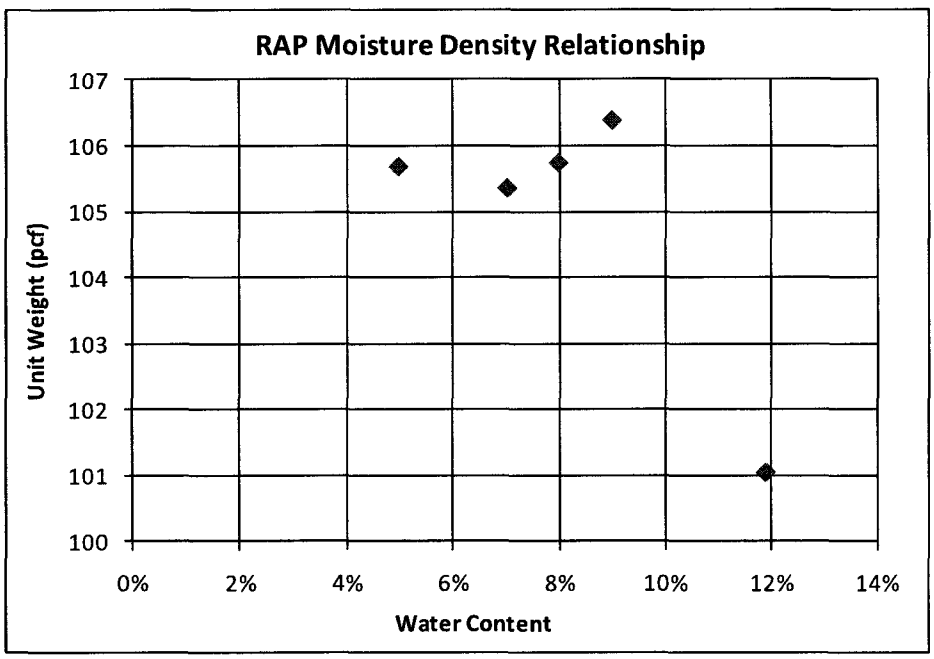

Figure 48: RAP Moisture Density Curve

As can be seen in the concrete and brick moisture density curves, the data varied widely. This is due to the significant amount of coarse material in the

gradation and the highly variable properties of both brick and concrete. This is particularly notable in the brick blend, whose wide range of moisture-density values can be attributed to the amount of core versus "fire skin" particles in each blend, whose absorption properties vary widely. The optimum moisture content was approximately 12% for both materials, so all blends of concrete and brick were prepared at 12% water content.

The RAP moisture density curve is shown in Figure 48. As expected, RAP has a slightly lower optimum moisture content, with maximum density reached at 8.8%. The lower optimum moisture content results from the asphalt binder reducing the absorption of the crushed stone aggregate particles, which generally have lower absorption than concrete or brick. All 100% asphalt blends were prepared at 8.8%. When the asphalt was blended with concrete the optimum water content was adjusted based on the amount of RAP and concrete in each blend.

Upon determination of the optimum water content for each material, standard compaction methods needed to be used to establish benchmark density values. Finding density values by using standard, easily reproducible methods ensures reproducibility of results. The method selected for this research was the Standard Proctor Test (AASHTO T-99). Five specimens each of concrete, brick, asphalt, and crushed stone were tested. The results for Standard Proctor Testing are shown in Table 7.

Table 7: Average Standard Proctor Densities for Components of BDA

Component	Maximum Dry Density (pcf)
Crushed Stone	125.7
Concrete	99.7
Brick	100.1
RAP	105.3

RAP had the highest density, followed by brick, concrete, and crushed stone. The standard proctor delivers a known amount of energy to the material to establish a benchmark density for the given material. If there is the need to evaluate other materials using the methods in this research, the densities from each respective method can be recorded as a multiplier of the values in Table 7. This way the optimum water content can be determined for a different material, which can then be compacted to a density similar to the samples in this research, allowing comparison between different materials.

4.2 Abrasion Resistance Results

The purpose of abrasion resistance testing was to determine how the material would handle stresses incurred during transportation, handling, and compaction of the material. It is critical that abrasion resistance meets minimum requirements so the material can maintain characteristics like roughness and angularity, which have a direct effect on performance. This test was only performed on crushed brick and concrete because this research is primarily concerned with the effects of brick content on BDA. Although the Micro-Deval test specifies that the material must be saturated before testing, unsaturated samples were also tested to determine the effects of saturation on performance.

Figure 49 shows the Micro-Deval wearing results for saturated and unsaturated samples of crushed brick and concrete. The allowable limits for base and subbase as defined by AASHTO T-327 are shown as solid and dashed lines. The results show that crushed concrete meets abrasion resistance criteria for use as base and subbase. On the other hand, unsaturated brick did not meet performance criteria for base and saturated brick did not meet the threshold for either base or subbase. Since AASHTO T-327 specifies that samples be tested in saturated conditions, brick is not a suitable material for use as highway base and subbase. However because this research is exploring the potential for use of mixed BDA, conclusions must be drawn about the maximum amount of brick that can be allowed in a given sample of BDA before it is considered unsuitable for use as a highway base and subbase.

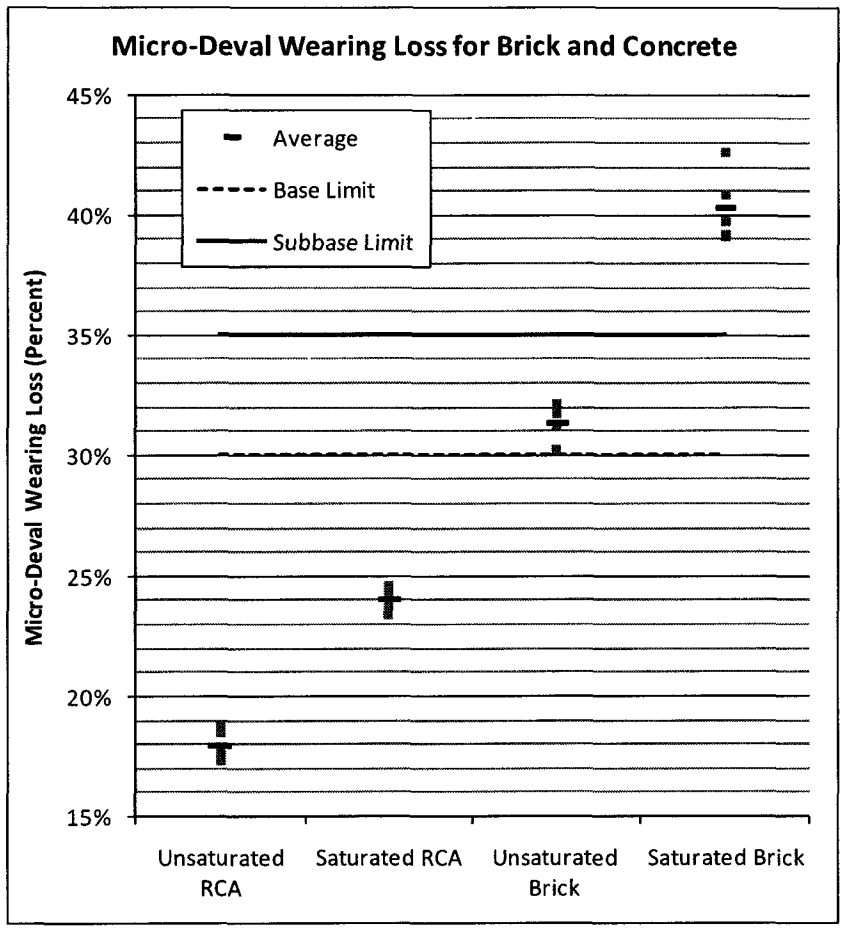

Figure 49: Micro-Deval Wearing Results for Brick and Concrete

4.2.1 Allowable Brick Content Based on Abrasion Resistance

Based on the saturated results, the average wearing loss for crushed concrete is 24.0%, and the average loss for brick is 40.3%. However, in order to obtain more accurate results more mid range data points were needed. Since it is unlikely that brick contents will ever exceed approximately 20% due to RCA being the primary component of BDA, a blend of 10% brick was tested to obtain raw data within a more practical range. The results are shown in Figure 50.

As expected, the allowable brick content has a relatively high variance, which is common when dealing with geotechnical materials. Figure 50 shows

that the maximum brick content should be 31% based on a 95% confidence interval. Previous research has shown that the Micro-Deval generally yields repeatable results (Cuelho, et al., 2008), suggesting that the five specimens tested per sample should provide reliable enough data to draw strong conclusions from. Figure 50 shows the saturated Micro-Deval Results plotted with 95% confidence intervals, which contain the majority of the raw data points.

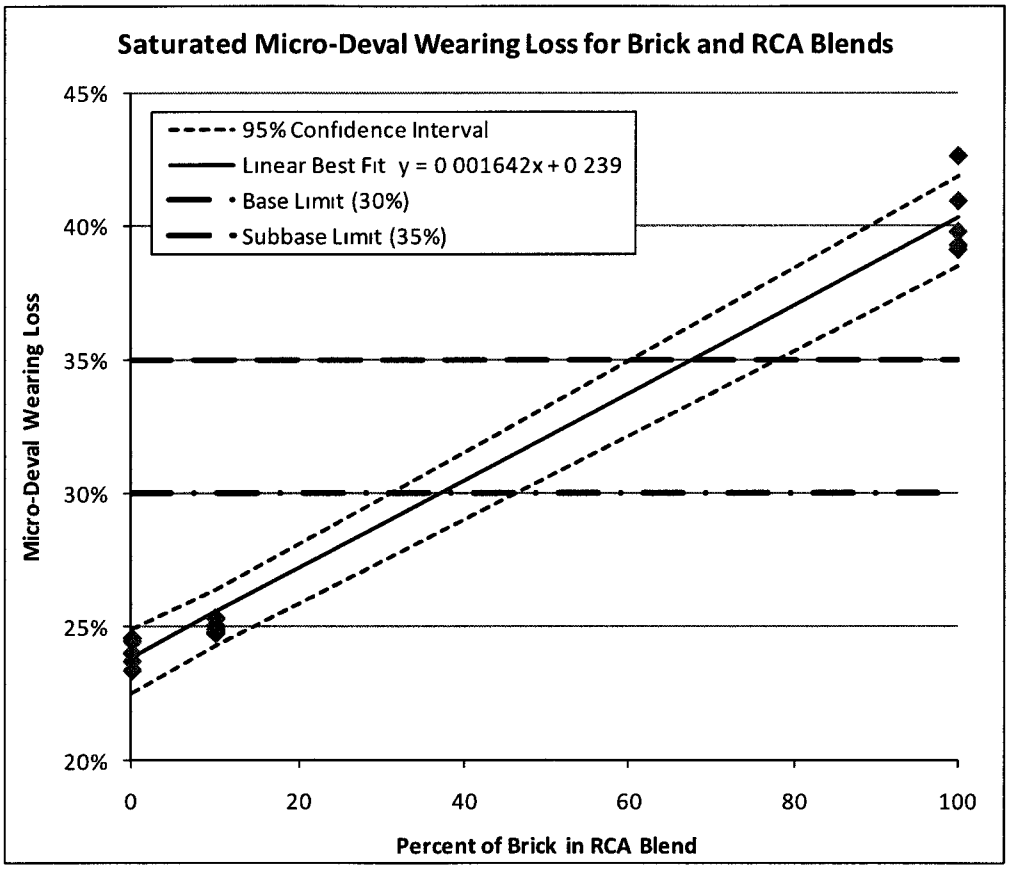

Figure 50: Saturated Micro-Deval Results with 95% Confidence Interval

However, one of the conclusions drawn by Cuelho (2008) recommended that "If the Micro-Deval test is selected as the primary test for evaluating aggregate durability, the authors recommend that an alternate test be implemented whenever Micro-Deval results fall between 18 and 27 percent loss."

This may be cause for some concern with the saturated and unsaturated RCA data, most of which falls within this range.

4.2.2 Effects of Saturation of Abrasion Resistance

As shown in Figure 49, saturation caused abrasion resistance to decrease in both crushed brick and concrete. As mentioned earlier the effects of saturation on the performance on brick were a major concern due to the methods of manufacture, particularly with older bricks. Figure 51 shows the increase in Micro-Deval wearing loss due to saturation. The data shows an average increase of 33.9% for RCA and 28.7% for brick. This shows that saturation has a greater effect on the abrasion resistance of RCA than brick. However it must be noted that the C_V for RCA is 18.4%, compared to 12.2% for brick. Both are high enough to prevent strong conclusions, but the C_V for RCA is almost 50% higher than brick, suggesting that if more tests were run the effects of saturation may be approximately the same for brick and RCA.

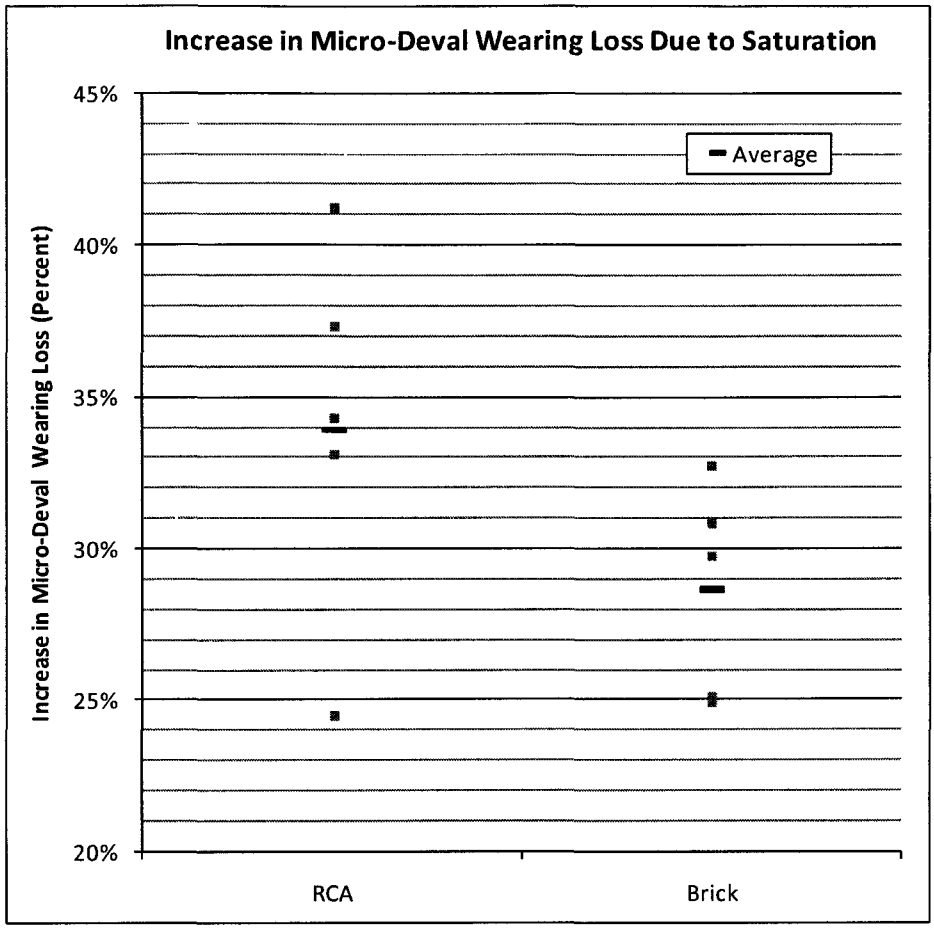

Figure 51: Increase in Micro-Deval Wearing Loss Due to Saturation

4.3 Durability Results

Freeze-thaw durability testing is a particularly important test because of the extreme freeze-thaw stress encountered in roadways throughout the Northeast. Freezing water generates significant stresses when confined, which can rapidly lead to deterioration of a material if it cannot withstand those stresses. For this research two samples of 100% brick and 100% concrete were fully immersed and subjected to 41 freeze-thaw cycles. Upon completion of the testing the samples were oven dried to constant mass and sieved over the 5/8" sieve to determine percent loss. The results for freeze-thaw testing are shown in Figure 52.

Interestingly the concrete showed a significantly higher susceptibility to freeze-thaw than the brick, with an average loss of 22%. The brick was much tougher than the concrete, with an average loss of just over 4%. This is due to the homogeneity of the brick compared to the concrete. The bricks contain a well mixed blend of sand and clay, which form a homogenous structure with a uniform coefficient of thermal expansion. The concrete, on the other hand, is composed of coarse aggregate and cement paste, which each have different coefficients of thermal expansion. The temperature swing caused by the repeated freeze-thaw cycles caused differential stresses between the aggregate and cement paste, which progressively degraded the individual particles.

Brick has shown considerably greater resistance to freeze-thaw conditions than concrete. However, the NHDOT does not currently specify a limit for freeze-

thaw resistance, so there was no statistical analysis performed on this data to establish a maximum allowable percentage of brick or concrete.

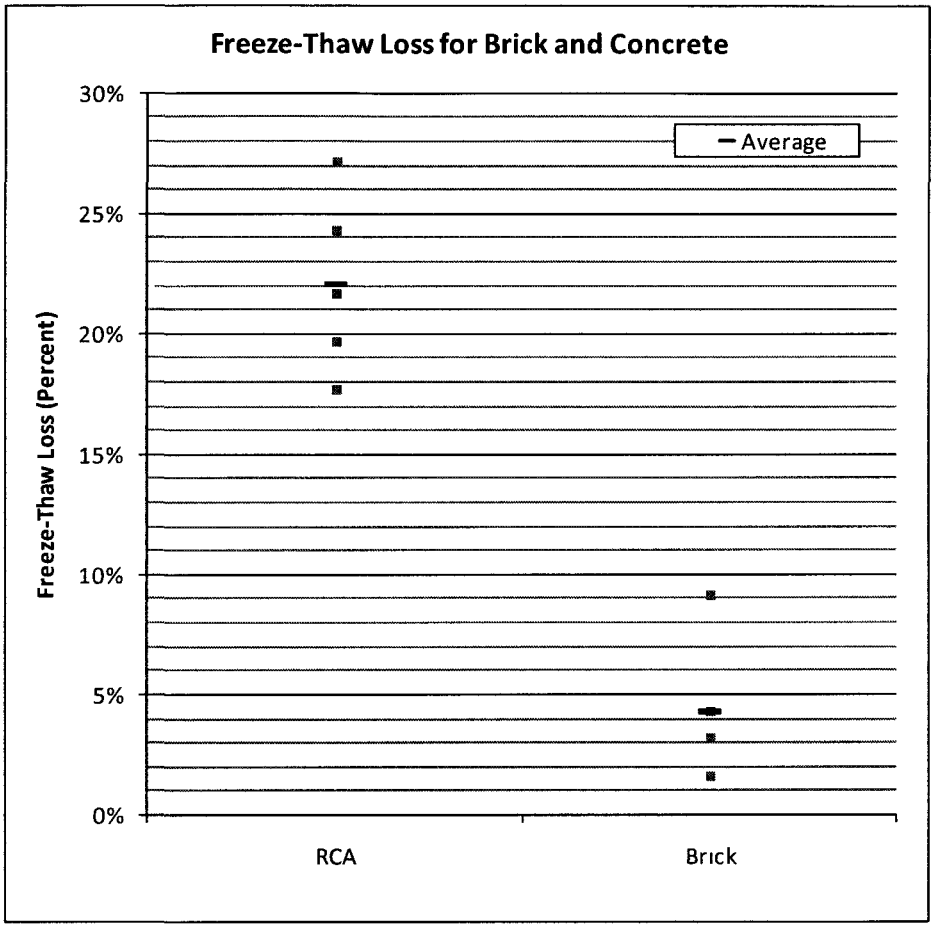

Figure 52: Freeze-thaw Loss for Brick and Concrete

4.4 California Bearing Ratio Results

All CBR testing was performed according to AASHTO T-198 using the loadframe described in Chapter 3. The loadframe was connected to a data acquisition system and controlled using the GCTS CATS software. This software allowed the display of real time load and deformation data. The constantly updating data output allowed the operator to monitor the progression of the test to ensure everything was running according to plan.

Due to the large amount of samples that needed to be evaluated, 5 specimens of each sample were tested with the exception of 100% RCA blends, of which 10 specimens were tested. The RCA was the base material for all the blends tested, so a reliable benchmark needed to be established to ensure representative results. Each sample was tested in saturated and unsaturated conditions to examine the effects of water on material performance.

4.4.1 Recycled Concrete Aggregate

The first material tested was recycled concrete aggregate. The specimens were blended and compacted at optimum moisture content as described in Chapter 3. The results for unsaturated and saturated RCA are shown in Figure 53 and Figure 54. Both unsaturated and saturated samples showed an increase in CBR with an increase in dry density at a 95% confidence level. The average dry density for unsaturated and saturated specimens was 107.7 pcf. The unsaturated RCA had an average CBR of 159% with a C_V of 30.3%. Saturated RCA had a slightly higher average CBR of 167% with a slightly lower C_V of 23.9%.

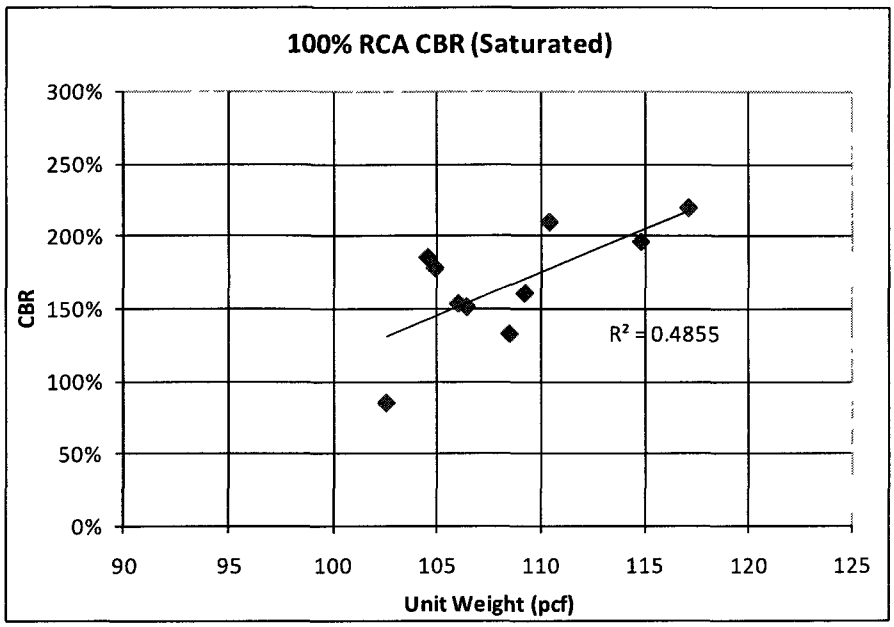

Figure 53: CBR Results for Unsaturated RCA

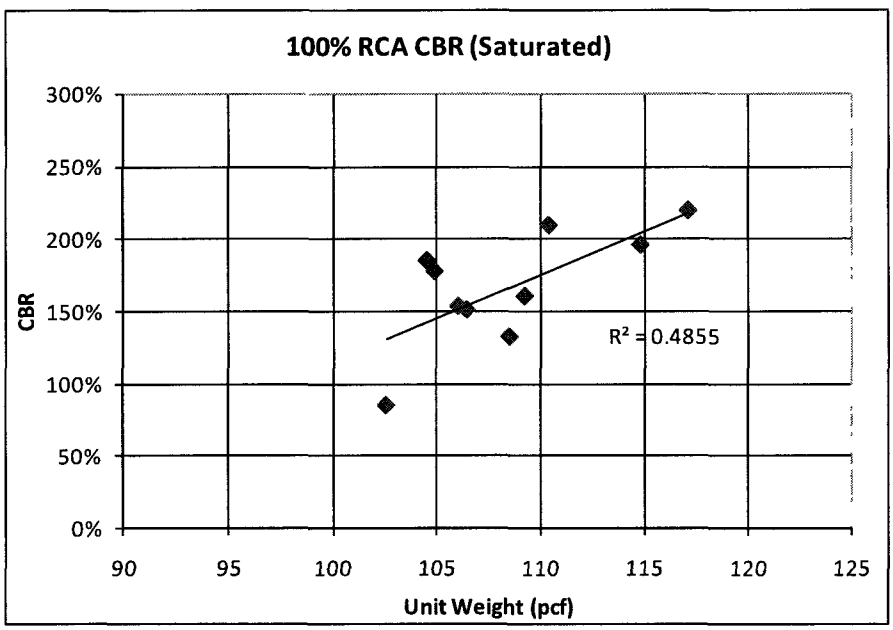

Figure 54: CBR Results for Saturated RCA

4.4.2 Brick

The brick was blended to the same gradation as the RCA to ensure comparable results. Water was added to optimum moisture content and the specimen was compacted in the same way described in Chapter 3. It is unlikely that pure brick will ever be used as a highway base and subbase, so the focus of this research is primarily on the effects of brick content on blends of RCA. Because of this only 5 specimens each of saturated and unsaturated brick were tested. The results for unsaturated and unsaturated brick are shown in Figure 55 and Figure **56**.

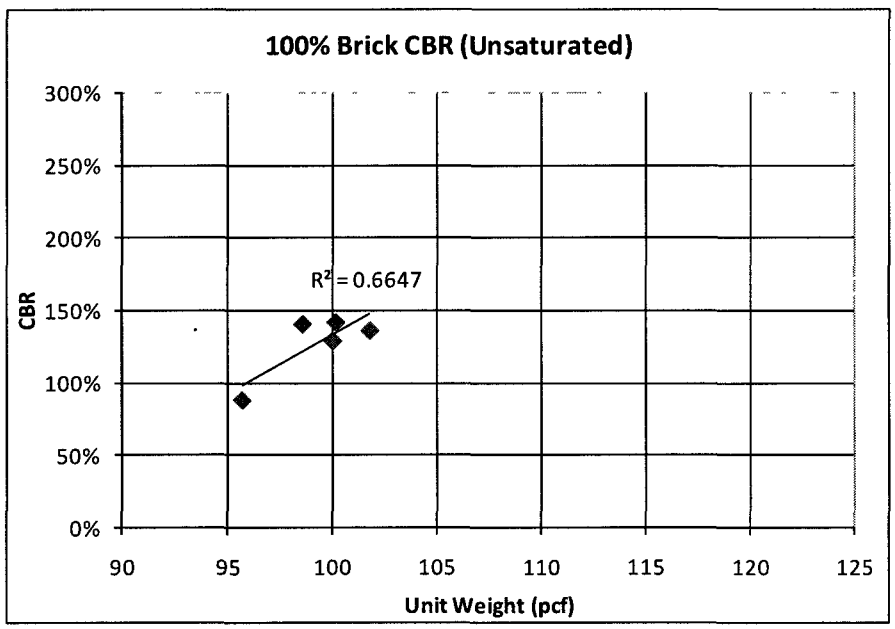

Figure 55: CBR Results for Unsaturated Brick

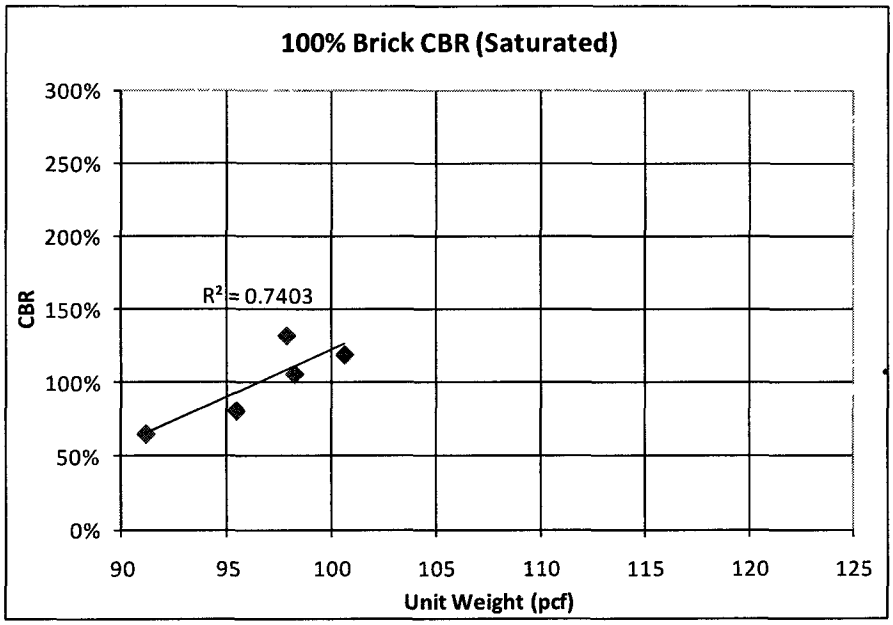

Figure 56: CBR Results for Saturated Brick

The brick samples showed an increase in CBR with an increase in dry density with a 90% confidence level. The average dry density for both saturated and unsaturated brick was 97.9 pcf, approximately 9.1% lower than RCA. Unsaturated brick had an average CBR 127% with a C_V of 17.6%. Saturated brick had an average CBR of 101% with a C_V of 26.8%.

4.4.3 Effects of Saturation on CBR for Brick and Concrete

Saturation tends to decrease the bearing capacity of most geotechnical materials; however this research yielded some interesting results. Since RCA is composed of crushed concrete, it contains trace portions of residual Portland cement which have not formed into a paste. When allowed to soak for an extended period of time, this Portland cement reacts with the water to create a binding effect, increasing strength. This was shown in the CBR results. The effects of saturation on CBR are shown in Figure 57.

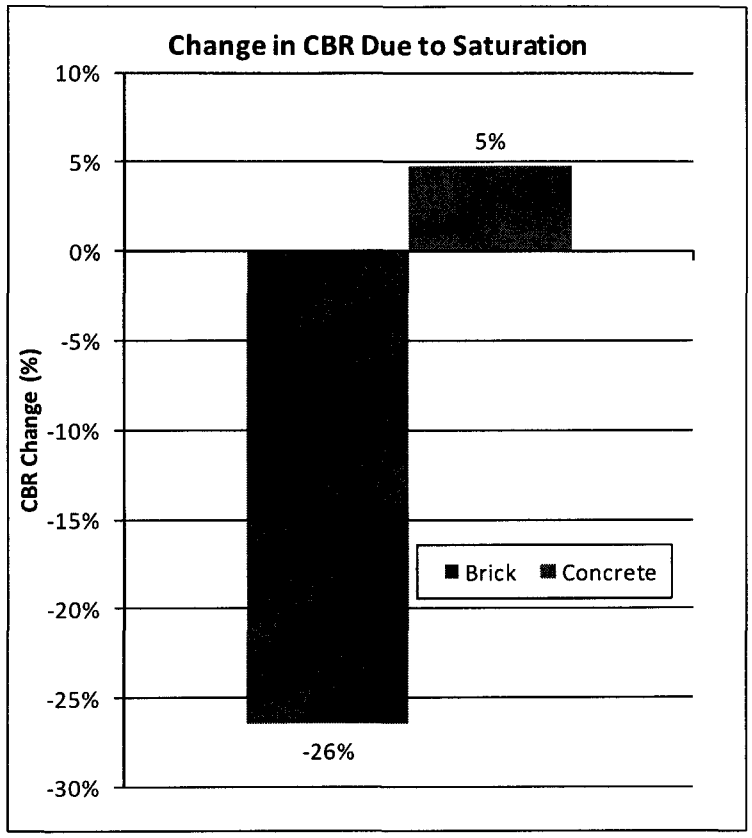

Figure 57: Effects of Saturation on CBR for Brick and Concrete

Crushed concrete showed a gain in bearing capacity of nearly 5%. On the other hand brick did not perform as well, showing a significant decrease in bearing capacity. This is likely due to water softening the inner core portions of the brick that were exposed during crushing. Once saturated the core portions show behavior similar to clay and sand, the primary components used to manufacture bricks. This significant decrease in material performance was also observed in the Micro-Deval testing, where the saturated bricks' abrasion resistance was markedly less than the unsaturated brick.

4.4.4 Effects of Brick Content on Density

Both saturated and unsaturated specimens were prepared in the same fashion. The saturated specimens were weighed prior to soaking so they could be compared with unsaturated specimens. As mentioned in 4.4.2, the average brick density was 9.1% lower than the RCA density. Densities were also obtained for each blend of brick and concrete, these are shown in Figure 58.

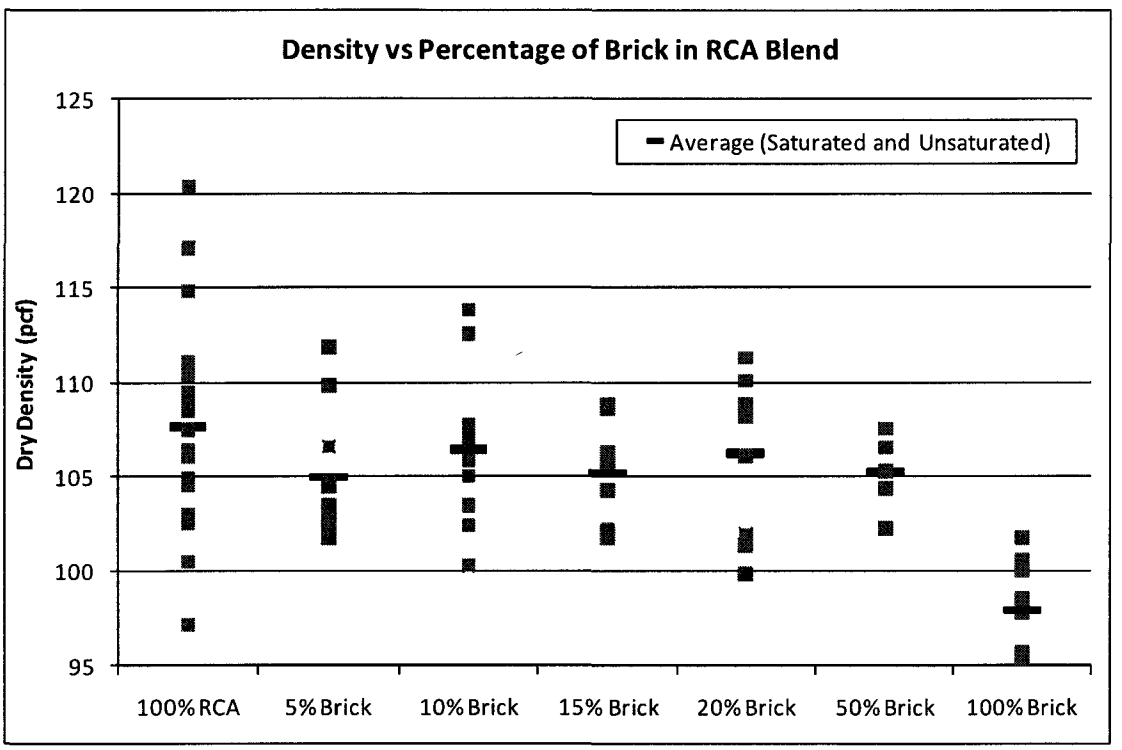

Figure 58: Brick Blend Densities

Although the density has a relatively high variability with a C_V of 0.314, a general downward trend in density is shown with increasing brick content. However, in order to establish a reliable relationship between density and brick content many more specimens would need to be prepared.

4.4.5 Effects of Brick Content on CBR

The CBR is currently the most common method of evaluating highway base and subbase used by state agencies. As described in Chapter 3, the CBR is determined by comparing the stress of the material being tested to a reference material at the same deformation. The reference material is crushed California limestone, and is considered an excellent material for use as a base and subbase, so a CBR of 100% means the material being tested should be an excellent base and subbase. Because of this most design methodologies limit the CBR used for calculation to 100%, so even if the material has a CBR value greater than 100%, the CBR used for design will always be 100%. Since this is common practice, all CBR values from this research that exceeded 100% were considered acceptable.

As shown earlier in this chapter, unsaturated brick on average had a CBR value 20.1% less than unsaturated RCA. Saturated samples showed a greater difference, with bricks CBR 39.5% lower than RCA's CBR. CBR values for unsaturated and saturated brick blends are shown in Figure 59and Figure 60.

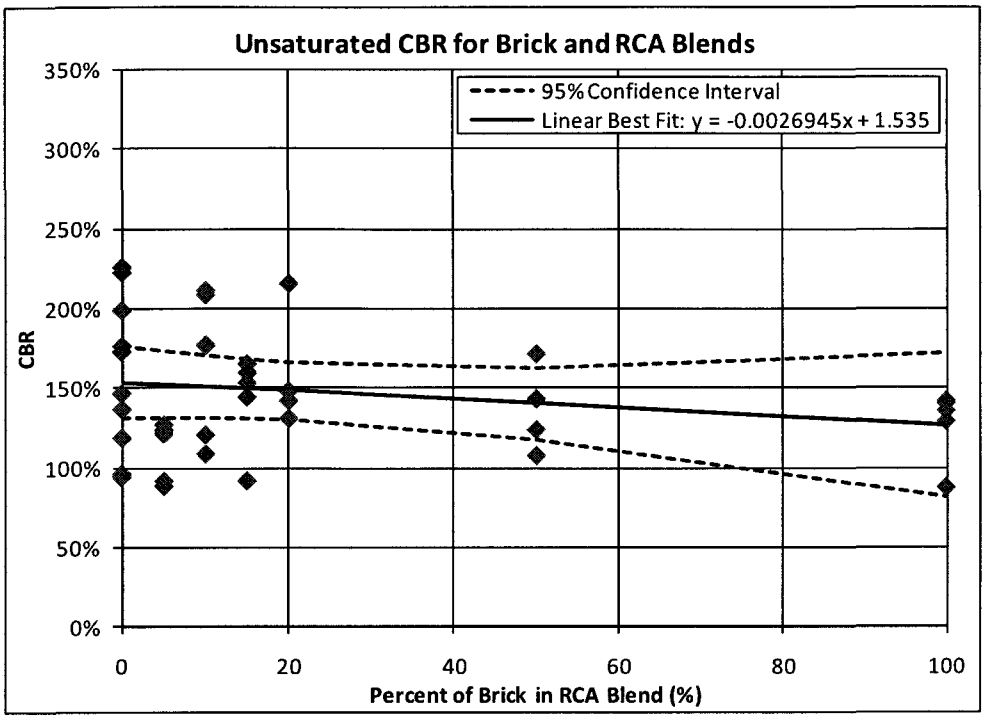

Figure 59: Unsaturated Brick Blend CBR Values

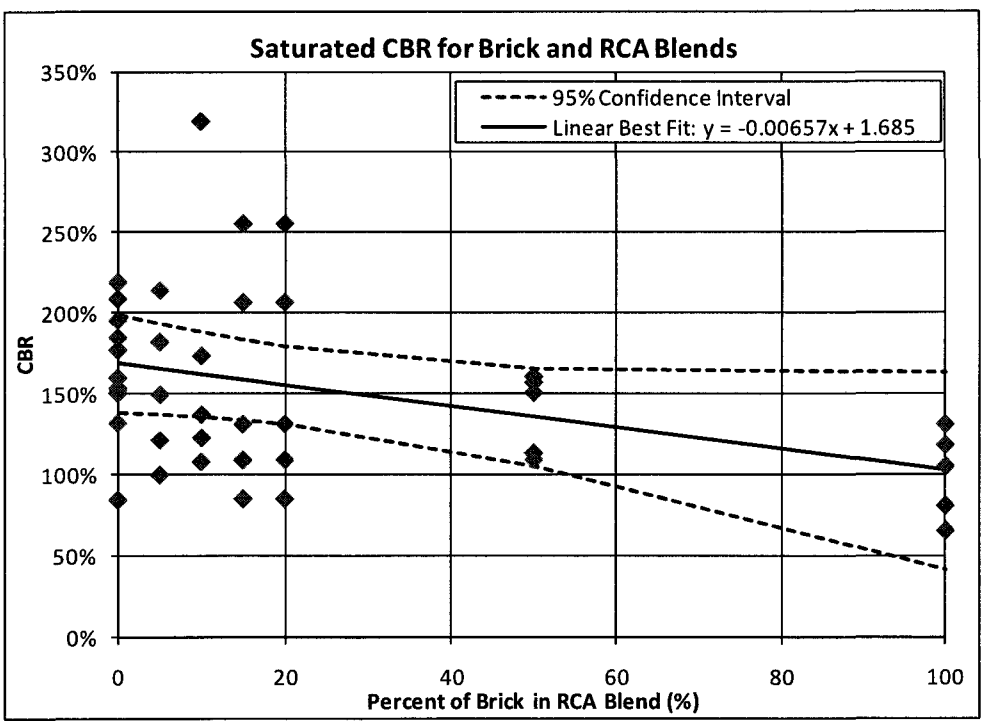

Figure 60: Saturated Brick Blend CBR Values

Upon analysis of the CBR data, it was observed that a disproportionate amount of data points were outside the 95% confidence interval. As can be shown in Figure 59 and Figure 60, this is more pronounced around the lower brick contents. Since brick contents will likely not exceed 20% in practice, a better statistical representation was needed. To do this, the CBR data for brick contents up to 20% was compared against the linear fits from Figure 59 and Figure 60. The results of this refined analysis are shown in Figure 61 and Figure 62.

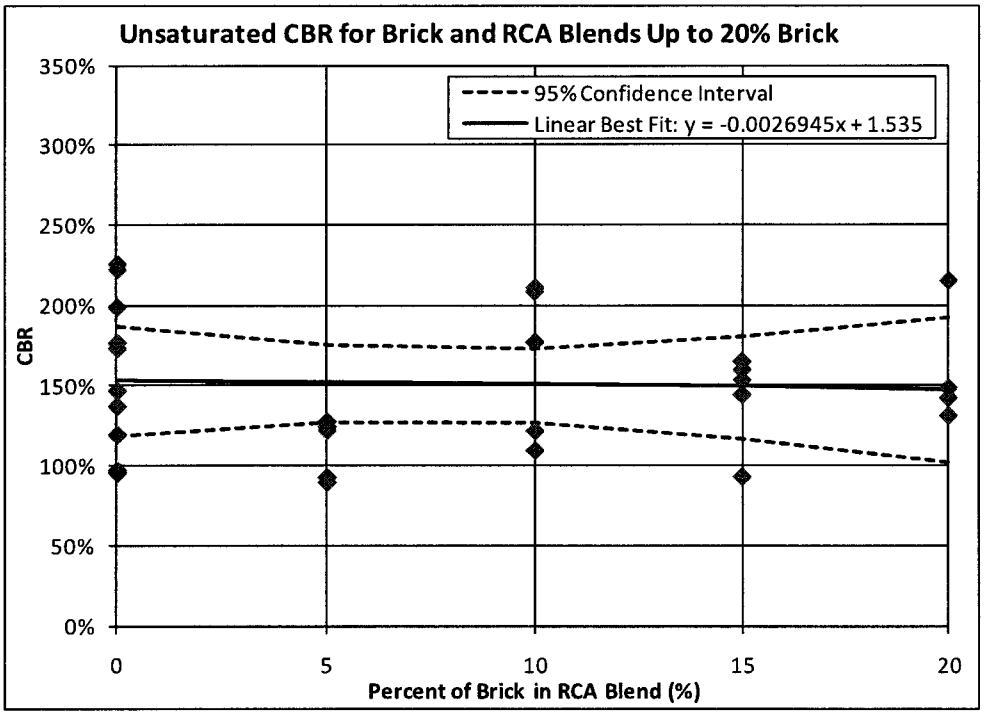

Figure 61: Unsaturated CBR Data with Refined Confidence Intervals

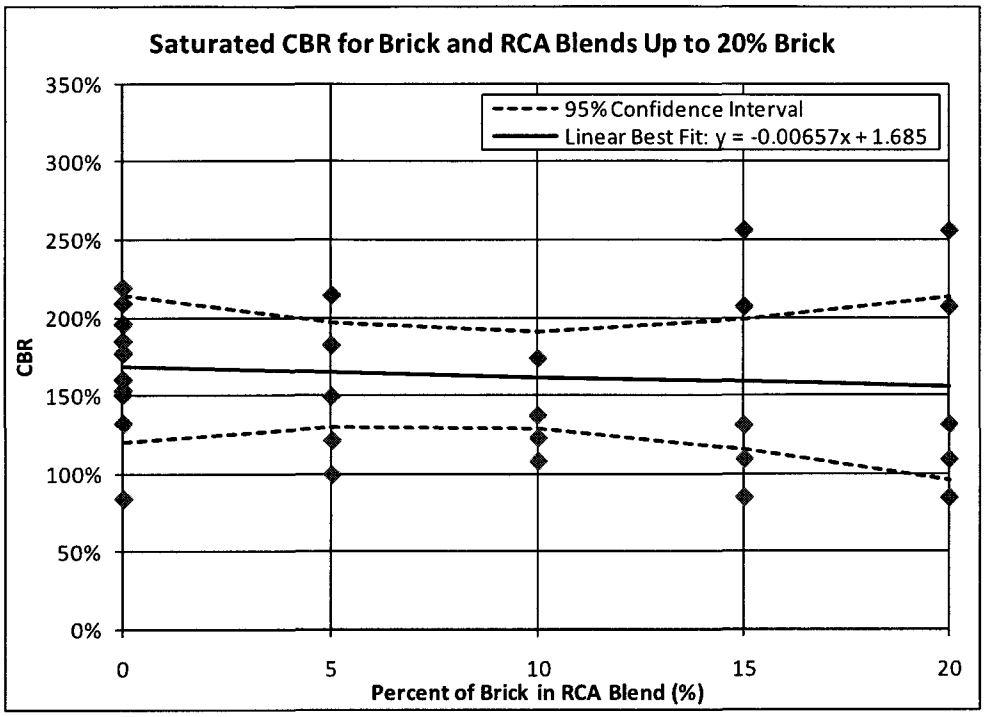

Figure 62: Saturated CBR Data with Refined Confidence Intervals

The refined linear regression analysis brought more data points within the 95% confidence interval, allowing for more representative predictions of the effects of brick content on CBR performance within a practical range of brick contents.

4.4.6 Allowable Brick Content for CBR

In order to establish allowable brick contents for BDA blends based on CBR values, a relationship between brick content and CBR had to be established. This was done using the statistical methods described in Chapter 3. Linear regression using a 95% confidence interval was used for this research. The linear fit with 95% confidence intervals is shown for unsaturated and saturated CBR results in Figure 59 and Figure 60. As mentioned previously, most design methodologies limit the CBR to 100%, so it was determined that the

best way to evaluate the effect of brick content on CBR was to use a reference value of 100% to represent high quality material. By using this approach, the point where the brick content brings the CBR below 100% becomes the allowable brick content.

The allowable brick content was initially determined by using the lower 95% confidence interval about the linear fit shown in Figure 59 and Figure 60. Using the lower 95% confidence interval provides a more conservative value than the linear fit. This method determined the maximum allowable brick content for blends with RCA shown in Table 8.

Table 8: Max. Allowable Brick Content for BDA Blends Based on Original 95% CI

	Maximum Allowable Brick Content
Unsaturated BDA	74%
Saturated BDA	54%

Once the confidence interval was reconfigured around CBR values for brick contents lower than 20%, the maximum allowable brick content needed to be adjusted. The maximum allowable brick content for the refined confidence interval is shown in Table 9.

Table 9: Max. Allowable Brick Content for BDA Blends Based on Refined 95% CI

	Maximum Allowable Brick Content
Unsaturated BDA	21%
Saturated BDA	18%

As seen in Table 8 and Table 9, refining the confidence interval to better fit brick contents that are more likely to be observed in the field significantly reduces the allowable brick content. Because the second regression analysis better represents the data in the lower brick content range, it provides a better estimate of the effects of brick content on CBR performance for the majority of tests performed in this research. Because of this the results shown in Table 9 should be considered the most conservative estimate CBR performance with relation to brick content.

4.5 Summary Resilient Modulus Results

Once the CBR testing was completed, Summary Resilient Modulus testing was conducted. All tests were performed using the GCTS triaxial testing setup described in Chapter 3. Five tests were run on each blend of material. Although more tests generally provide better data, this number was chosen to balance data quality with the amount of time spent on testing. In order to obtain the best possible data, all tests results were carefully analyzed, and any test that showed signs of a system malfunction was rerun so a minimum of five acceptable datasets were obtained for each blend.

4.5.1 Performance of Crushed Stone

In order to establish control data for this research, the same crushed stone used in Mr. Corey Clark's research was tested using the same procedure as the BDA from this research. This crushed stone was obtained from the testing pit in room S123 of Kingsbury hall, shown in Figure 63.

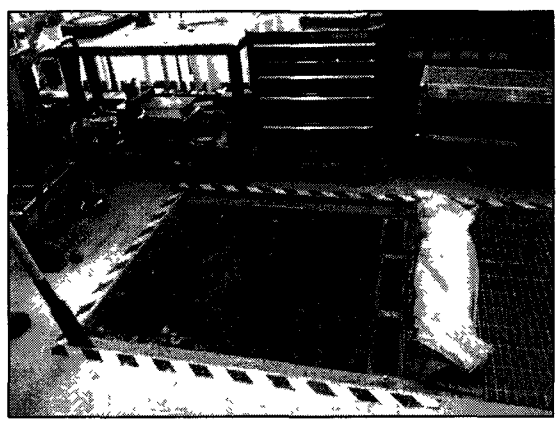

Figure 63: Test Pit in Kingsbury S123

Due to the size of the pit, slightly larger particles were present in the gradation. To address this all material greater than 3/4" was scalped. Since the material in

this research was blended to match the gradation used in Clark (2010), no alterations needed to be made. Once the material was scalped and dried, it was blended at optimum water content and tested using the same procedure as the rest of the resilient modulus testing in this research. The results of this testing are shown in Figure 64.

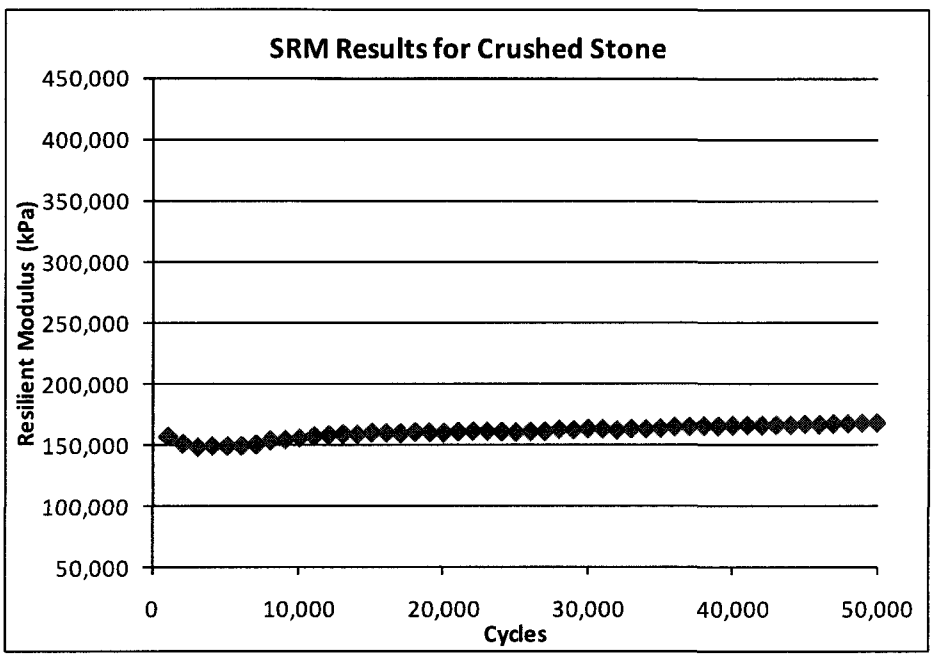

Figure 64: Resilient Modulus Results for Crushed Stone (θ = 208 kPa)

4.5.2 Effects of Brick Content on BDA Performance

The SRM blends tested in this research vary slightly from the CBR blends tested. This is because of a high degree of variability observed at smaller increments during CBR testing. In attempts to reduce this variability and better establish the effects of brick in BDA, all SRM blends were tested at 10%, 20%, 30%, 50%, 70%, and 100% brick, as opposed to 5% increments up to 20%, and 50% brick with the CBR. Since M_R is a more important factor in material performance, testing a wide range of blends better established the effects of

brick content on M_R for design purposes. Results for all brick blends are shown in Figure 65.

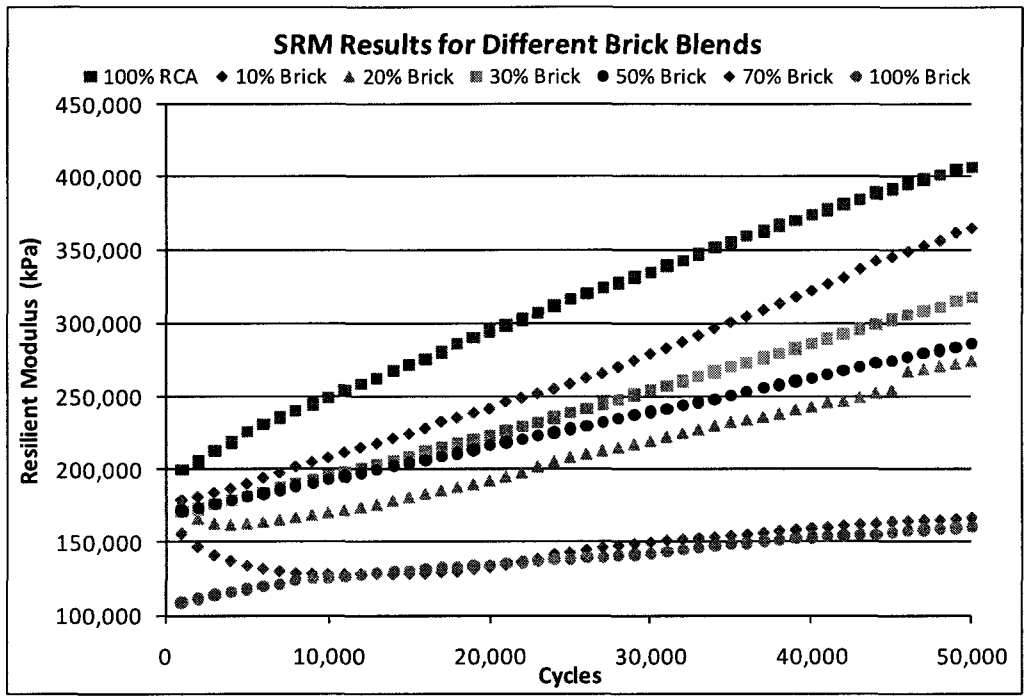

Figure 65: Results of SRM Testing for Different Brick Blends (θ = 208 kPa)

All blends showed some degree of M_R gain over the course of the test. This is likely due to an increase in density as loading progressed. A general decrease in M_R with increasing brick content was observed. The initial M_R increase is less pronounced with increased brick content as well, this is particularly evident in the 70% brick blend, where M_R continues to drop until approximately 9,000 loading cycles, where it behaves just like 100% brick. This is likely the point where there is enough brick to prevent the concrete from establishing effective bonds, so the brick properties control once the bonds have been broken.

4.5.3 Saturated and Unsaturated Results for Brick and RCA Blends

In order to establish the effects of saturation on the performance of BDA, both saturated and unsaturated SRM tests were performed on blends of 100% RCA, 100% brick, and a 50% blend of both materials. The results from this testing are shown in

Figure **66** and Figure **67**.

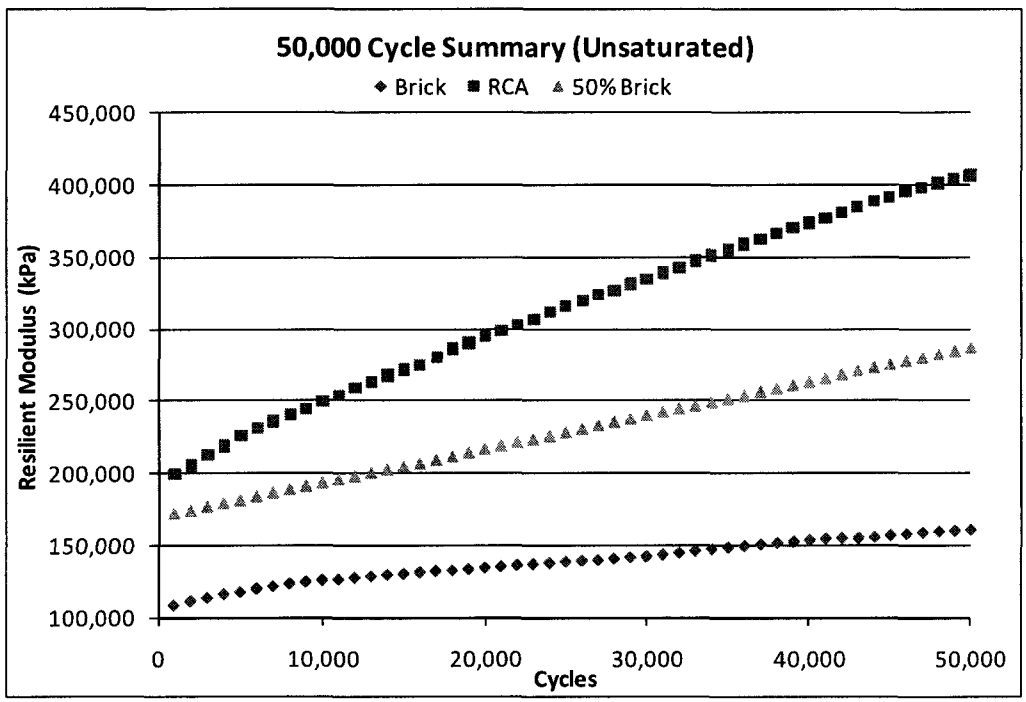

Figure 66: Average Unsaturated SRM Results for Brick and RCA (θ = 208 kPa)

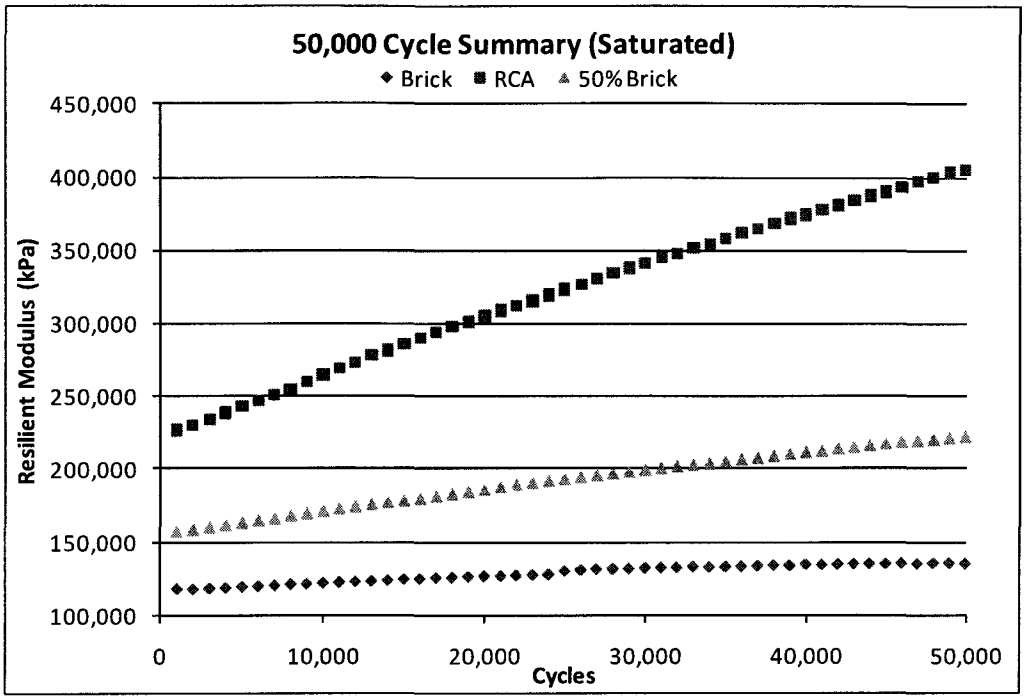

Figure 67: Average Saturated SRM Results for Brick and RCA (θ = 208 kPa)

Since saturation tends to accelerate material degradation under loading, the effects of saturation are more apparent after many loading cycles. Because of this, the SRM_I was not used to evaluate the effects of saturation on BDA blends. Instead the average M_R reading at 50,000 cycles was used. As can be seen in Figure 66 and Figure **67**, saturation led to a decrease in final M_R for all materials. The average final M_R for each saturated and unsaturated blend is shown in Table 10.

Table 10: Comparison of Final M_R Values for Brick and RCA Samples

Blend	Final M_R Average(kPa)		% Change
	Unsaturated	Saturated	
100% RCA	406,686	404,926	N/A
50% RCA / 50% Brick	286,025	221,681	-22.5%
100% Brick	160,382	135,329	-15.6%

Saturation had little effect on the RCA, showing a decrease in final M_R of less than one percent. Saturation had a more significant effect on the brick blends, both showing a decrease in M_R of greater than 15%. This decrease, as with the CBR results, is likely due to degradation of the brick particles into sand and clay. One interesting observation is a greater decrease in M_R for the 50% concrete blend, which is likely due to the relatively small sample size and the inherent variability of geotechnical testing data.

4.5.4 Effects of RAP Content on BDA Performance

RAP blends tested in this research were blended in the same fashion as the brick blends discussed earlier to ensure comparability of data. Less RAP testing was done in this research due to greater availability of data compared to brick (Lee, et al., 2001). However, most available data analyzes the effects of higher RAP contents. Because of this, the effects of lower RAP contents were analyzed in this research. For this testing, five specimens each of 10% RAP and 20% RAP were blended at optimum water content, prepared and tested using the same procedures as the brick blends. The results of this testing are shown in Figure 68.

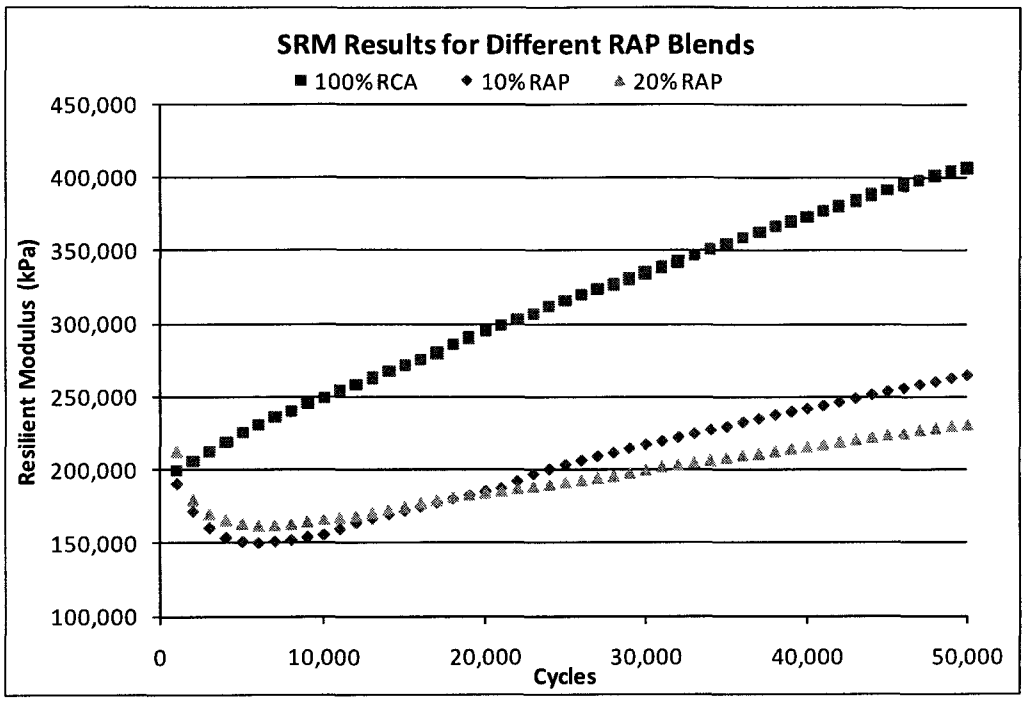

Figure 68: SRM Results for Different RAP Blends (θ = 208 kPa)

RAP had a noticeably different and much more pronounced effect on the blend than brick. Figure 68 shows both RAP blends lost nearly 25% of their initial M_R in the first 5,000 loading cycles before starting a trend of increasing M_R similar to what has been observed in other results from this research. This initial reduction in M_R may be attributed to the deformability of the asphalt binder, which may have caused slippage between particles.

4.5.5 Time Dependent Stiffness

As discussed earlier, equipment errors lead to uncharacteristic results during some of the tests. For the purpose of this research, the results had to be discarded. However, the observed material behavior may lead to a better understanding of the in-situ behavior of recycled concrete aggregate. Of the two tests in question, one was run overnight and the other over a weekend.

Approximately halfway through the test, the Rv value exceeded 1.3, causing the test to pause. Since the tests were being run while no one was in the lab, the specimen remained under the confining and overburden pressures without being loaded until the test was resumed. Once the test was resumed, unusually high MR values were observed. The results of each test are shown in

Figure **69** and

Figure 70.

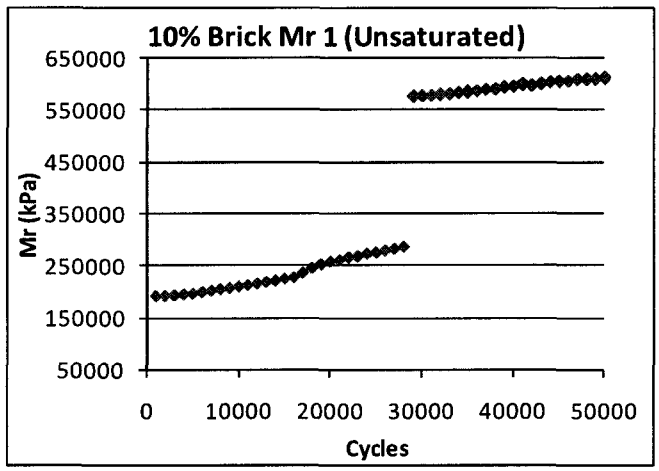

Figure 69: M_R Increase after Pause over Weekend

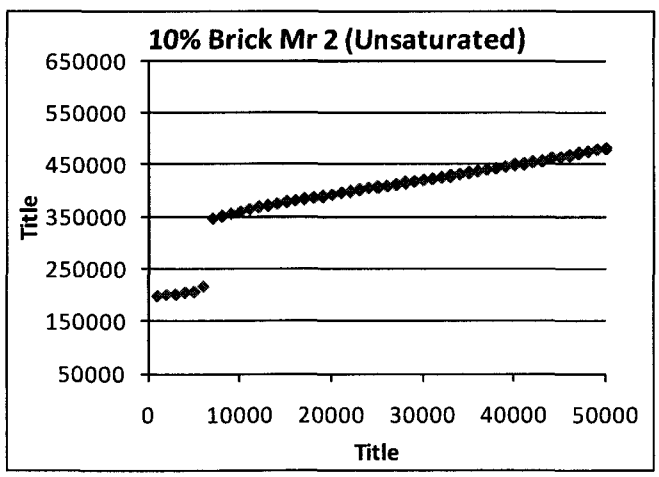

Figure 70: M_R Increase After Pause Overnight

Both pauses resulted in increased M_R, which became more significant over time. This suggests that BDA, in particular BDA with a large portion of RCA, will stiffen over time, even if it is not being subjected to traffic loads. More controlled research done using a Light-Weight Deflectometer (LWD) on a test pit has shown that the stiffness of BDA will nearly double over a two-week period (Martin, et al., 2011). The results of this research are shown in Figure 71.

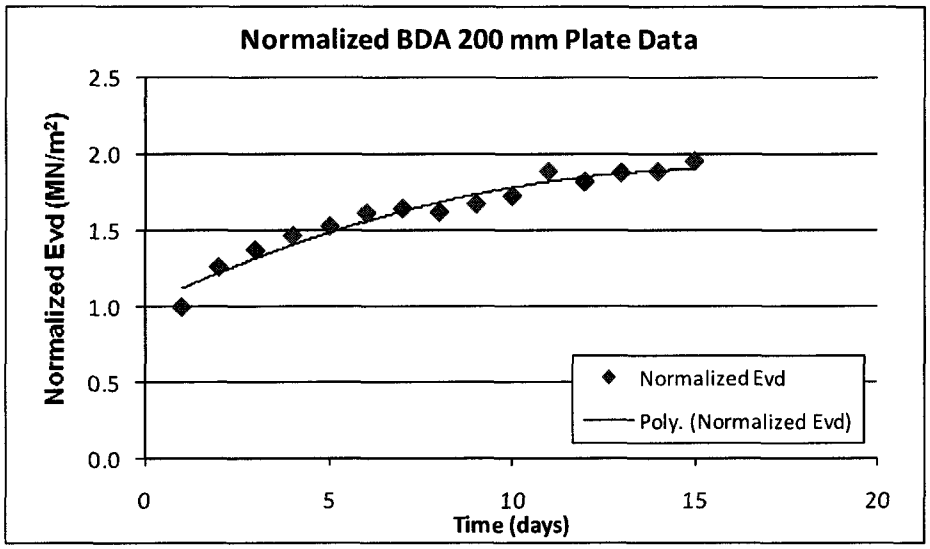

Figure 71: Normalized LWD Stiffness Over Time (Martin, et al., 2011)

The results show a progressive increase in stiffness which levels off after approximately two weeks. This testing was performed in a laboratory test pit using a LWD, which is comparable with RLT results depending on the density of the material (Clark, 2010).

4.5.6 The Initial Summary Resilient Modulus

Reporting a conservative resilient modulus value for use in the MEPDG proved to be a challenge in this research. Materials respond differently when subjected to different loading conditions, as determined in previous research

using AASHTO T-307 (Clark 2010, DeRocchi 2008). Since AASHTO T-307 uses 15 different loading conditions over a short term, the resilient modulus is typically reported as an average of all 15 values. The Summary Resilient Modulus uses one loading condition over a long term, so a different approach for determining the resilient modulus was necessary. When analyzing the data from the long term testing, a general increase in resilient modulus was observed with all materials except for crushed stone. An example of the increase in resilient modulus for a specimen of RCA is shown in Figure 72.

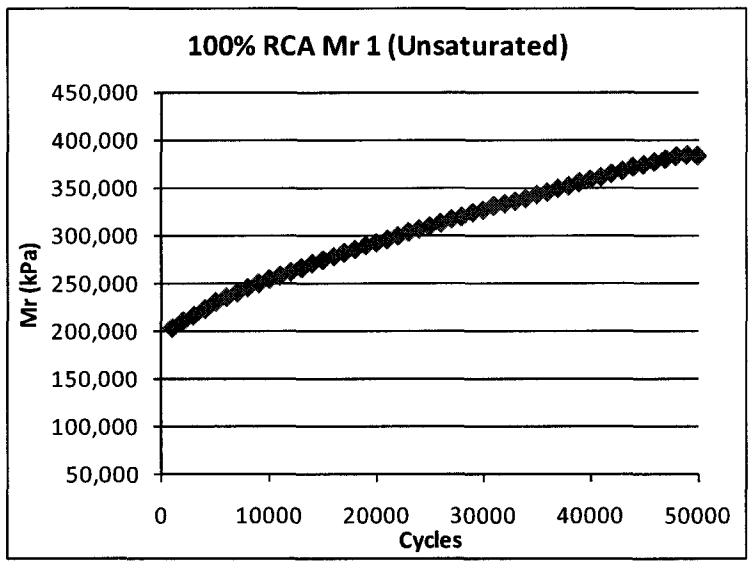

Figure 72: Sample of Increase in M_R (θ = 208 kPa)

This led to a problem in determining which value would representatively model the effects of M_R on pavement performance. Since M_R increases as the loading progresses, taking an average would likely lead to inadequate prediction of performance early in the pavement life, which could possibly result in rutting failure. In order to address this, it was decided that an "in place" M_R value must be determined to best model the material as it is just before traffic loading begins.

Since the M_R increase generally progresses in a linear fashion, it was decided that a linear fit be used with the data, shown in Figure 73.

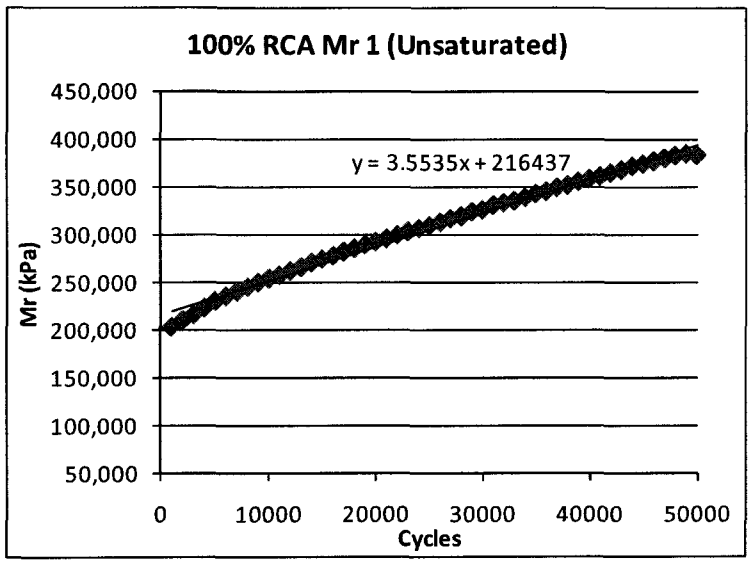

Figure 73: SRM Data with Linear Fit

This data fit could then be associated with a linear equation, shown in Figure 73. Using this equation the M_R could be calculated back to theoretical "zero load" point which would represent the material as it is placed and compacted. Note that the intercept of the linear fit is higher than the initial M_R at 1,000 load cycles; this was typical of the majority of the linear fits. Due to the lack of a seating sequence for this test a slightly higher initial stiffness value was desirable because it would provide a more representative stiffness corresponding to 2,000-3,000 loading cycles, which would act as the seating sequence.

It was decided that this value would be called the initial summary resilient modulus, or the SRM_I. SRM_I values for different brick and RAP contents are shown in Figure 74 Figure 75. These values were used for modeling with the

MEPDG to compare BDA blends with different brick and RAP contents with respect to rutting performance.

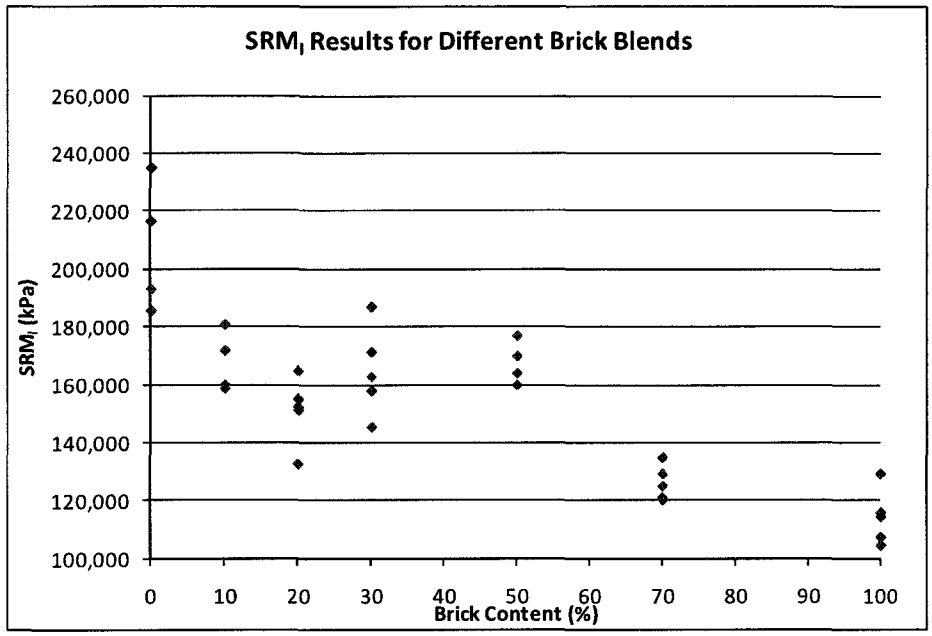

Figure 74: SRM$_I$ vs Brick Content

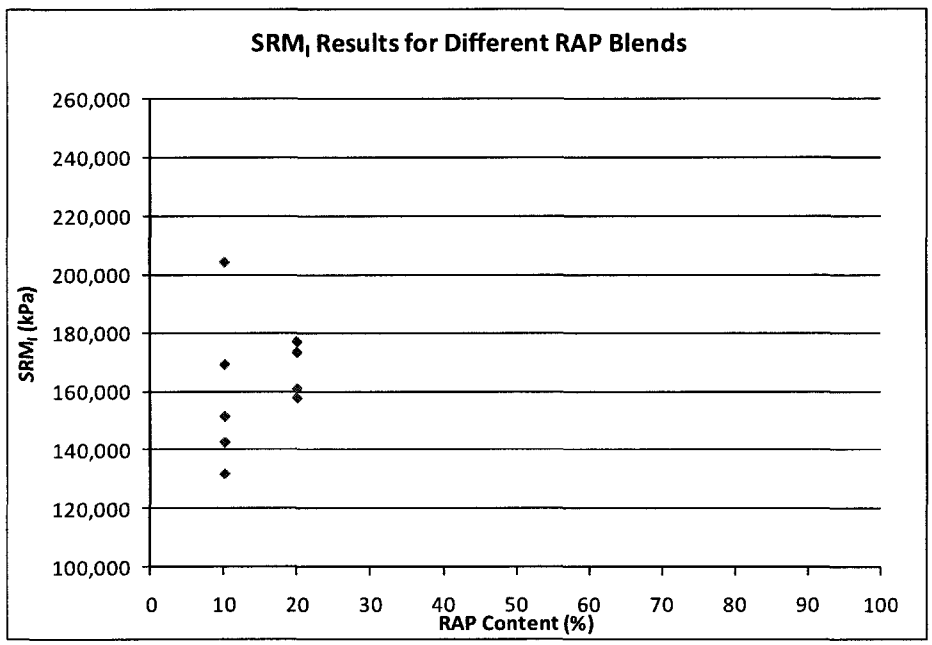

Figure 75: SRM$_I$ vs RAP Content

4.6 MEPDG Results

Flexible pavement design, as mentioned earlier, models the pavement system as several layers with varying thicknesses and corresponding stiffnesses the end goal of bringing the stresses produced by traffic loads to an acceptable level for the natural soil on site. When designing using resilient modulus values, there is no defined minimum M_R, just a range of typical values based on soil type. Because of this the effect of BDA brick content cannot be evaluated based on M_R alone. In order to compare different blends of BDA based on accepted performance standards the M_R results were used to model rutting performance in the MEPDG.

4.6.1 Effects of Brick Content of Unsaturated BDA Samples

As observed earlier in this chapter, M_R generally decreases with increasing brick content. In order to determine whether the M_R decrease was significant enough to affect rutting performance, all the SRMI values were modeled in the MEPDG. All results are shown in Figure 76. Note that the zero percent brick corresponds to 100% RCA. Full scale rut depth is shown on the right side of Figure 74 for reference.

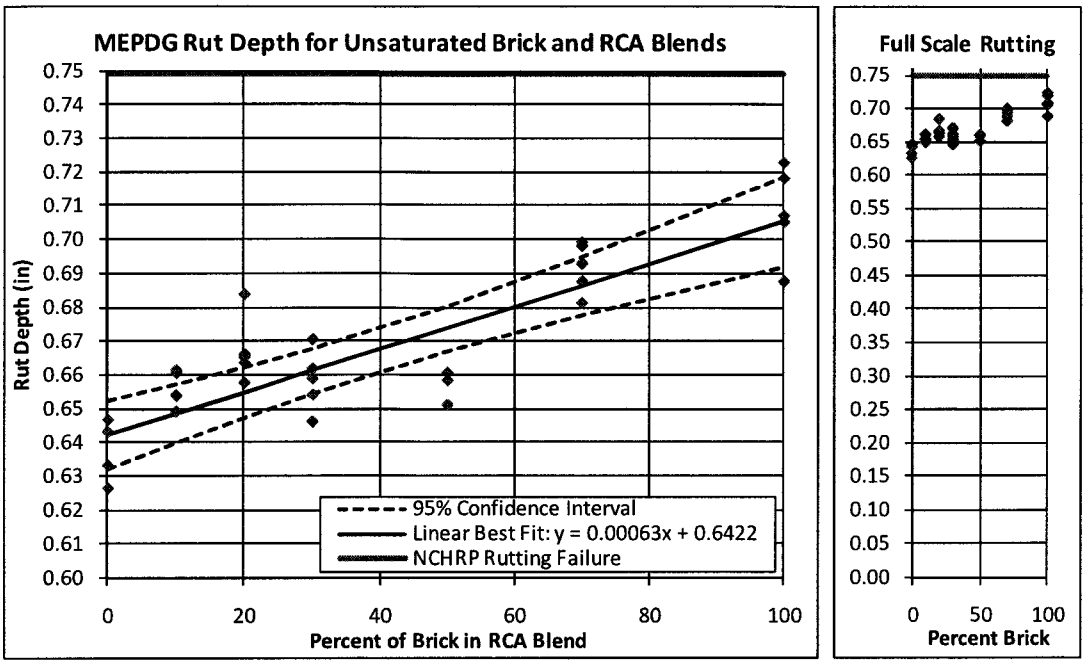

Figure 76: MEPDG Model Results for Unsaturated Brick Blends

The model results show that BDA is acceptable as a highway base or subbase when considering rutting performance. These model results are based on specific input parameters, and are not completely influenced by the quality of the base and base and subbase. Because of this results may vary depending on site specific conditions.

4.6.2 Effects of Saturation on Brick Blends

As discussed in Section 4.5, brick showed a greater decrease in M_R due to saturation than RCA. In order to get a better idea of the effects of saturation on brick and concrete, the SRM_I values from the saturated samples were modeled in the MEPDG. The results of the MEPDG model are shown in Figure 77.

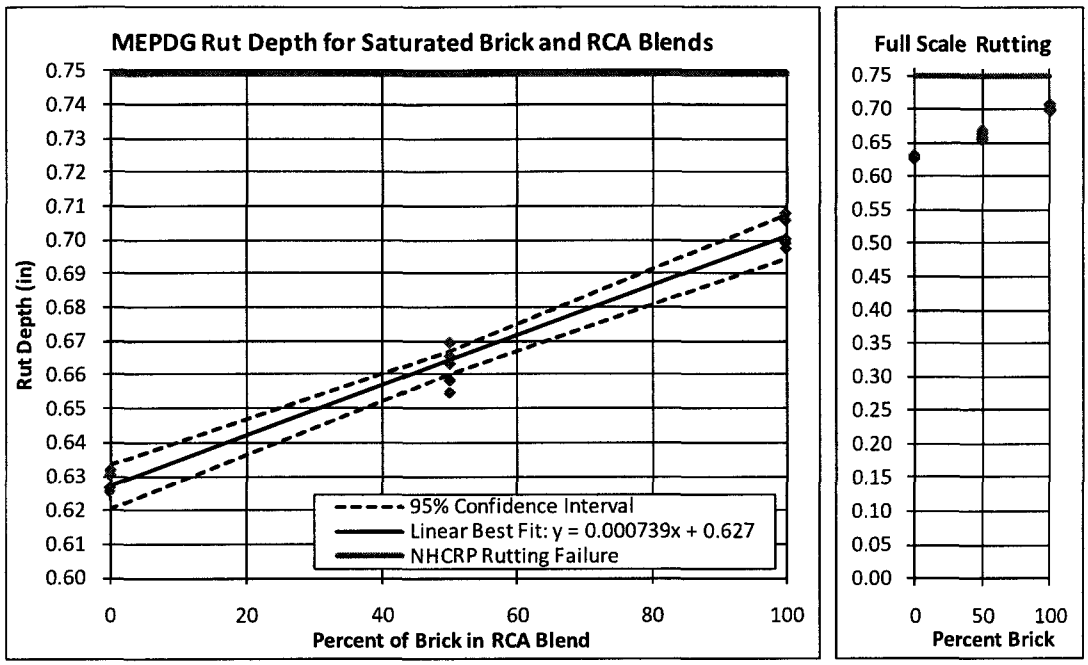

Figure 77: MEPDG Model Results for Saturated Brick Blends

The rutting results from the MEPDG model show that all BDA is acceptable for use as a highway base and base and subbase, even with the 95% confidence interval. It should also be noted that when rutting performance is shown on a full scale, shown on the right side of Figure 76 and Figure **77**, the effects of brick content appear even more insignificant, particularly when the MEPDG simulation for 5 crushed stone samples showed an average rut depth of 0.673 in. That being said, the model was also influenced by many other factors, so site specific results could be very different than suggested in Figure 77. However, these results do show that BDA, regardless of brick content, has properties similar to conventional highway construction materials.

4.6.3 Effects of RAP on Unsaturated BDA Samples

RAP blends showed different M_R results than the brick blends, with an initial decrease up until approximately 10,000 loading cycles before increasing. The same method was used to determine the SRM_I because the linear fit brought the intercept to a value slightly above the minimum stiffness. These SRM_I values were input into the MEPDG, the results are shown in Figure 78.

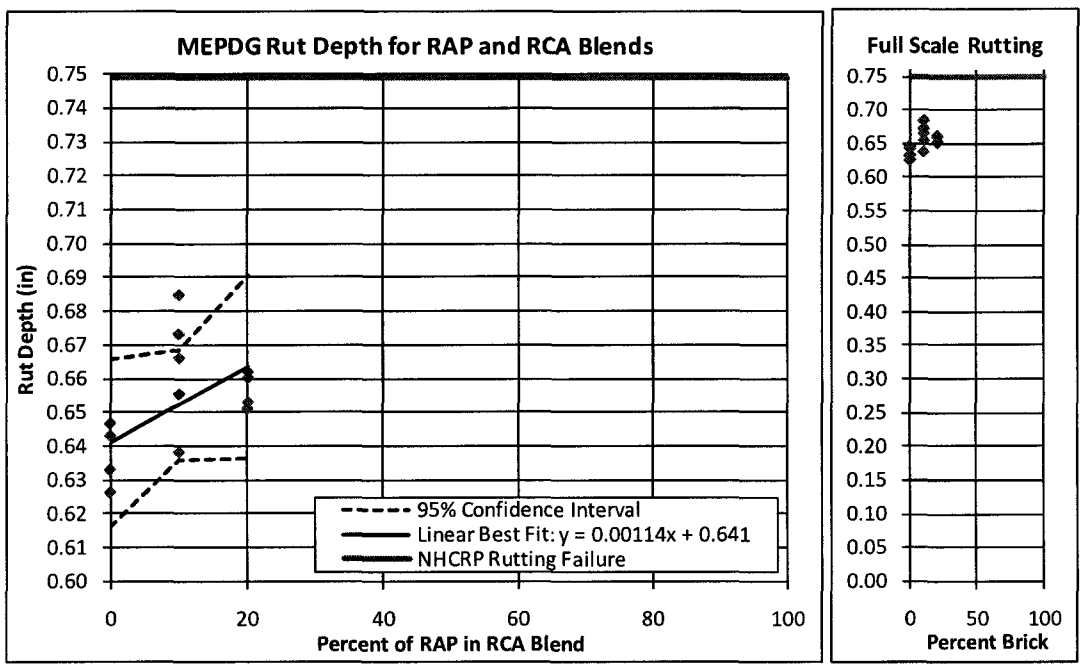

Figure 78: MEPDG Rutting Values for RAP Blends

The RAP blends show a visibly higher degree of scatter than both the saturated and unsaturated brick blends; however, based on a 95% confidence interval the RAP blends tested in this research will not exceed the NHCRP rutting failure value.

4.7 Correlations between CBR and SRM_I

As discussed in Chapter 2, the California Bearing Ratio does not effectively model the fatigue failure mode that highway base and subbase experience. However, because the CBR is relatively easy to perform and highly repeatable compared to the resilient modulus, many attempts have been made at establishing a correlation between resilient modulus and CBR. Previous research done by DeRocchi (2008) and Clark (2010) has shown that these correlations do not provide an accurate representation of resilient modulus values determined in the lab. Since the method of obtaining resilient modulus in this research was slightly different than DeRocchi or Clark, a comparison between predicted and actual SRMI values was prepared using Equation 2. The results of this comparison are shown in Figure 79.

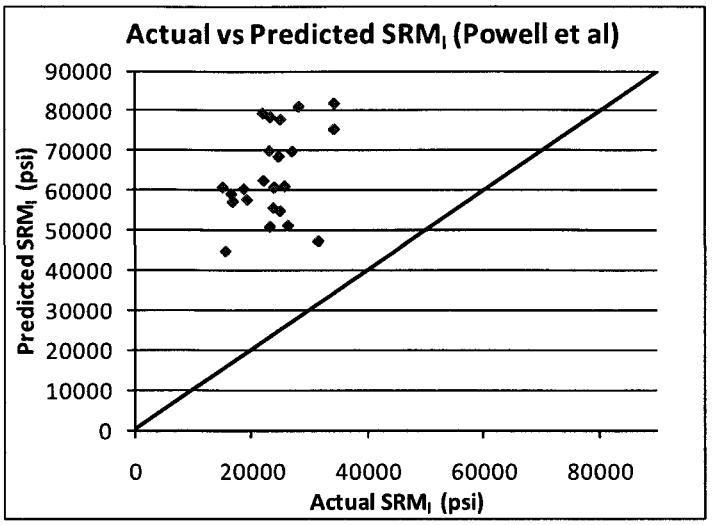

Figure 79: Actual vs Predicted SRM_I Values Using Equation 2

The Powell et al. correlation method dramatically over estimates SRM_I values observed in the laboratory. These results are similar to the findings of Clark (2010) and DeRochhi (2008), shown in Figure 80 and Figure **81**, respectively.

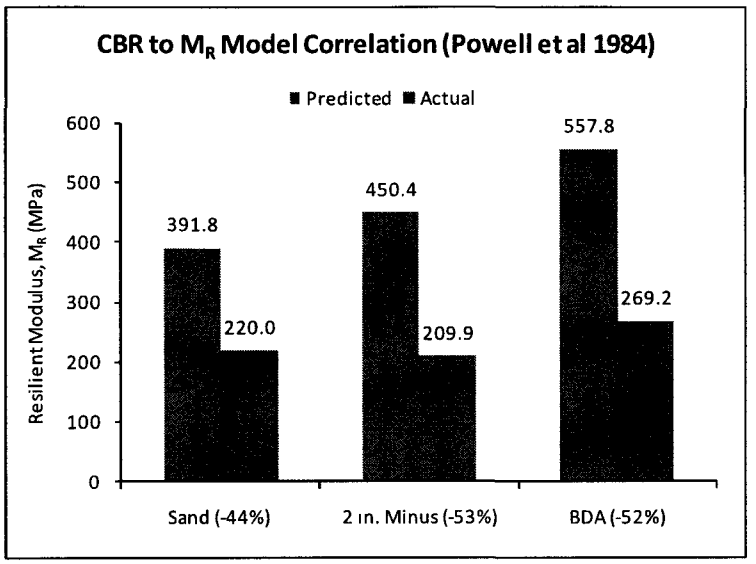

Figure 80: CBR Predicted M_R vs Actual M_R (Clark, 2010)

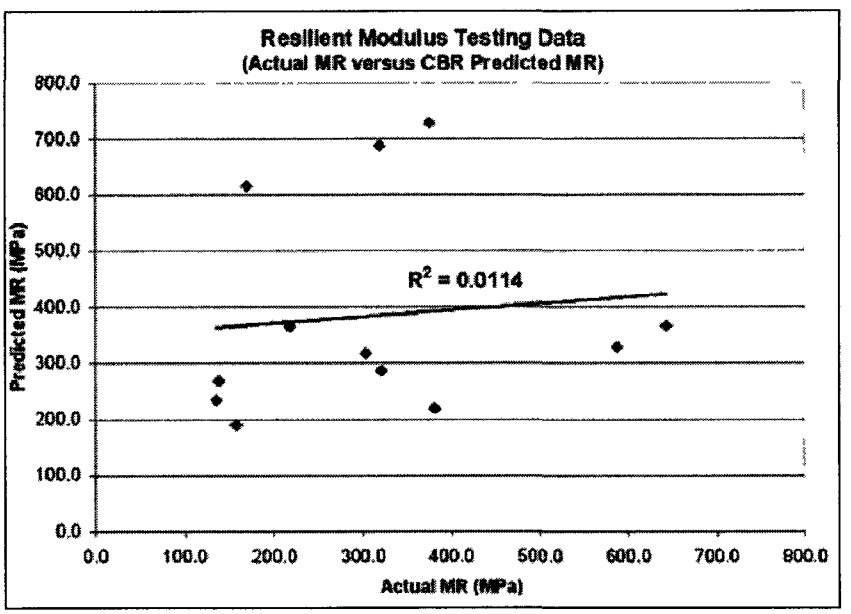

Figure 81: CBR Predicted M_R vs Actual M_R (DeRocchi, 2008)

CHAPTER 5

CONCLUSIONS AND RECOMMENDATIONS

5.1 Introduction

This purpose of this research was to determine the affect of brick content on controlled blends of BDA, in particular with respect to long term performance under non- ideal conditions. Since brick is composed of clay and sand which has been modified for weather resistance, concerns have arisen with respect to performance of the brick core, which is exposed upon crushing. In order to evaluate this performance, samples of crushed brick were tested for strength, stiffness, durability, and abrasion resistance in saturated and unsaturated conditions. These samples were compared to crushed concrete, the other major component of BDA. Additionally blends of brick and crushed concrete were tested to establish the point at which brick has a significant effect on the performance of BDA as a highway construction material.

The material selection was made to best represent BDA materials in the C&D waste stream in New England. All testing methods used in this research are nationally recognized as state of the art for evaluating flexible pavement systems. Once all data had been collected, the effects of brick content on material performance were compared to accepted standards to establish a maximum allowable brick content.

5.2 Conclusions

A total of five different tests were performed on different blends of brick and RCA in order to establish allowable levels of brick based on different mechanisms of material performance. The results were compared to nationally accepted values for high quality materials. Due to regional variations in the composition of construction materials, which in turn affect the composition of the C&D waste stream, the results of this research can only be considered valid for sources of BDA within the Northeast United States. The conclusions for allowable brick content based on test data are shown in the following sections.

5.2.1 Micro-Deval Performance

The Micro-Deval test evaluates a materials resistance to abrasion. This is important because highway construction materials generally go through blasting, sieving, transportation, placement, and compaction before they go into service. All of these processes are highly abrasive, and if a material does not have adequate abrasion resistance key characteristics such as angularity and gradation can be significantly affected, resulting in poor performance. Both saturated and unsaturated samples were tested, however AASHTO T-327 specifies that the test be run in saturated conditions. Because of this the allowable brick content was established using the saturated results only.

By testing 5 specimens each of brick and RCA, a linear relationship between Micro-Deval wearing loss and BDA brick content was established. In order to address any potential issues with data variability, a 95% confidence interval about the mean response was established. Using the conservative end

of the confidence interval, it was established that the BDA brick content shall not exceed 31% when considering abrasion resistance. This was based on an allowable wearing loss of 30% for base material defined by AASHTO.

5.2.2 Freeze-Thaw Resistance

Due to the climatic conditions in the Northeast, freeze-thaw resistance is a very important material property. During the winter the ground typically freezes approximately 4-5 feet deep or greater, depending on location and the severity of the winter. This is well within range of highway base and base and subbase materials. During the spring the daytime temperatures increase, causing snowmelt which raises the water table. However, the night time temperatures remain low, resulting in freeze-thaw cycles. This subjects any submerged material to extreme stresses resulting from the expansion of water which can have a significant effect on material performance over time.

Freeze-thaw testing was done on 5 specimens each of 100% brick and 100% RCA. After 41 freeze-thaw cycles the results showed that RCA has an average loss of 22% and brick had an average loss of 4%.

5.2.3 California Bearing Ratio

The CBR is one of the most common methods used by state agencies for evaluating highway construction materials. Although it is frequently used as a design parameter, it does not effectively evaluate stiffness, the primary mechanism for base and subbase failure. However, since there is plentiful CBR data for many different geotechnical materials, it is useful for comparison.

Most design methods, including the MEPDG, limit the CBR of any material to 100% because it is considered an excellent material at that point. Because of this a CBR of 100% was used as a baseline for comparing the effects of brick on BDA. All saturated and unsaturated CBR data was organized so that a linear relationship could be established between brick content and CBR. Once this was done statistical methods were used to define a 95% confidence interval. Based on the lower 95% confidence interval, the maximum allowable brick content for unsaturated BDA is 21%. Saturation caused a slight decrease in bearing capacity, resulting in a maximum allowable brick content of 18%.

5.2.4 Repeat Load Triaxial Testing

Stiffness is the best indicator of the quality of base or base and subbase. Currently the best method for obtaining stiffness values is the RLT test, which determines the M_R. Because of this, the bulk of this research focused on RLT testing to examine the effects of brick content on blends of BDA. Because stiffness is also affected by layer thickness, there is no benchmark value for stiffness that determines a quality material. To evaluate the effects of brick content on material performance, M_R values obtained from RLT testing were input to the MEPDG.

5.2.5 MEPDG Models

The initial summary resilient modulus (SRM_i) was determined from each RLT test and used in a MEPDG model which simulated 10 years of traffic loading in environmental conditions typical to New England. The NCHRP has defined rutting failure at 0.75", so this value was used as a baseline for comparison of

different BDA blends. In order to isolate the effects of brick content on BDA blends, both the base and base and subbase layers were modeled using resilient modulus values obtained from testing. No other parameters were changed in the model to ensure accurate comparisons between data. Based on a 95% confidence interval, simulations using M_R values obtained from unsaturated and saturated samples resulted in a maximum rut depth of 0.723". This is less than the threshold value of 0.75", so results of this research indicate that brick content has an insignificant effect on BDA rutting performance.

5.2.6 Summary

Based on the conclusions of this research, different brick contents affect the performance of BDA at varying degrees depending on the performance characteristic. Important findings of this research are listed below:

- Based on SRM_I values obtained from 5 SRM tests on 7 unsaturated and saturated blends, brick content does not have a significant effect on simulated rutting performance when BDA is used as a highway base and subbase.
- Based on SRM_I values obtained from 5 SRM tests on 2 unsaturated blends, RAP content does not have a significant effect of simulated rutting performance in proportions of up to 20% RAP.
- Based on CBR values obtained from 5 CBR tests on 12 unsaturated and saturated blends, brick content should be limited to 18% in BDA blends used as a highway base and subbase.

- Freeze-Thaw testing has shown that RCA has significantly less freeze-thaw resistance than brick.
- Five Micro-Deval tests on two blends of BDA have suggested brick content be limited to 31% in BDA blends used as highway base and subbase.
- Although CBR is not an accurate indicator of base and subbase performance, significant reduction in the bearing capacity of saturated brick raises concerns about the long term performance of brick over time, particularly in severe climates.
- Resilient modulus of BDA blends may significantly increase over cycles of loading and unloading similar to what is commonly seen on construction sites, potentially leading to better performance.

Currently the NHDOT specifies that no more than 5% of crushed material contain brick particles. The results of this study indicate that brick contents could be raised to 20% with little or no effect on performance. It should be noted that BDA, even among geotechnical materials, has a wide variability. This study was performed using material obtained from a stockpile located in New Hampshire with the intent of representing the C&D stream in New England. However, due to nationwide variation in construction materials, results from this study cannot be considered valid in regions outside of New England.

5.3 Recommendations

Throughout this research several issues arose which could not be addressed, primarily due to time considerations. The issues, if resolved, could help provide a better understanding of BDAs performance as a highway construction material.

5.3.1 Abrasion Resistance

As mentioned in Chapter 4, further abrasion resistance testing may need to be performed to obtain more accurate values for RCA. This conclusion is a result of research which compared several methods of testing abrasion resistance (Cuelho, et al., 2008). This research recommended that any material with Micro-Deval losses falling between 18-27% should be confirmed using an additional method due to poor repeatability within this range. The majority of RCA Micro-Deval losses fell between 18-27%, so a different method for evaluating abrasion resistance should be used to further validate results.

5.3.2 Time Dependent Stiffness

As discussed in Chapter 4, an increase in resilient modulus over time was observed for some RLT specimens. This behavior could be very important in determining more representative M_R values for BDA. During construction base and subbase is typically placed well before hot mix asphalt is laid on top of it. During this time the material is subjected to construction loads, which provide the loading simulated during RLT testing. However, due to construction schedules, these loads are intermittent, stopping over nights and weekends when work is

over. This leaves the base in an "in place" condition, just like the conditions simulated during the overnight and weekend pauses observed in Figure 69 and **Figure 70**.

Although research has shown an increase in stiffness over time, it was done using a LWD in a test pit. The LWD has shown limited comparability with RLT results, particularly at lower densities (Clark, 2010). Because of this, time dependent stiffness should be explored in a similar fashion to the research done by Martin, Halsey, and Melton using RLT testing. This would establish time dependent stiffness behavior of BDA using more comparable results.

5.3.3 Long Term Stiffness Behavior

All resilient modulus testing was done up to 50,000 loading cycles, however, some roads in the United States will experience 50,000 loading cycles in a single day. The data from this research indicates progressive increase in M_R over time, particularly when plotted on a semi-log scale, shown in Figure 82. The University of Wisconsin has performed longer term tests than done in this research on crushed stone, and observed a decrease in resilient modulus once a maximum density had been reached. Since this material will not likely continue to progressively gain MR as indicated in Figure 82, longer term testing should be done to determine the material behavior once a maximum density is reached. This can help determine material behavior over a realistic pavement design life, and prove particularly helpful if significant reductions in M_R are observed beyond maximum density.

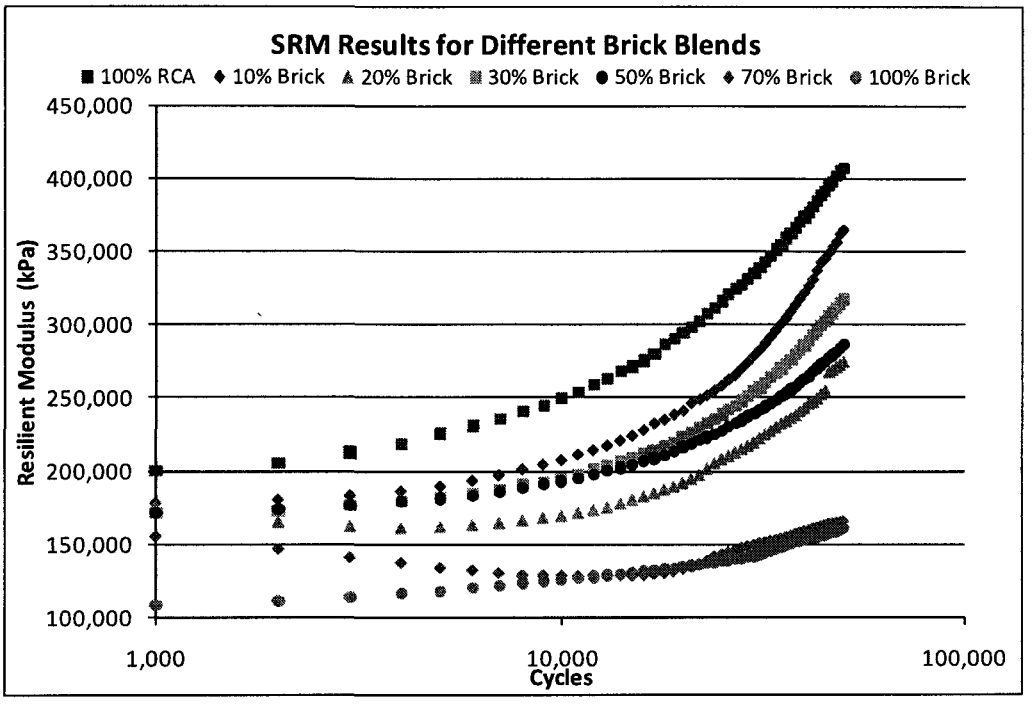

Figure 82: Brick Blend SRM Results Plotted on Logarithmic Scale

5.3.4 MEPDG M_R Input

As discussed in Chapter 4, a M_R value for each material needed to be obtained by placing a linear fit on each set of RLT results and using the y-intercept as the initial summary resilient modulus (SRM_I). This was done because the MEPDG requires a constant input for the M_R of each pavement layer. Unfortunately this does not accurately model the behavior of base and base and subbase over long term loading. As observed in all the results, M_R increased with loading cycles. Using the SRM_I allows for a conservative estimate of the material stiffness, however it will likely lead to over prediction of rutting. Since crushed materials are one of the most costly items used in the construction of roadways, the amount used has a great impact on the amount of roads an agency can construct in any given year. More accurate modeling of stiffness

behavior over long term loading can help create more efficient designs, which will ultimately help reduce the cost of roadway construction.

APPENDIX A

STANDARD PROCTOR RESULTS

Crushed Stone Specimen	**1**	**2**	**3**	**4**	**5**
Volume of Mold (m^3)	0.00212	0.00212	0.00212	0.00212	0.00212
Empty Mold Mass (kg)	6.7	6.7	6.8	6.7	6.8
Full Mold Mass (kg)	11.1	11.2	11.2	11.2	11.4
Mass of Sample in Mold (kg)	4.4	4.5	4.4	4.5	4.6
Moisture Content (%)	4.4%	4.4%	4.4%	4.4%	4.4%
Wet Density	2077.2	2122.0	2063.1	2114.9	2157.3
Dry Density (kg/m^3)	1989.7	2032.6	1976.2	2025.8	2066.4
Dry Density (lb/ft^3)	**123.9**	**126.6**	**123.1**	**126.2**	**128.7**

RCA Specimen	**1**	**2**	**3**	**4**	**5**
Volume of Mold (m^3)	0.00212	0.00212	0.00212	0.00212	0.00212
Empty Mold Mass (kg)	6.7	6.7	6.7	6.8	6.8
Full Mold Mass (kg)	10.4	10.6	10.5	10.9	10.9
Mass of Sample in Mold (kg)	3.7	3.9	3.8	4.2	4.1
Moisture Content (%)	12.0%	12.0%	12.0%	12.0%	12.0%
Wet Density	1745.2	1839.4	1792.3	1954.8	1940.7
Dry Density (kg/m^3)	1558.2	1642.3	1600.2	1745.3	1732.7
Dry Density (lb/ft^3)	**97.1**	**102.3**	**99.7**	**108.7**	**107.9**

Brick Specimen	**1**	**2**	**3**	**4**	**5**
Volume of Mold (m^3)	0.00212	0.00212	0.00212	0.00212	0.00212
Empty Mold Mass (kg)	6.7	6.7	6.7	6.7	6.7
Full Mold Mass (kg)	10.5	10.6	10.3	10.6	10.6
Mass of Sample in Mold (kg)	3.8	3.9	3.6	3.9	3.9
Moisture Content (%)	12.0%	12.0%	12.0%	12.0%	12.0%
Wet Density	1801.7	1820.5	1693.4	1858.2	1825.2
Dry Density (kg/m^3)	1608.7	1625.5	1511.9	1659.1	1629.7
Dry Density (lb/ft^3)	**100.2**	**101.3**	**94.2**	**103.3**	**101.5**

RAP Specimen	**1**	**2**	**3**	**4**	**5**
Volume of Mold (m^3)	0.00212	0.00212	0.00212	0.00212	0.00212
Empty Mold Mass (kg)	6.7	6.7	6.7	6.7	6.7
Full Mold Mass (kg)	10.6	10.6	10.6	10.5	10.6
Mass of Sample in Mold (kg)	3.9	3.9	3.9	3.8	3.9
Moisture Content (%)	8.0%	8.0%	8.0%	8.0%	8.0%
Wet Density	1820.5	1839.4	1830.0	1797.0	1844.1
Dry Density (kg/m^3)	1685.7	1703.1	1694.4	1663.9	1707.5
Dry Density (lb/ft^3)	**105.0**	**106.1**	**105.5**	**103.6**	**106.4**

APPENDIX B

CALIFORNIA BEARING RATIO RESULTS

100% RCA CBR (Unsaturated)

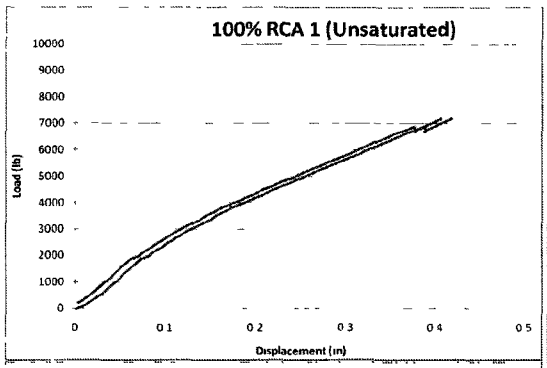

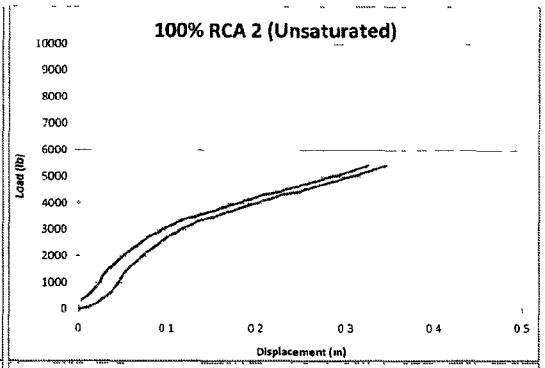

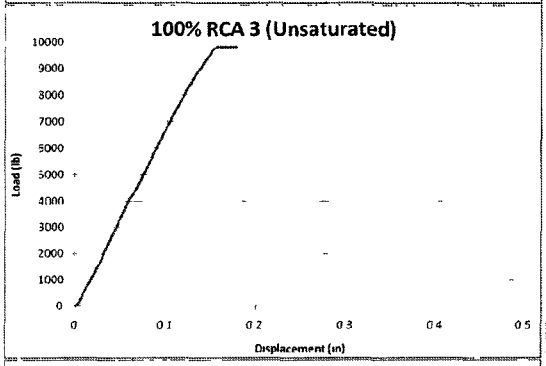

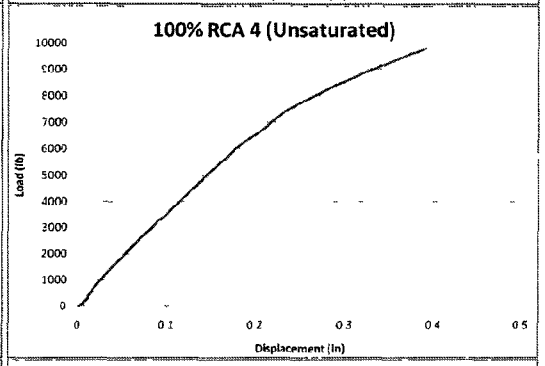

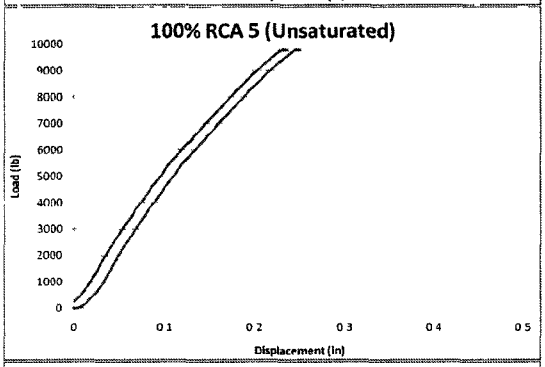

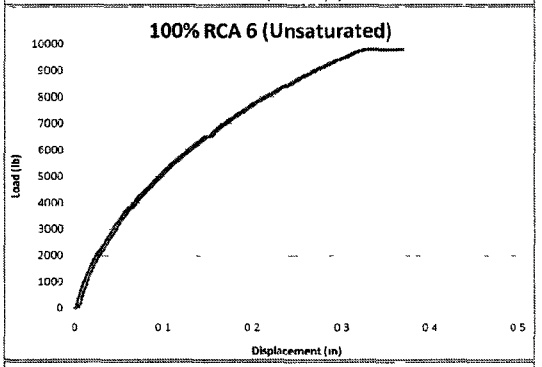

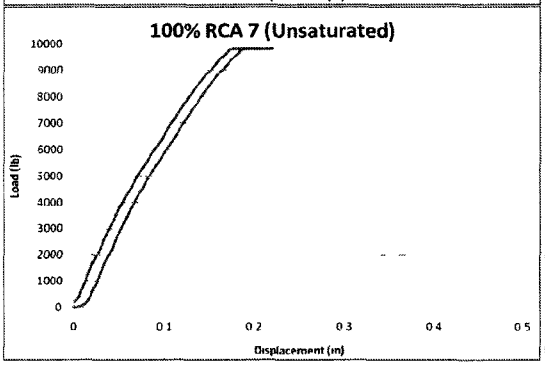

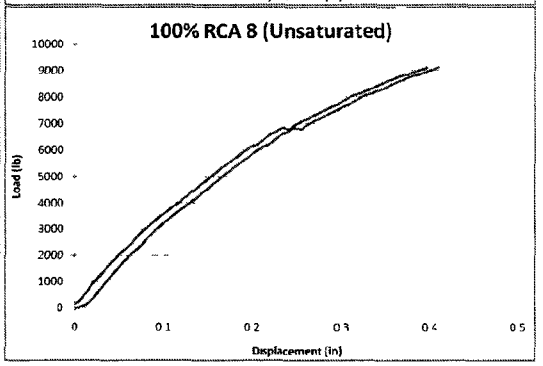

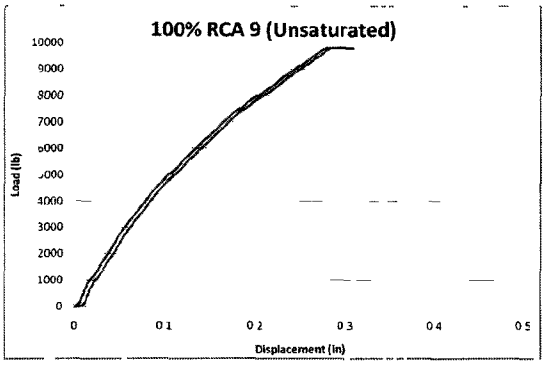

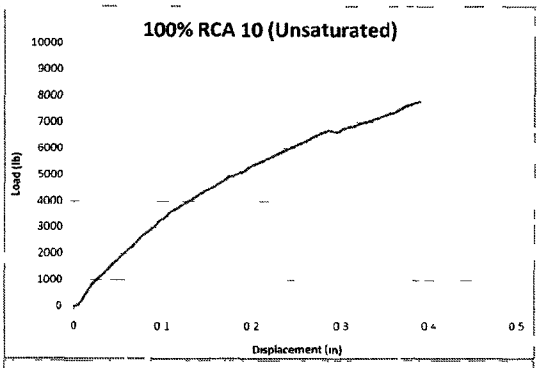

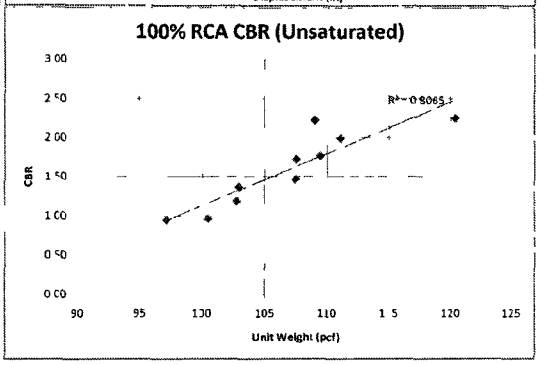

Sample	Unit Weight (pcf)	CBR
1	100.50	0.960
2	97.15	0.944
3	120.40	2.252
4	107.48	1.465
5	111.07	1.984
6	107.55	1.725
7	109.03	2.220
8	102.98	1.367
9	109.44	1.759
10	102.79	1.185

100% RCA CBR (Saturated)

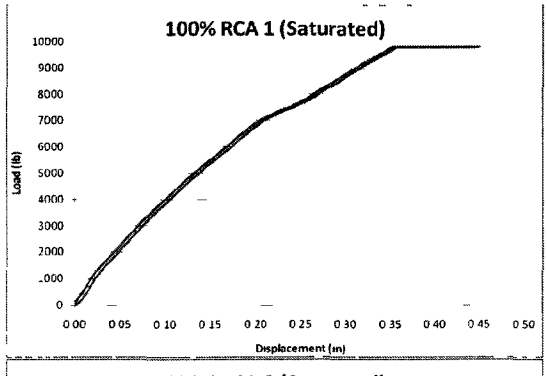

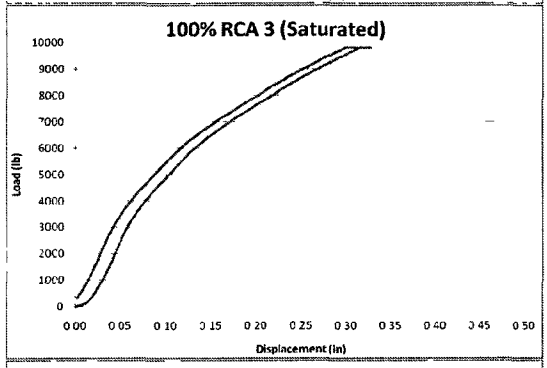

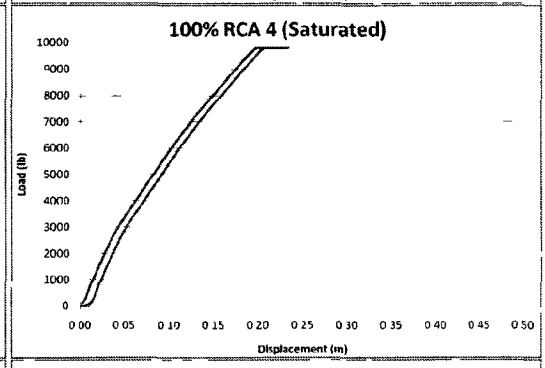

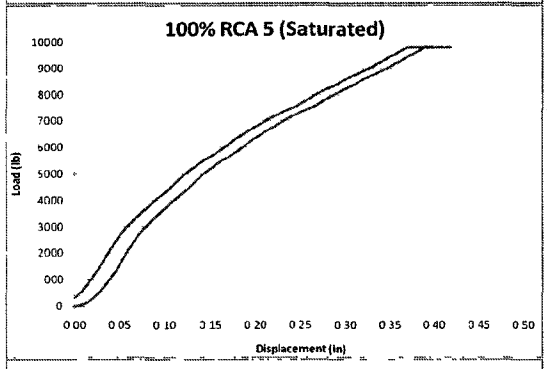

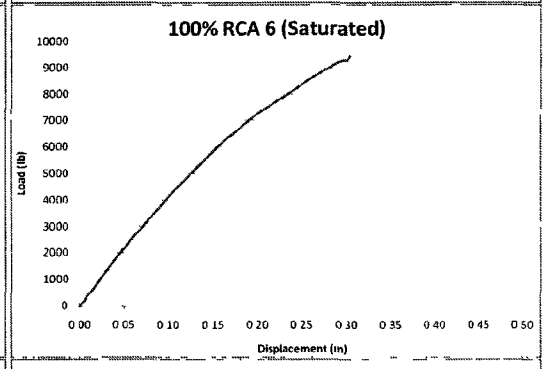

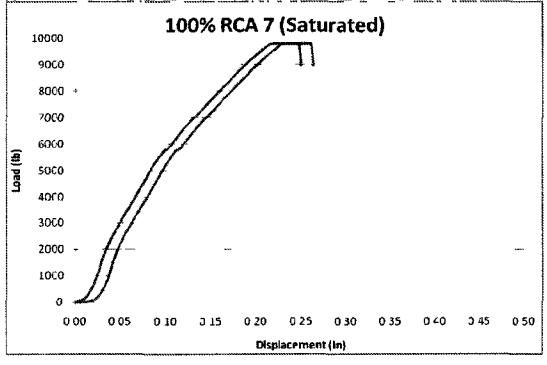

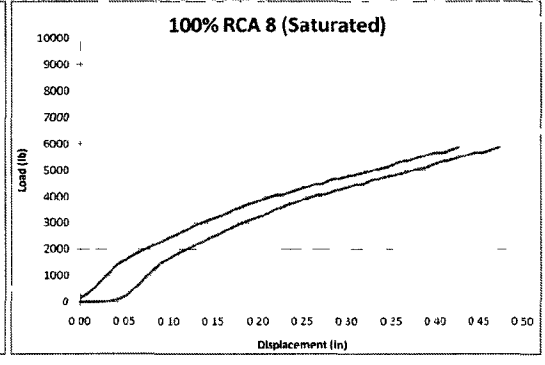

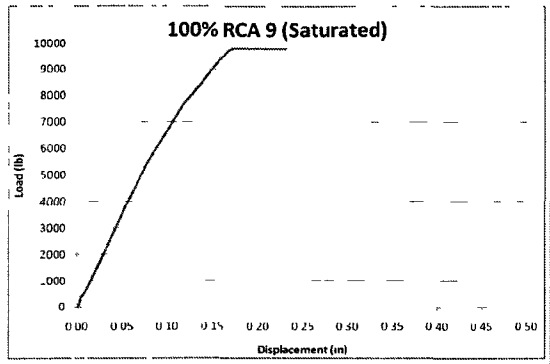

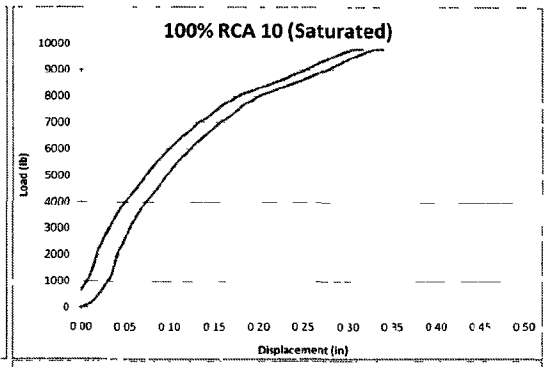

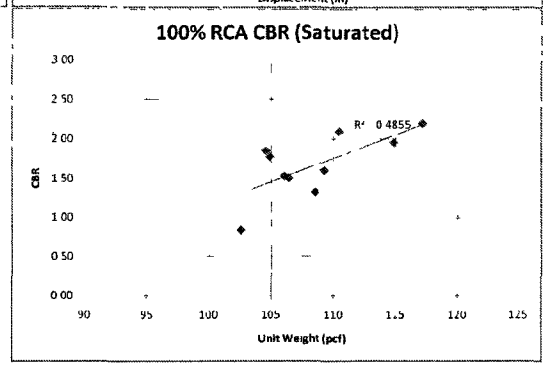

Sample	Unit Weight (pcf)	CBR
1	106.03	1.531
2	108.50	1.321
3	104.88	1.771
4	114.83	1.955
5	106.45	1.506
6	109.23	1.601
7	110.41	2.090
8	102.57	0.846
9	117.12	2.191
10	104.53	1.847

100% Brick CBR (Unsaturated)

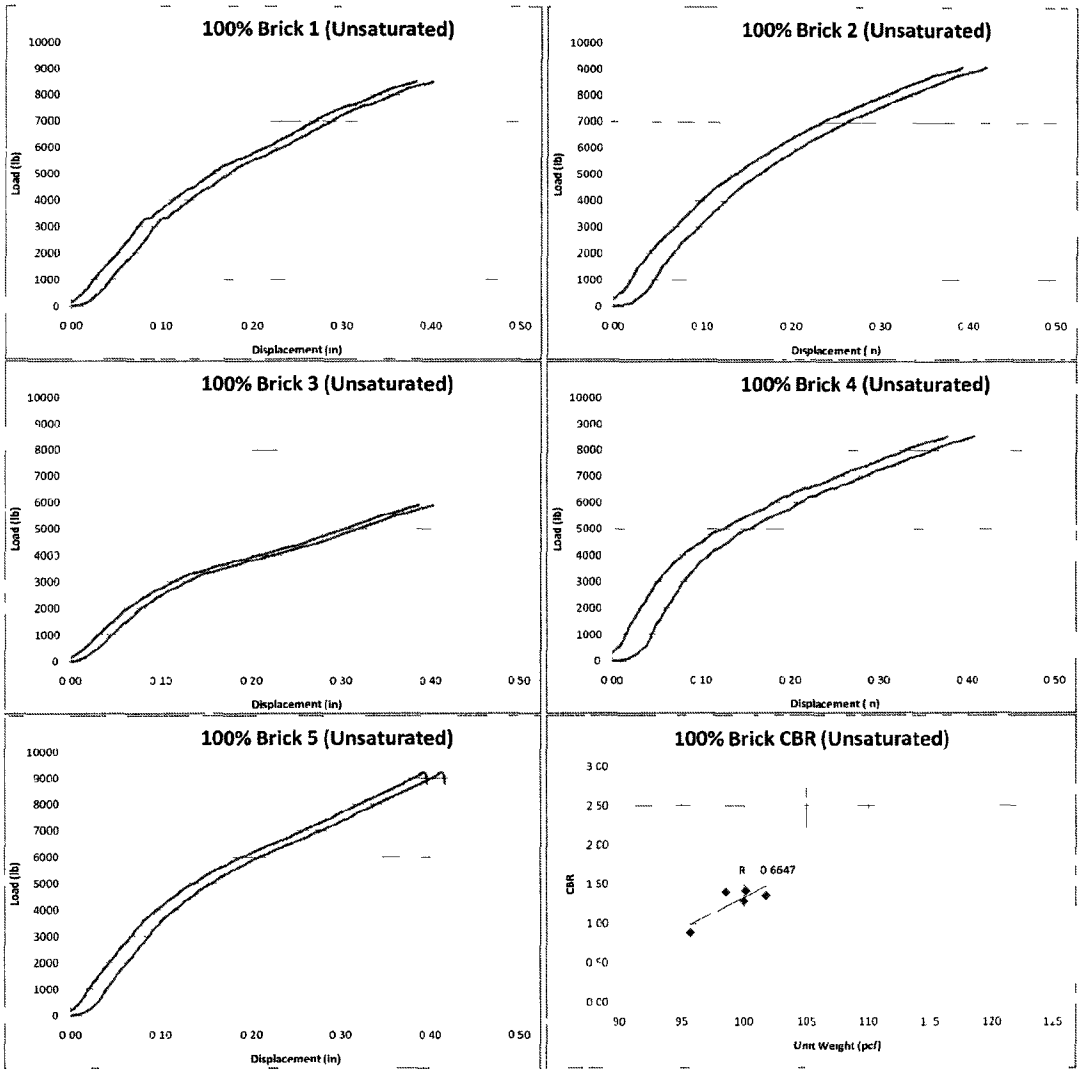

Sample	Unit Weight (pcf)	CBR
1	100.00	1.292
2	100.15	1.417
3	95 68	0.880
4	98.55	1 404
5	101.78	1.359

100% Brick CBR (Saturated)

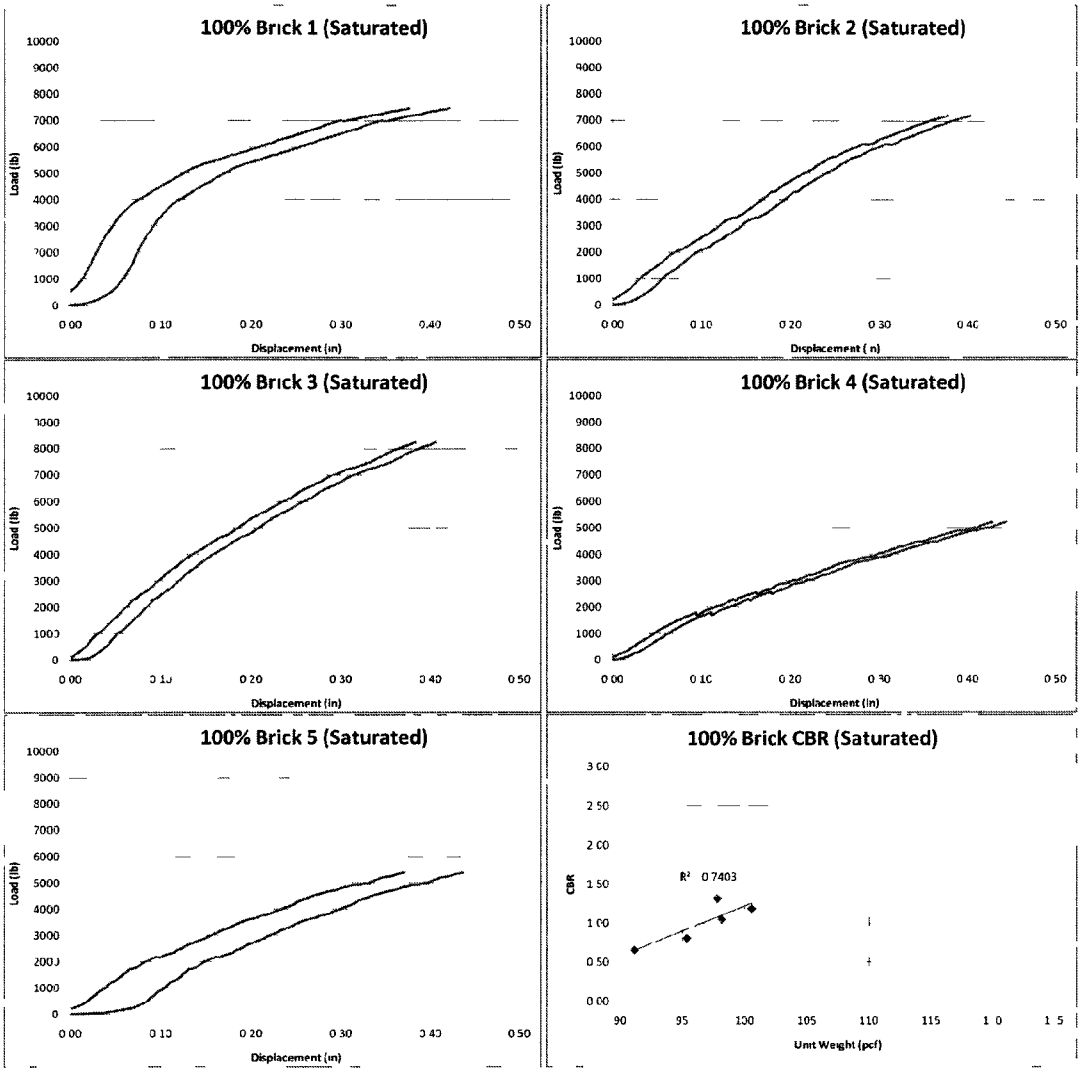

Sample	Unit Weight (pcf)	CBR
1	97.80	1 315
2	98.17	1.055
3	100.57	1.187
4	91.13	0.657
5	95.37	0 811

5% Brick CBR (Unsaturated)

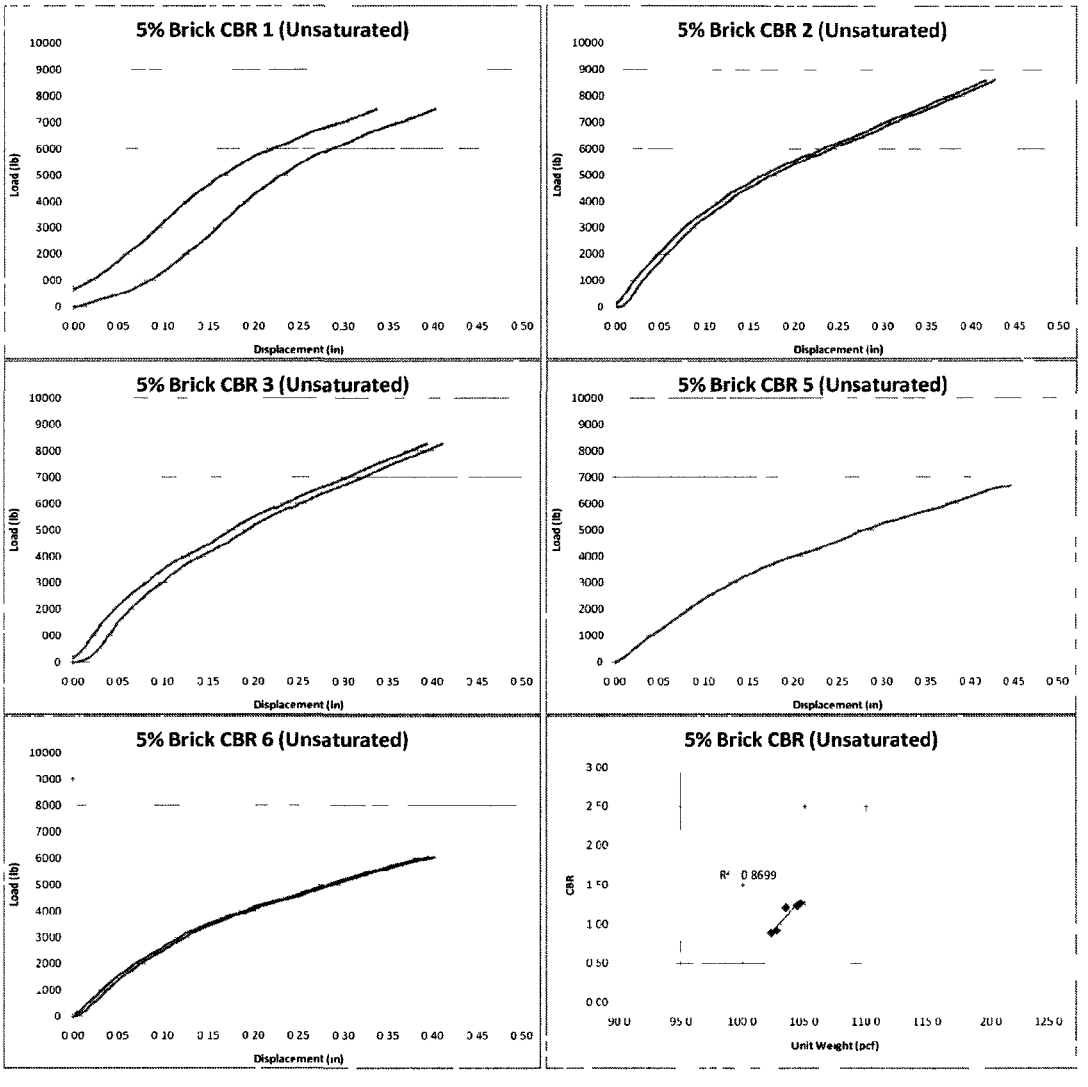

Sample	Unit Weight (pcf)	CBR
1	104.67	1.271
2	104.44	1 238
3	103.49	1.214
4		Bad Data
5	102.31	0.889
6	102.77	0.919

5% Brick CBR (Saturated)

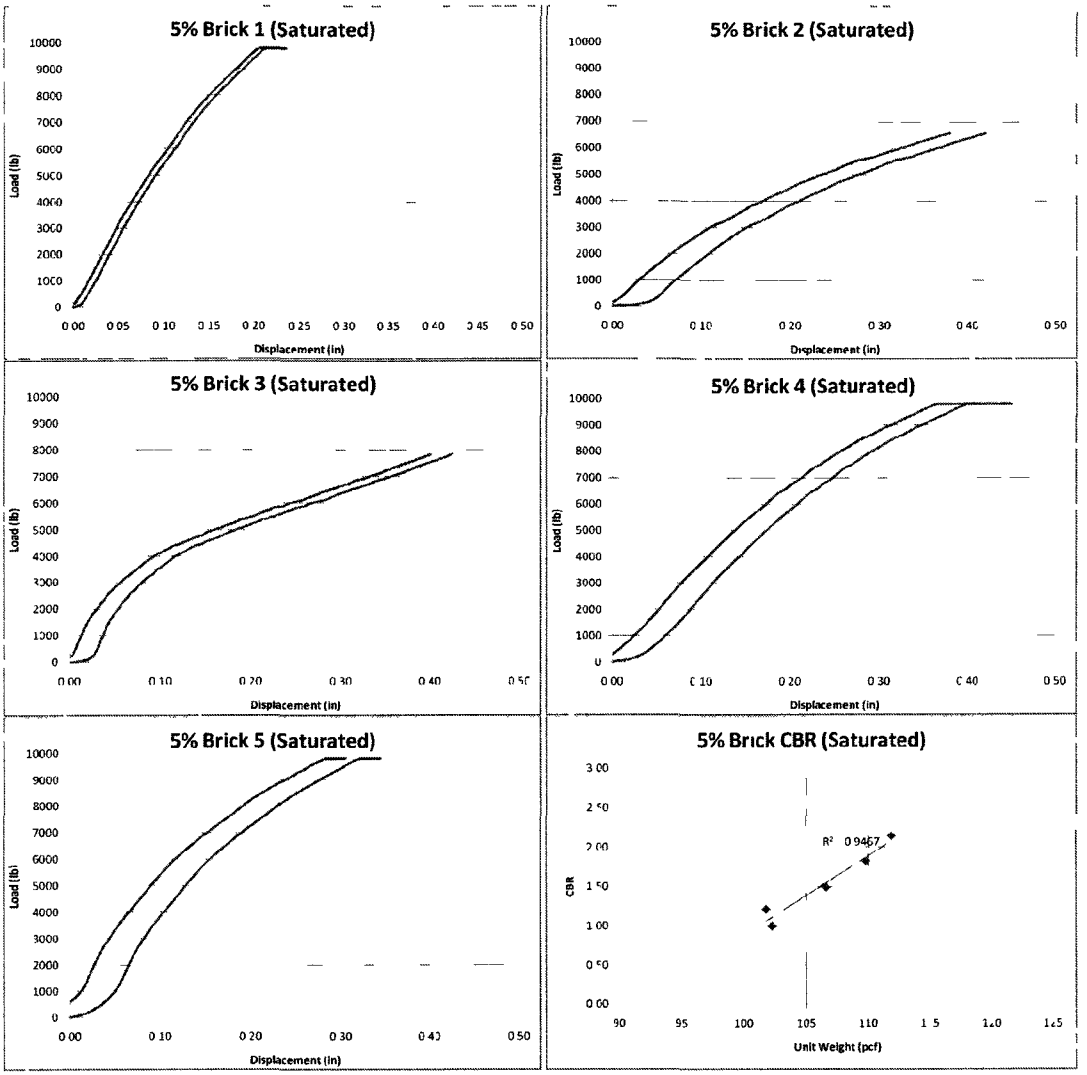

Sample	Unit Weight (pcf)	CBR
1	111.83	2 141
2	102 22	0.998
3	101.77	1 214
4	106.62	1.495
5	109.81	1.823

10% Brick CBR (Unsaturated)

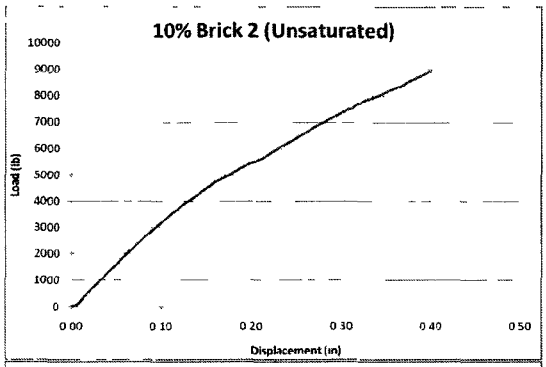

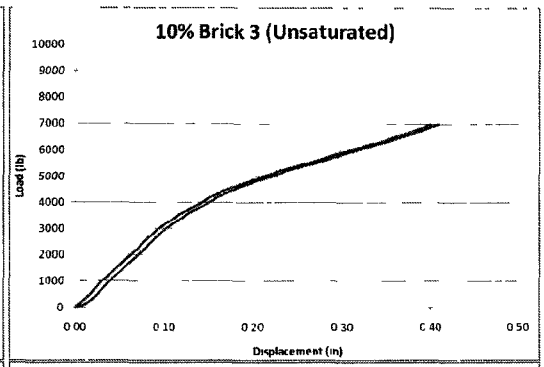

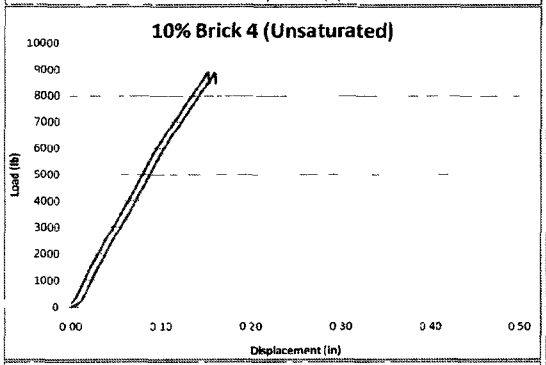

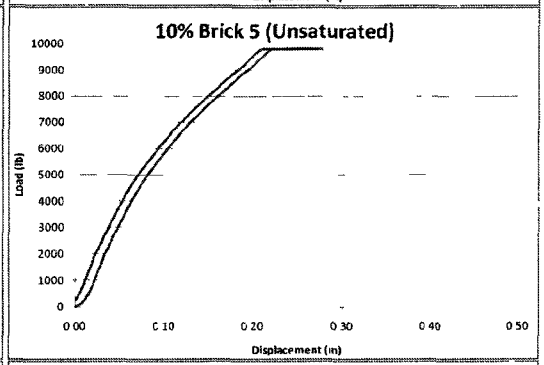

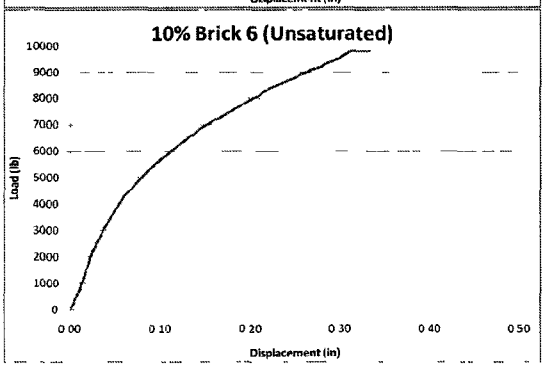

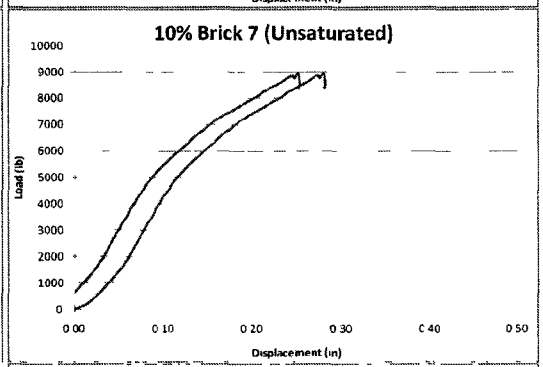

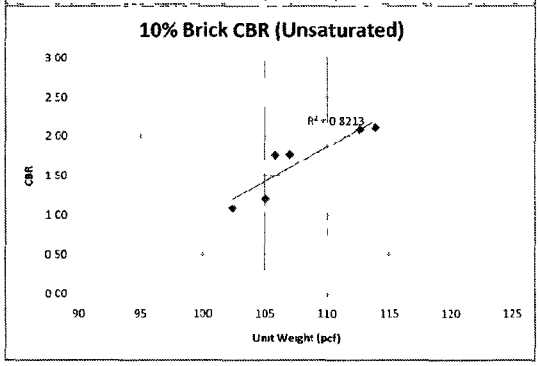

Sample	Unit Weight (pcf)	CBR
1		Bad Data
2	105.03	1.210
3	102.41	1.087
4	112.56	2.084
5	113.83	2.107
6	105.85	1.766
7	107.02	1.768

10% Brick CBR (Saturated)

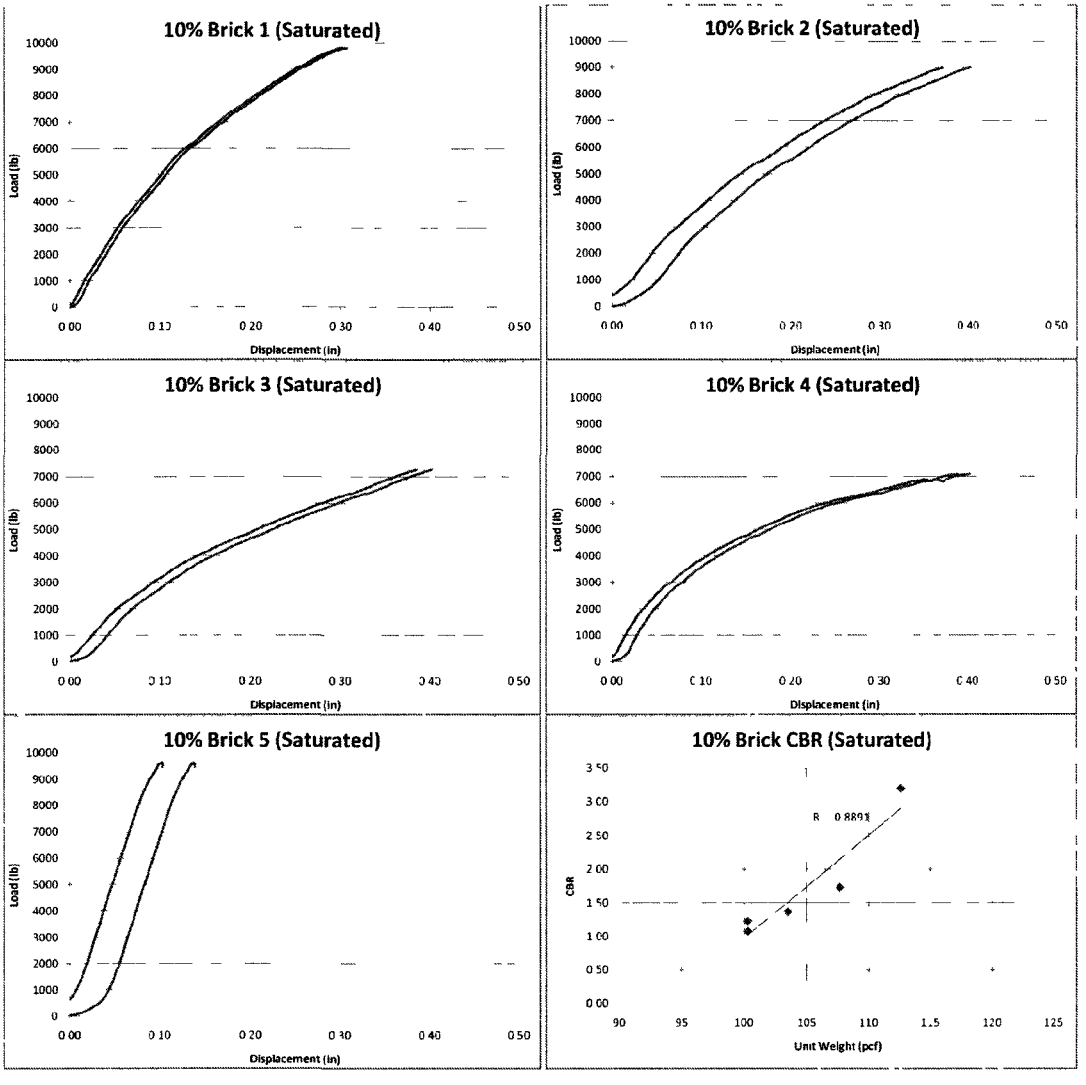

Sample	Unit Weight (pcf)	CBR
1	107.68	1.737
2	103.50	1.373
3	100.30	1.081
4	100.27	1.229
5	112.57	3.193

15% Brick CBR (Unsaturated)

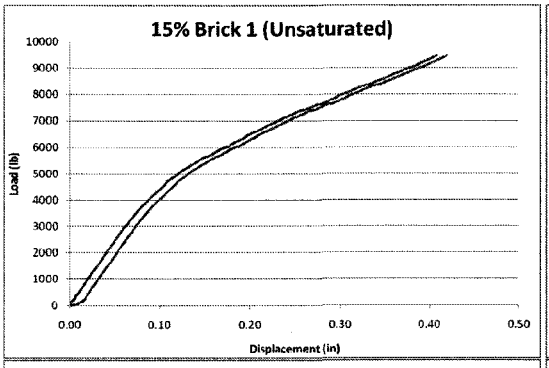

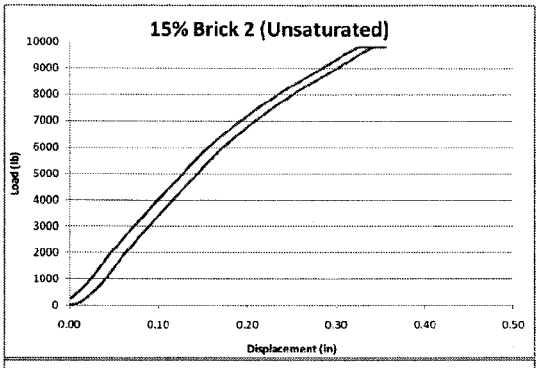

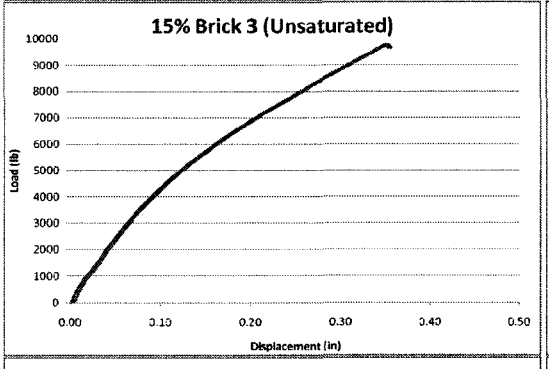

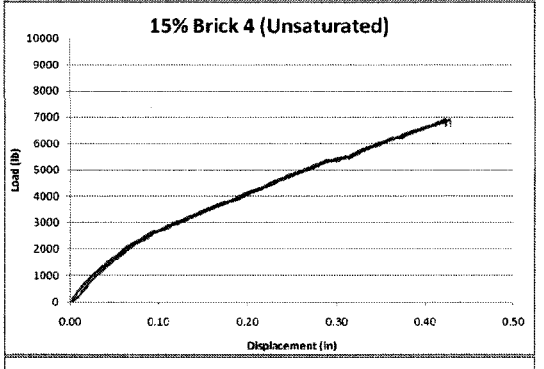

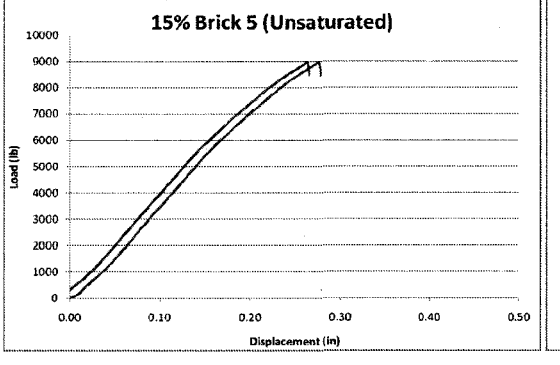

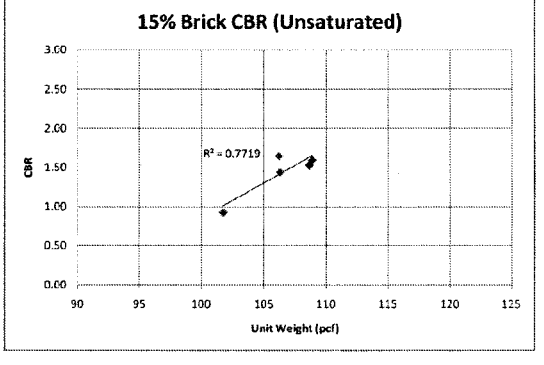

Sample	Unit Weight (pcf)	CBR
1	106.30	1.441
2	108.87	1.594
3	108.63	1.530
4	101.74	0.922
5	106.20	1.650

15% Brick CBR (Saturated)

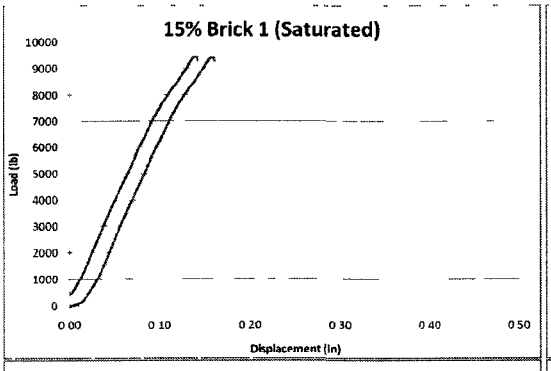

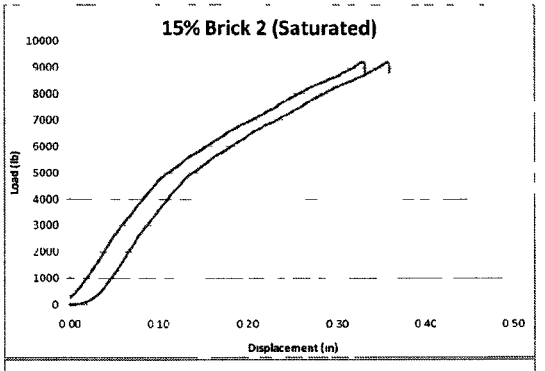

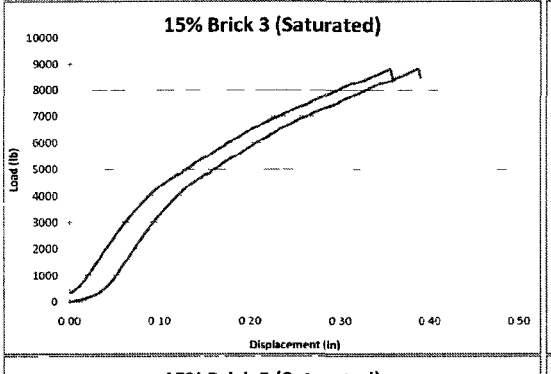

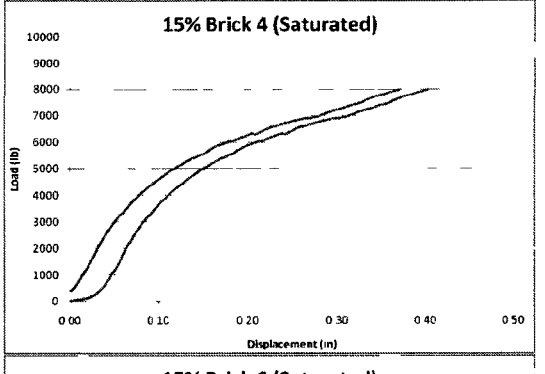

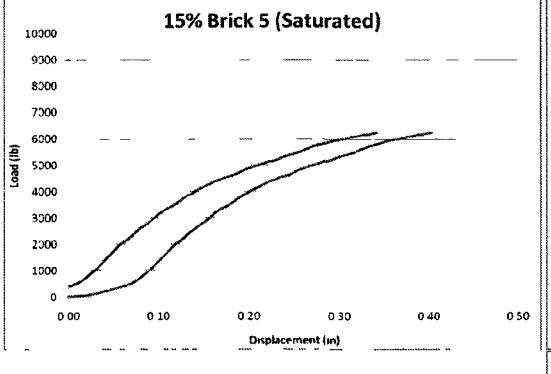

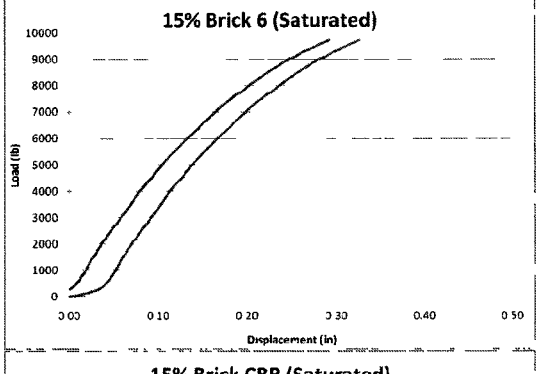

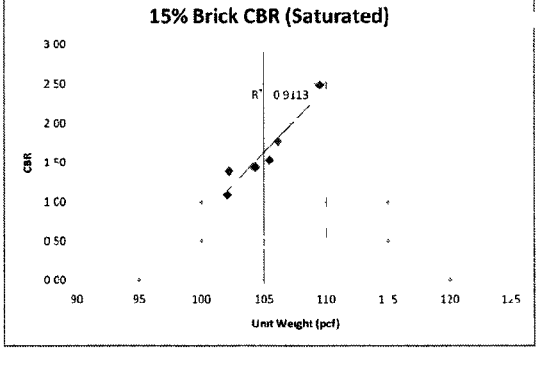

Sample	Unit Weight (pcf)	CBR
1	109.50	2.483
2	105.42	1.531
3	104.30	1.437
4	102.21	1.393
5	102.06	1.089
6	106.11	1.770

20% Brick CBR (Unsaturated)

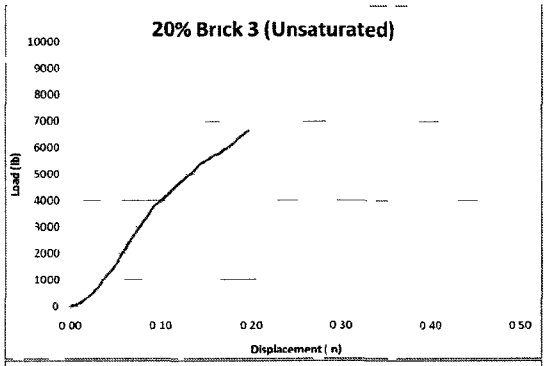

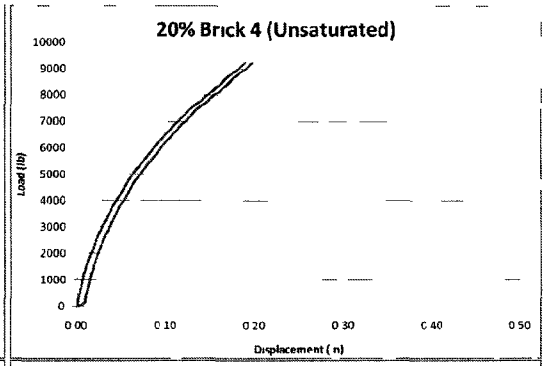

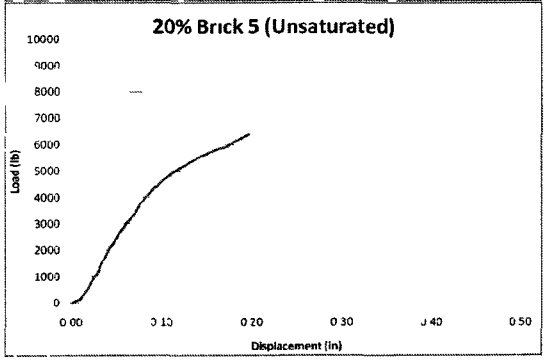

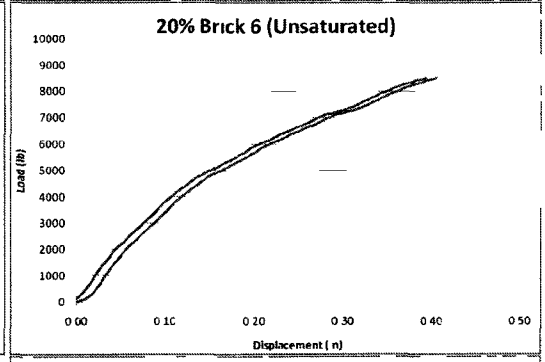

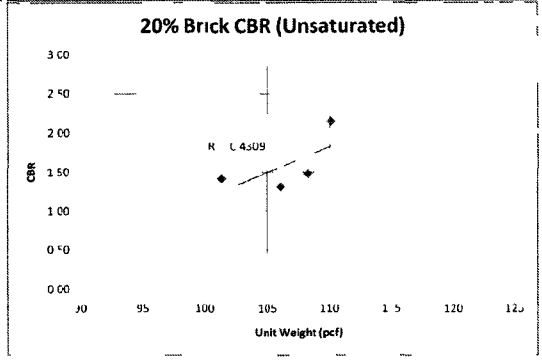

Sample	Unit Weight (pcf)	CBR
1		Bad Data
3	108 24	1 480
4	110 09	2 150
5	101 37	1 418
6	106 08	1 308

20% Brick CBR (Saturated)

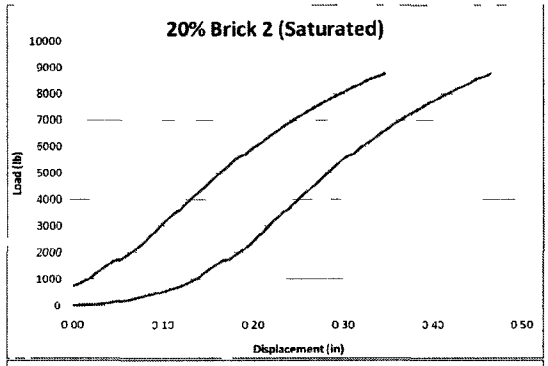

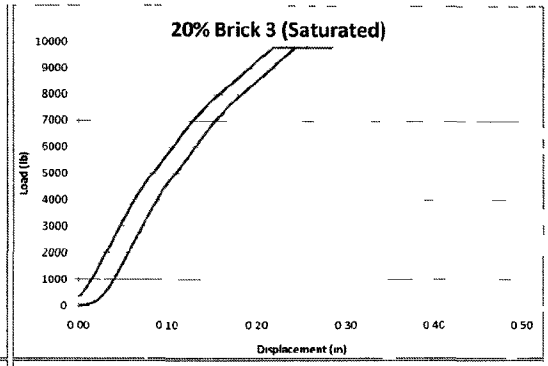

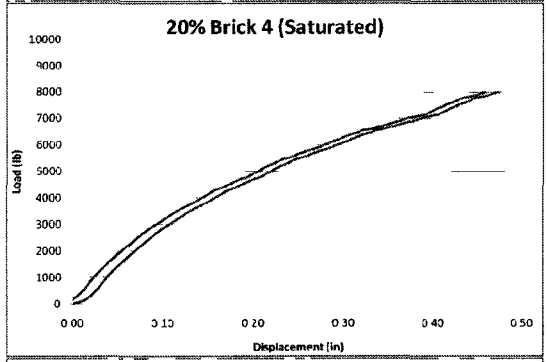

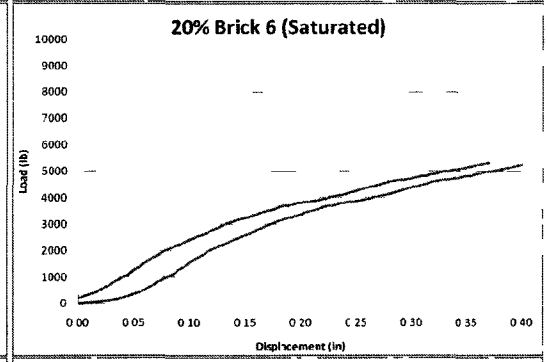

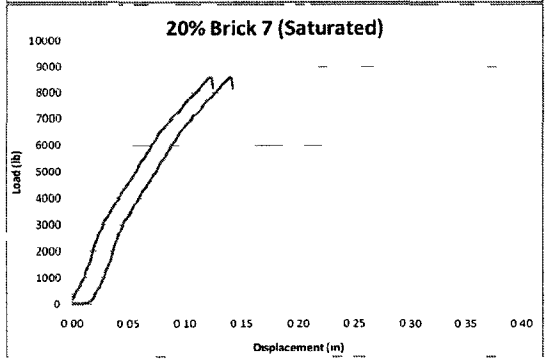

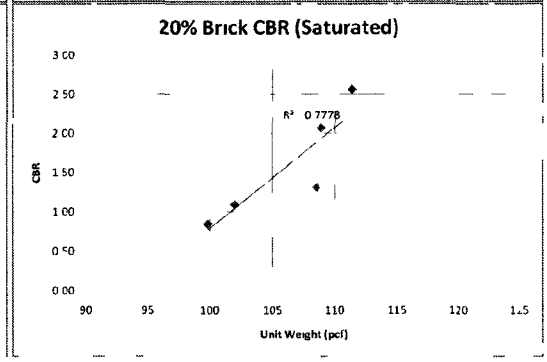

Sample	Unit Weight (pcf)	CBR
1		Bad Data
2	108.51	1.313
3	108.88	2.068
4	101.96	1.093
5		Bad Data
6	99.84	0.851
7	111.30	2.557

50% Brick CBR (Unsaturated)

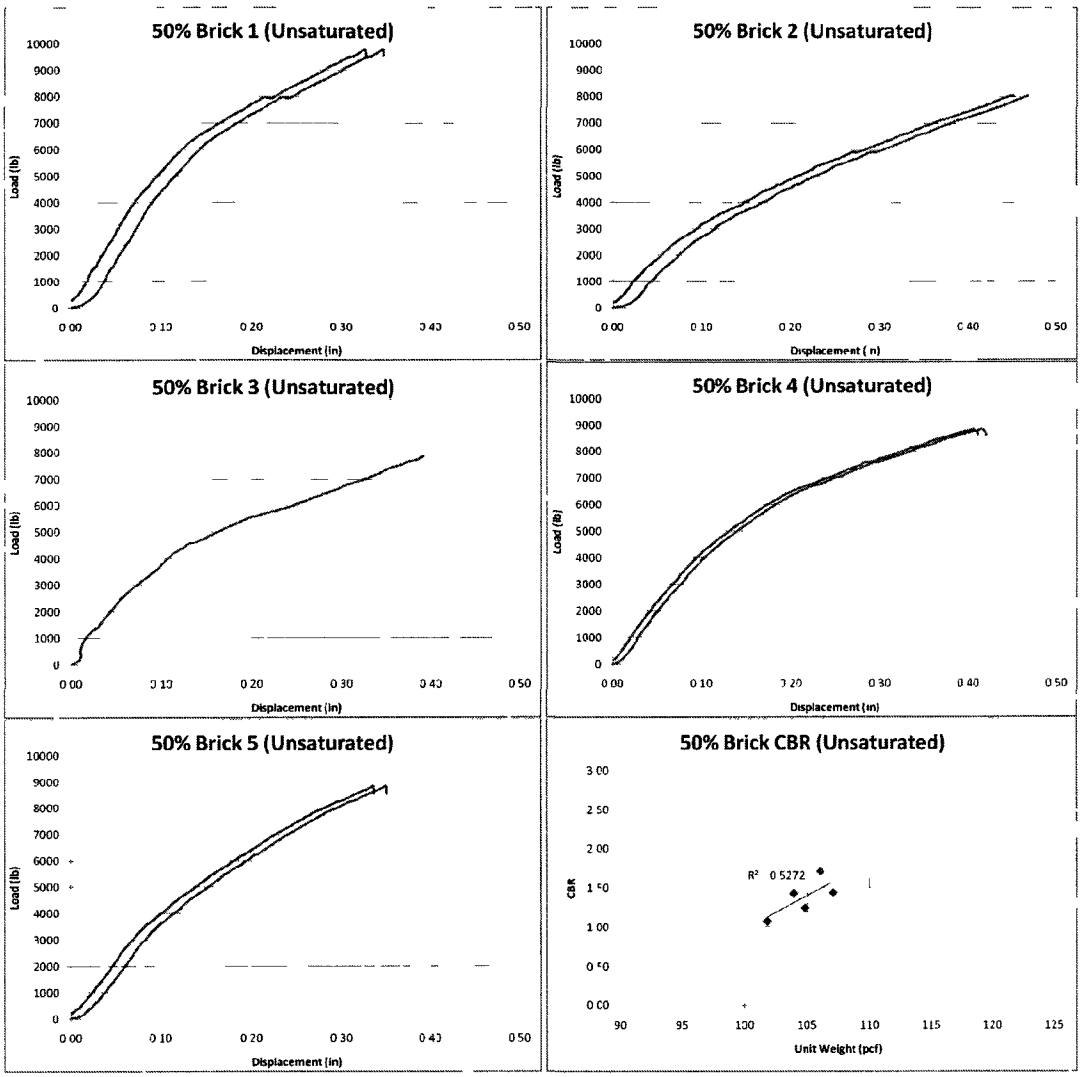

Sample	Unit Weight (pcf)	CBR
1	106.55	1.711
2	102.27	1.077
3	105.32	1.240
4	107.55	1.434
5	104.41	1.429

50% Brick CBR (Saturated)

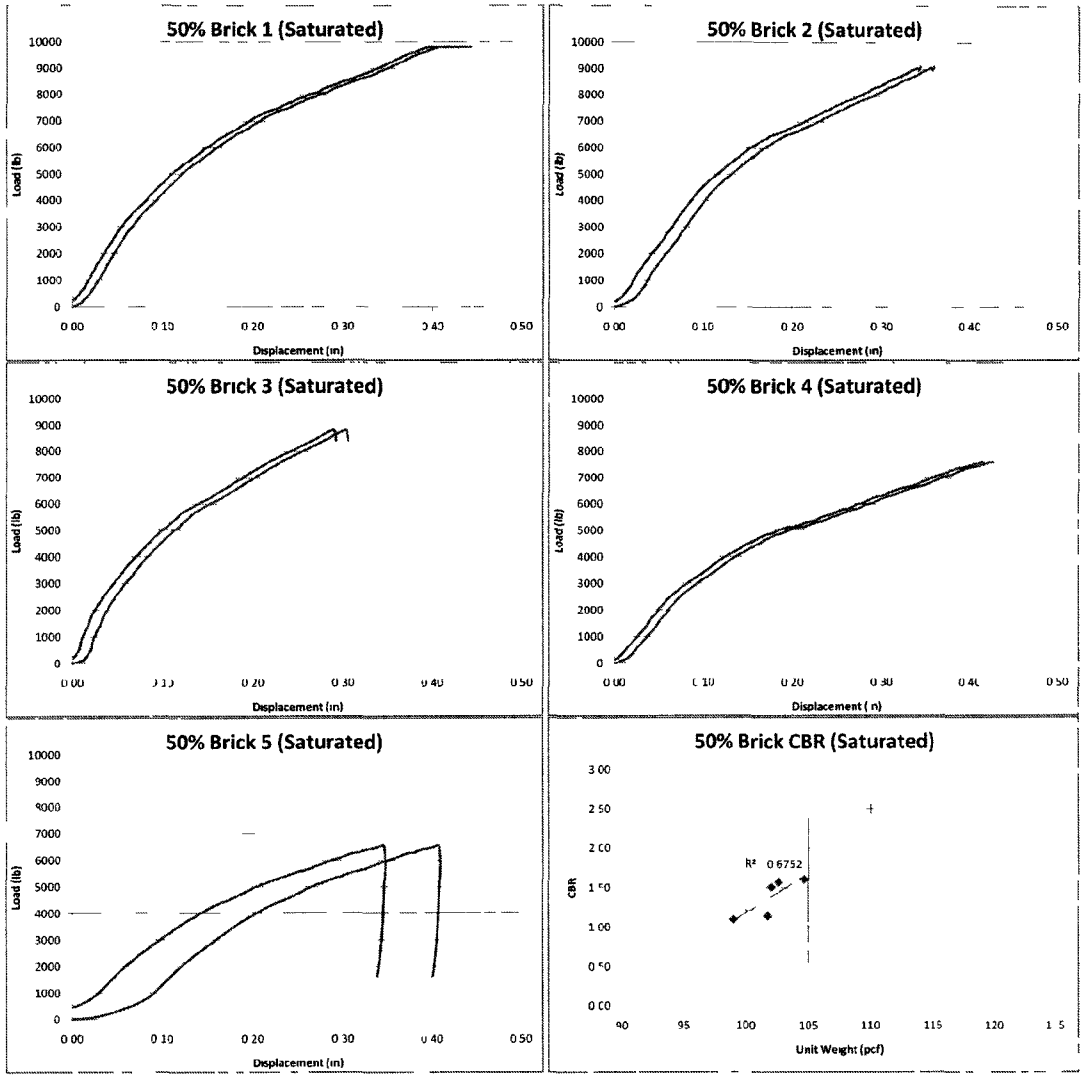

Sample	Unit Weight (pcf)	CBR
1	102.63	1.572
2	102.03	1.507
3	104.65	1.611
4	101.74	1.137
5	98.98	1.094

APPENDIX C

SUMMARY RESILIENT MODULUS RESULTS

100% RCA SRM (Unsaturated)

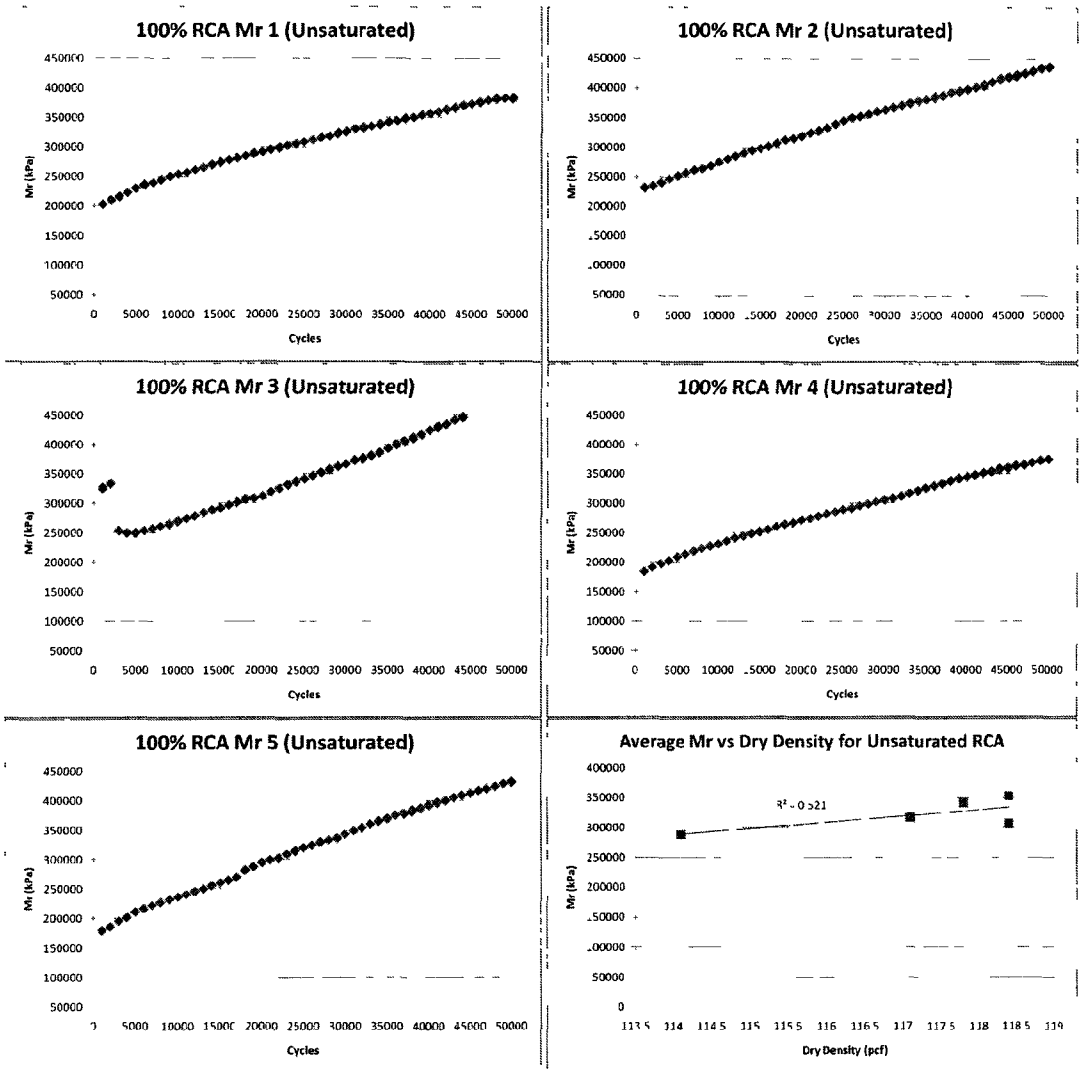

Specimen #		Linear Fit (kPa)	SRM_I (kPa)	SRM_I (psi)
100% RCA	1	y = 3.5535x + 216437	216,437	31,392
	2	y = 4.1757x + 234712	234,712	34,042
	3	y = 4.6196x + 234730	234,730	34,045
	4	y = 3.7673x + 192906	192,906	27,979
	5	y = 5.1445x + 185403	185,403	26,890

100% RCA SRM (Saturated)

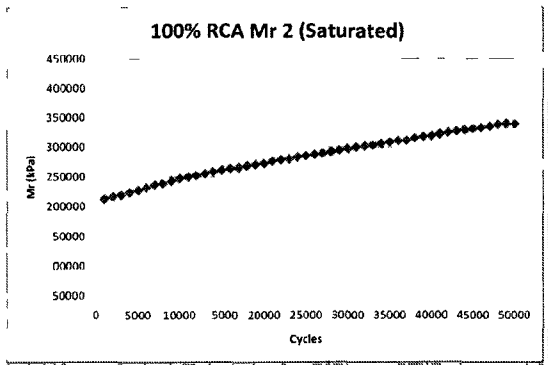

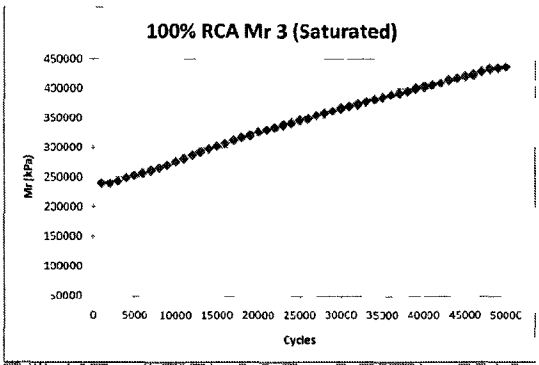

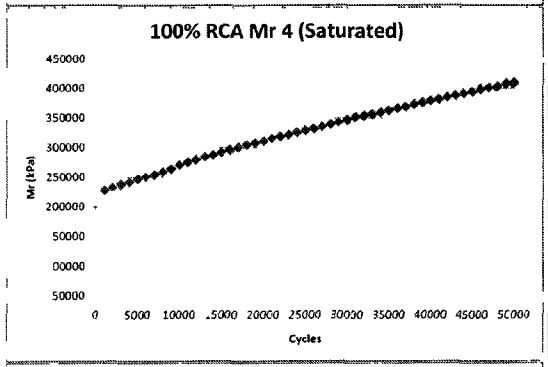

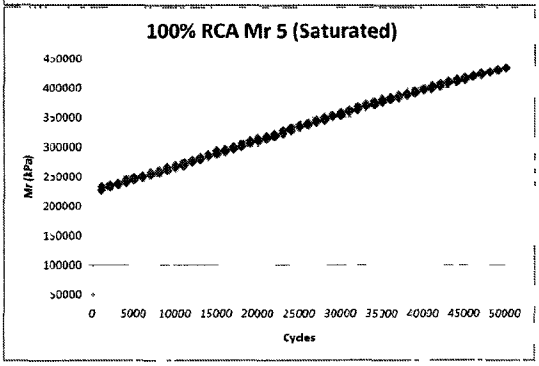

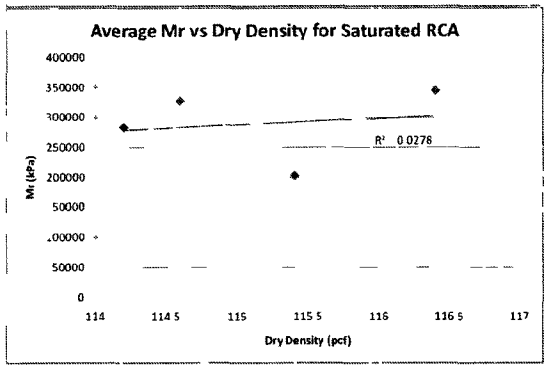

***NOTE: Specimen 1 was excluded due to equipment error

	Specimen #	Linear Fit (kPa)	SRM_I (kPa)	SRM_I (psi)
100% RCA	1	N/A	N/A	N/A
	2	y = 2.5157x + 219788	219,788	31,878
	3	y = 4.1968x + 236843	236,843	34,351
	4	y = 3.6555x + 233732	233,732	33,900
	5	y = 4.2795x + 223824	223,824	32,463

10% Brick SRM (Unsaturated)

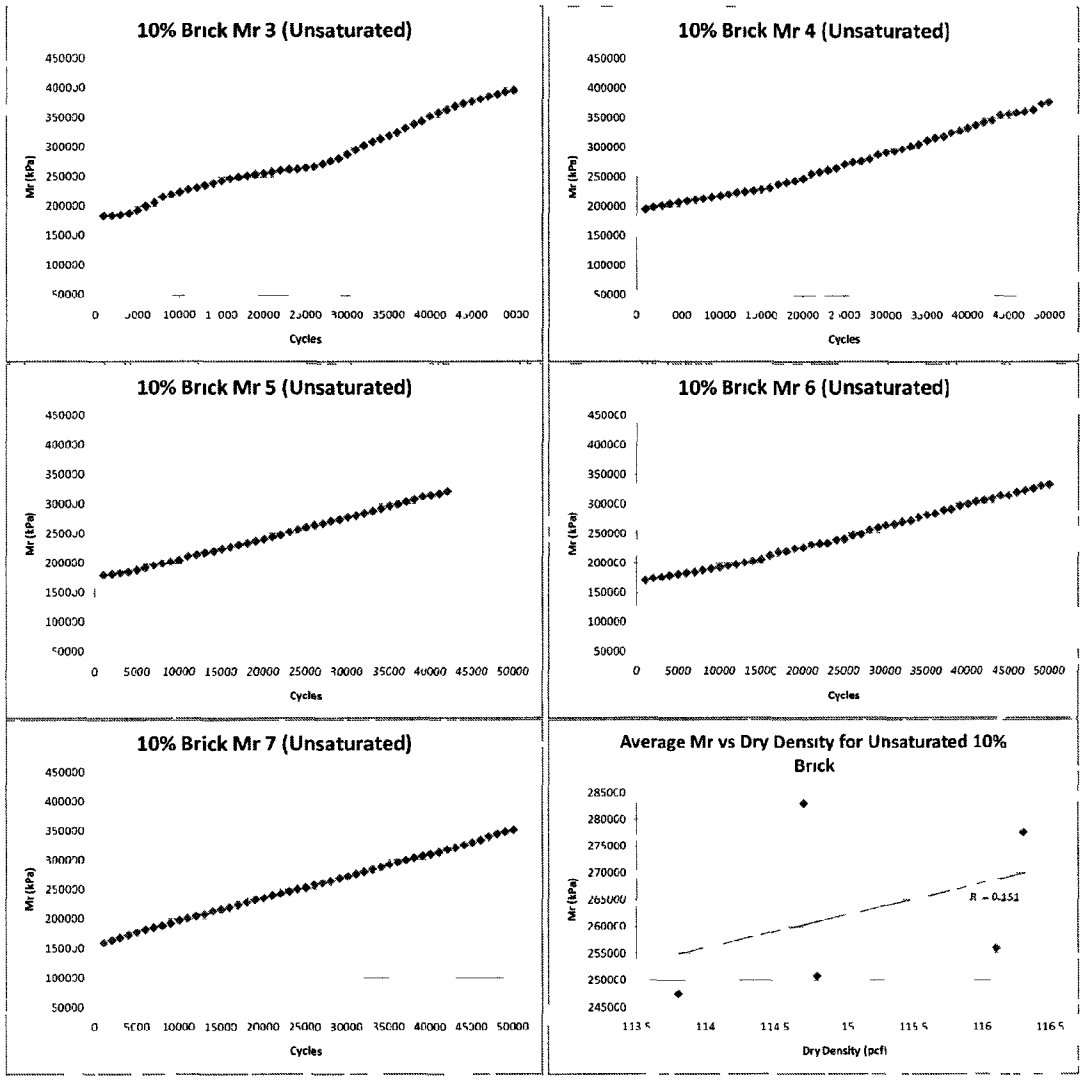

**NOTE. Specimen 1 and 2 were excluded due to equipment error

	Specimen #	Linear Fit (kPa)	SRM_I (kPa)	SRM_I (psi)
10% Brick	3	y = 4 3707x + 171480	171,480	24,871
	4	y = 3 8048x + 180575	180,575	26,190
	5	y = 3 543x + 171609	171,609	24,890
	6	y = 3 4385x + 159848	159,848	23,184
	7	y = 3 8294x + 158333	158,333	22,964

10% RAP SRM (Unsaturated)

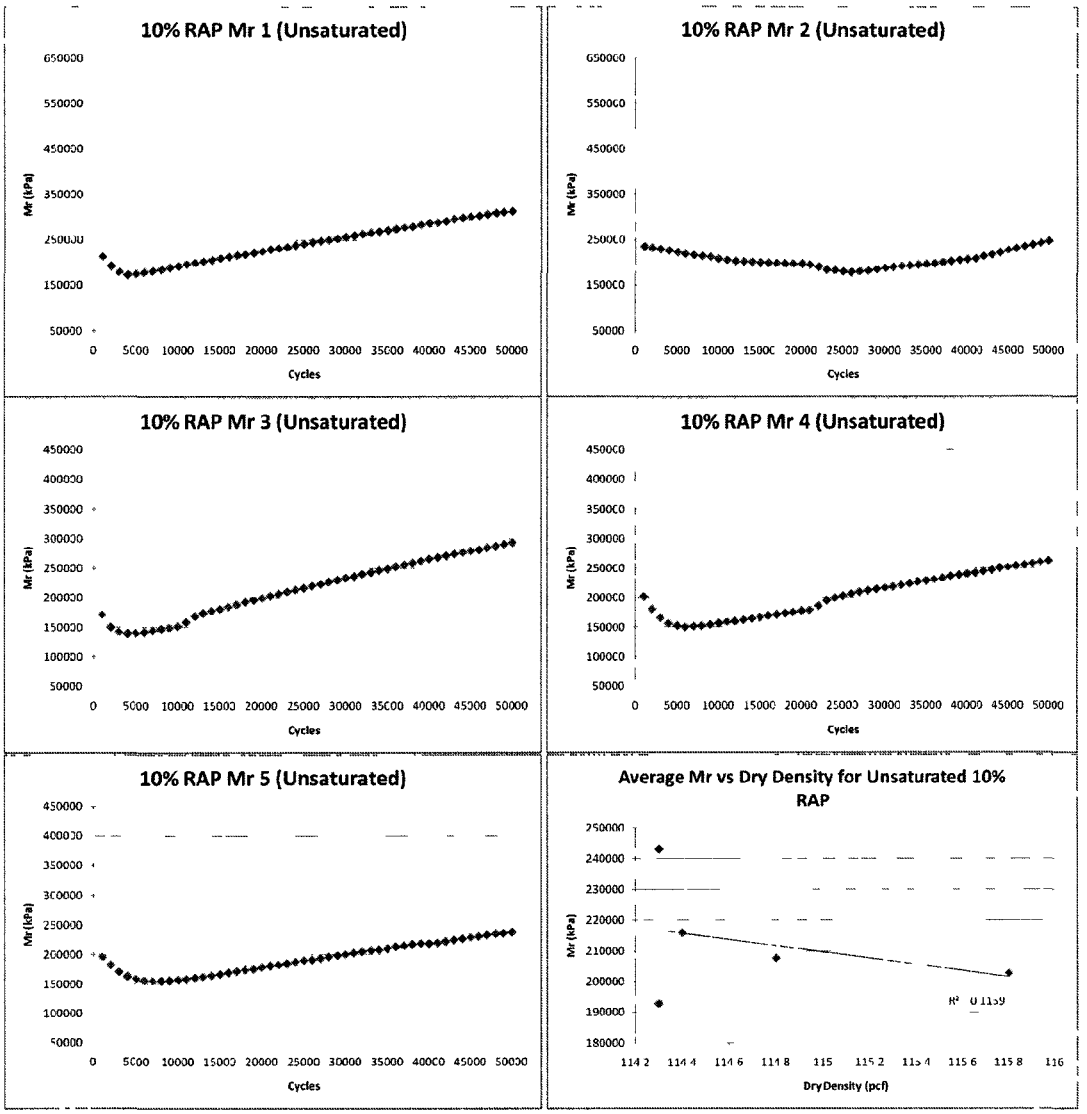

	Specimen #	Linear Fit (kPa)	SRM_I (kPa)	SRM_I (psi)
10% RAP	1	y = 2.9056x + 169024	169,024	24,515
	2	y = 0.142x + 204077	204,077	29,599
	3	y = 3.3046x + 131835	131,835	19,121
	4	y = 2.3709x + 142478	142,478	20,665
	5	y = 1.5964x + 151255	151,255	21,938

20% Brick SRM (Unsaturated)

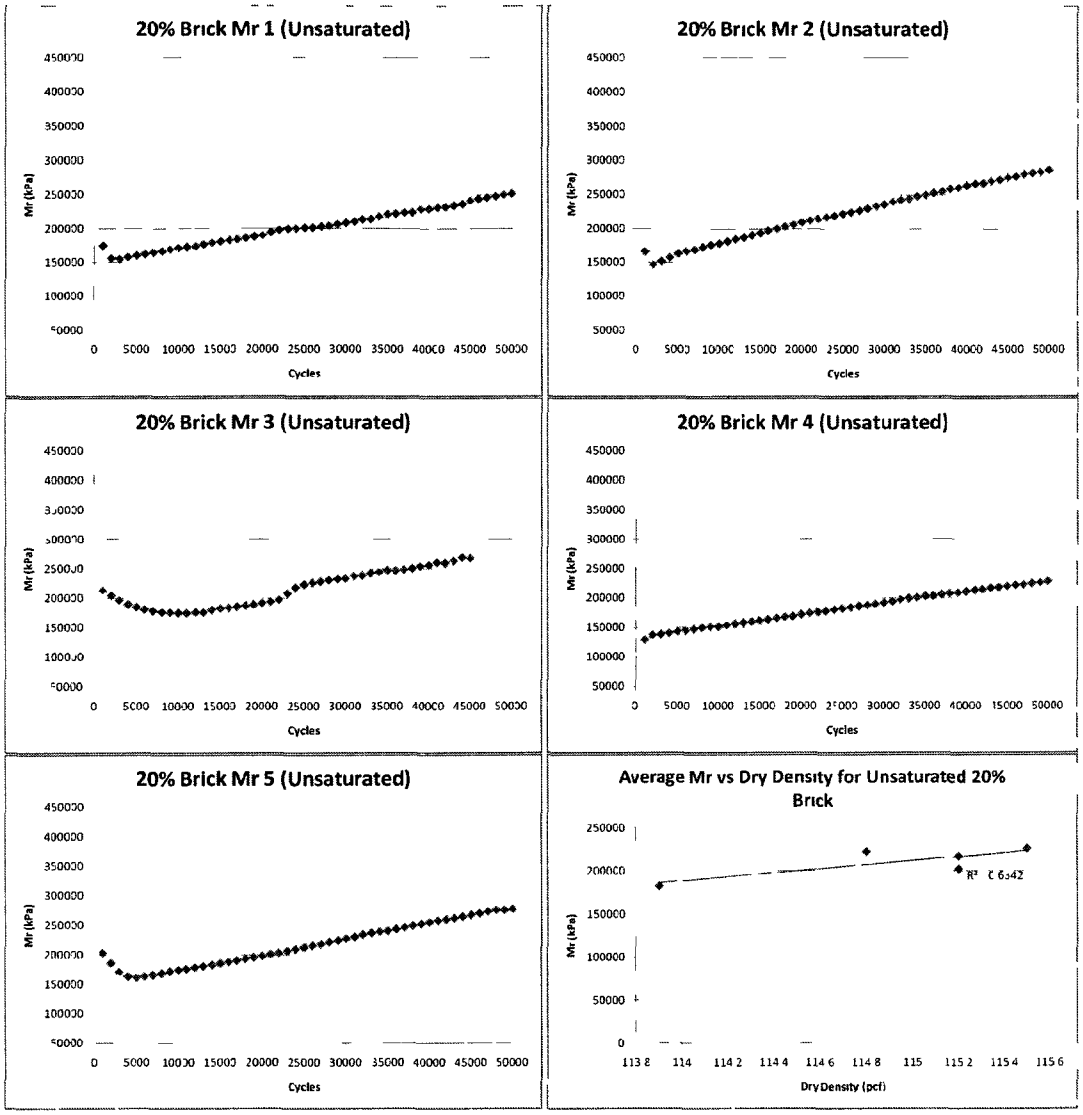

Specimen #		Linear Fit (kPa)	SRM_I (kPa)	SRM_I (psi)
20% Brick	1	y = 1 9342x + 152187	152,187	22,073
	2	y = 2 7989x + 150880	150,880	21,883
	3	y = 2 1853x + 164617	164,617	23,876
	4	y = 1 9501x + 132421	132,421	19,206
	5	y = 2 4297x + 154914	154,914	22,468

20% RAP SRM (Unsaturated)

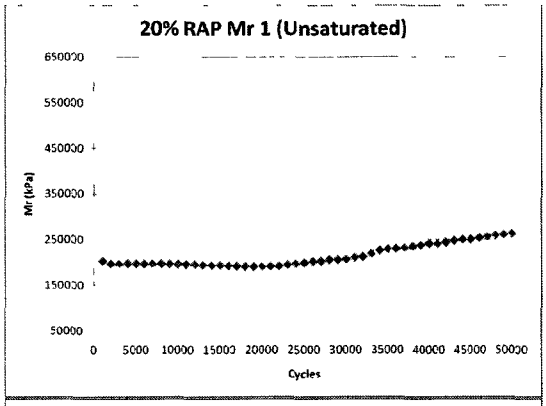

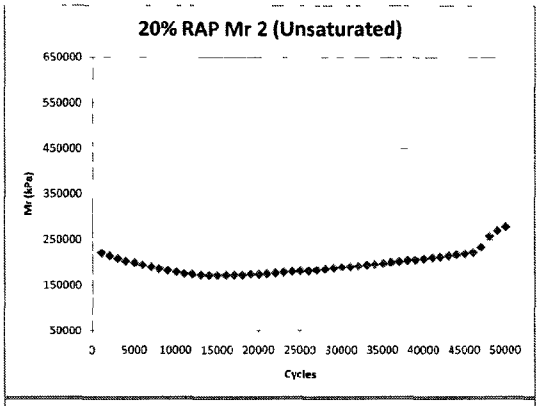

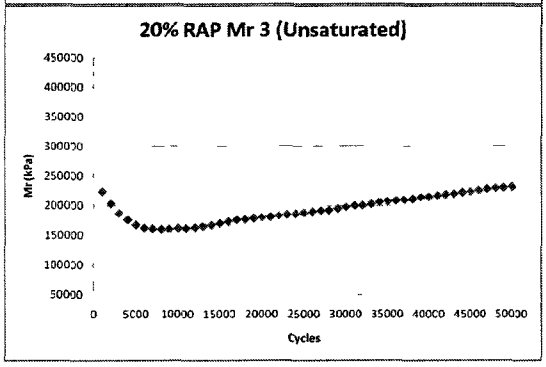

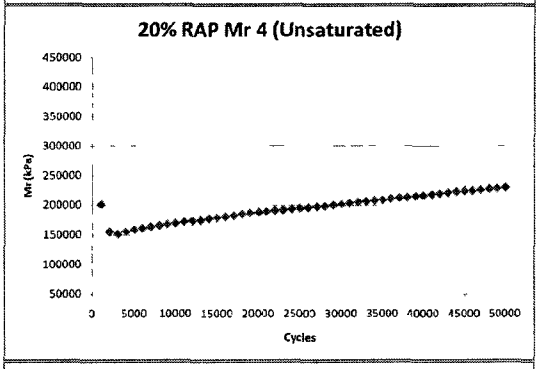

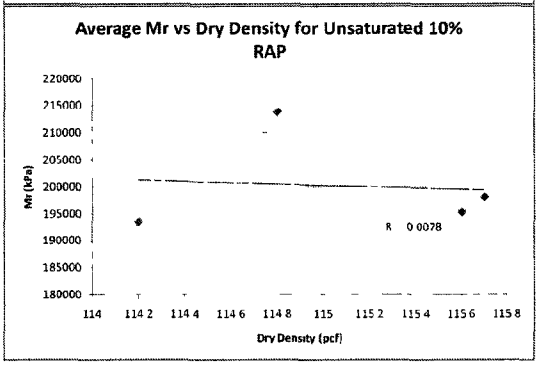

	Specimen #	Linear Fit (kPa)	SRM_I (kPa)	SRM_I (psi)
20% RAP	1	y = 1.4495x + 176874	176,874	25,653
	2	y = 0.9808x + 173079	173,079	25,103
	3	y = 1.2864x + 160743	160,743	23,314
	4	y = 1.4824x + 157643	157,643	22,864

30% Brick SRM (Unsaturated)

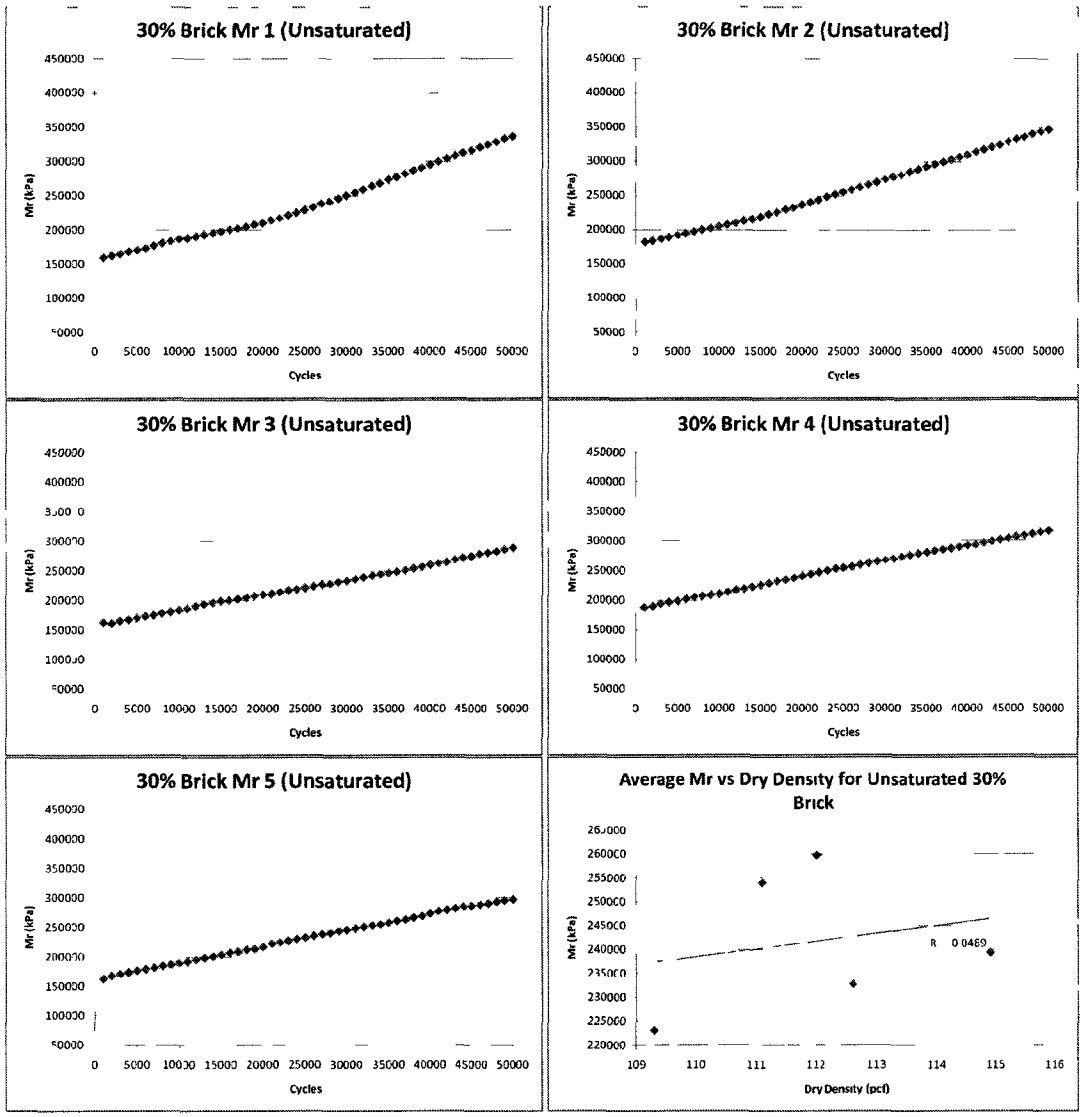

Specimen #		Linear Fit (kPa)	SRM_I (kPa)	SRM_I (psi)
30% Brick	1	y = 3.694x + 145164	145,164	21,054
	2	y = 3 4716x + 171211	171,211	24,832
	3	y = 2 5579x + 157720	157,720	22,875
	4	y = 2.6356x + 186735	186,735	27,084
	5	y = 2.7513x + 162569	162,569	23,579

50% Brick SRM (Unsaturated)

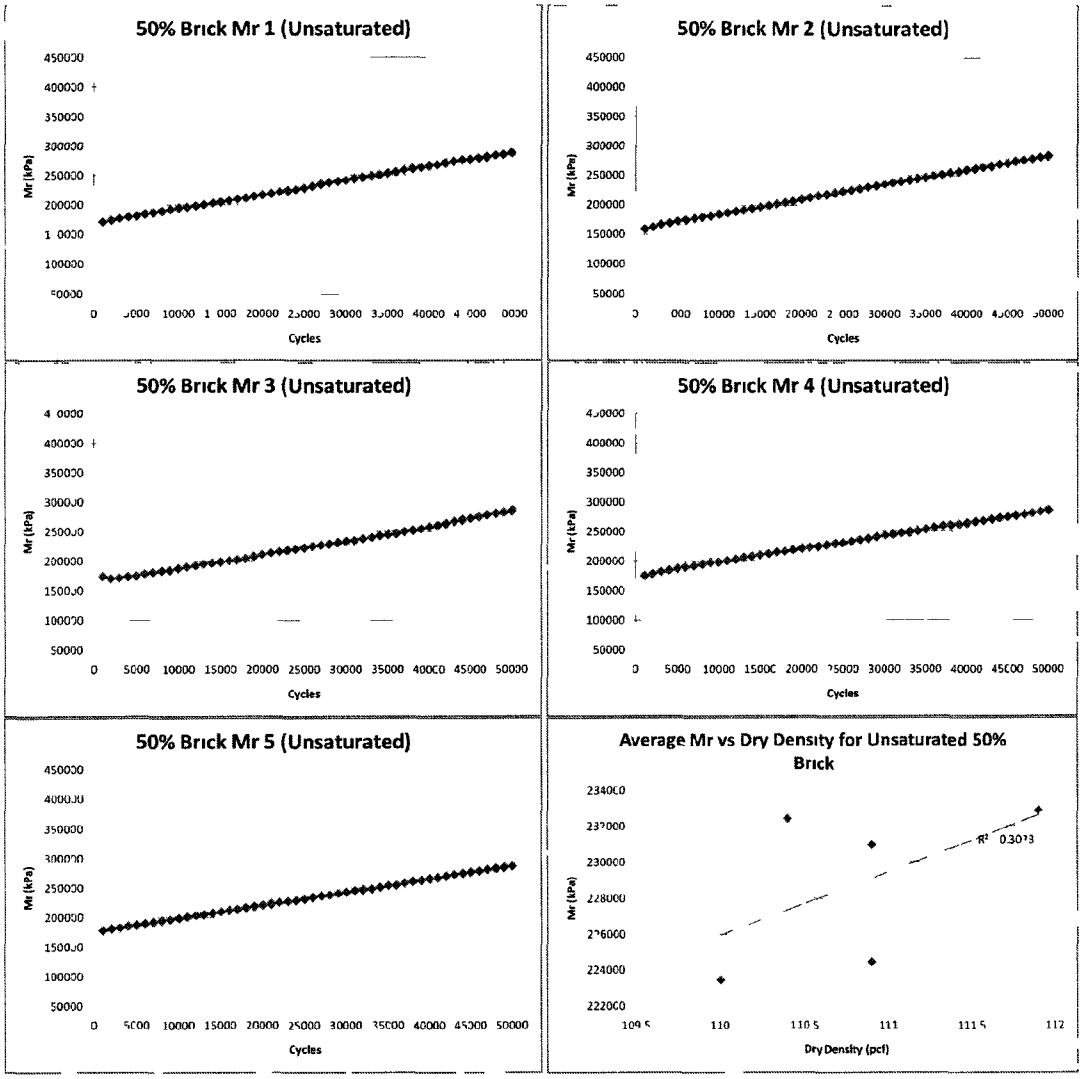

	Specimen #	Linear Fit (kPa)	SRM_I (kPa)	SRM_I (psi)
50% Brick	1	y = 2 4034x + 169710	169,710	24,614
	2	y = 2 4999x + 159702	159,702	23,163
	3	y = 2 3804x + 163739	163,739	23,748
	4	y = 2 1839x + 176758	176,758	25,637
	5	y = 2 2073x + 176618	176,618	25,616

50% Brick SRM (Saturated)

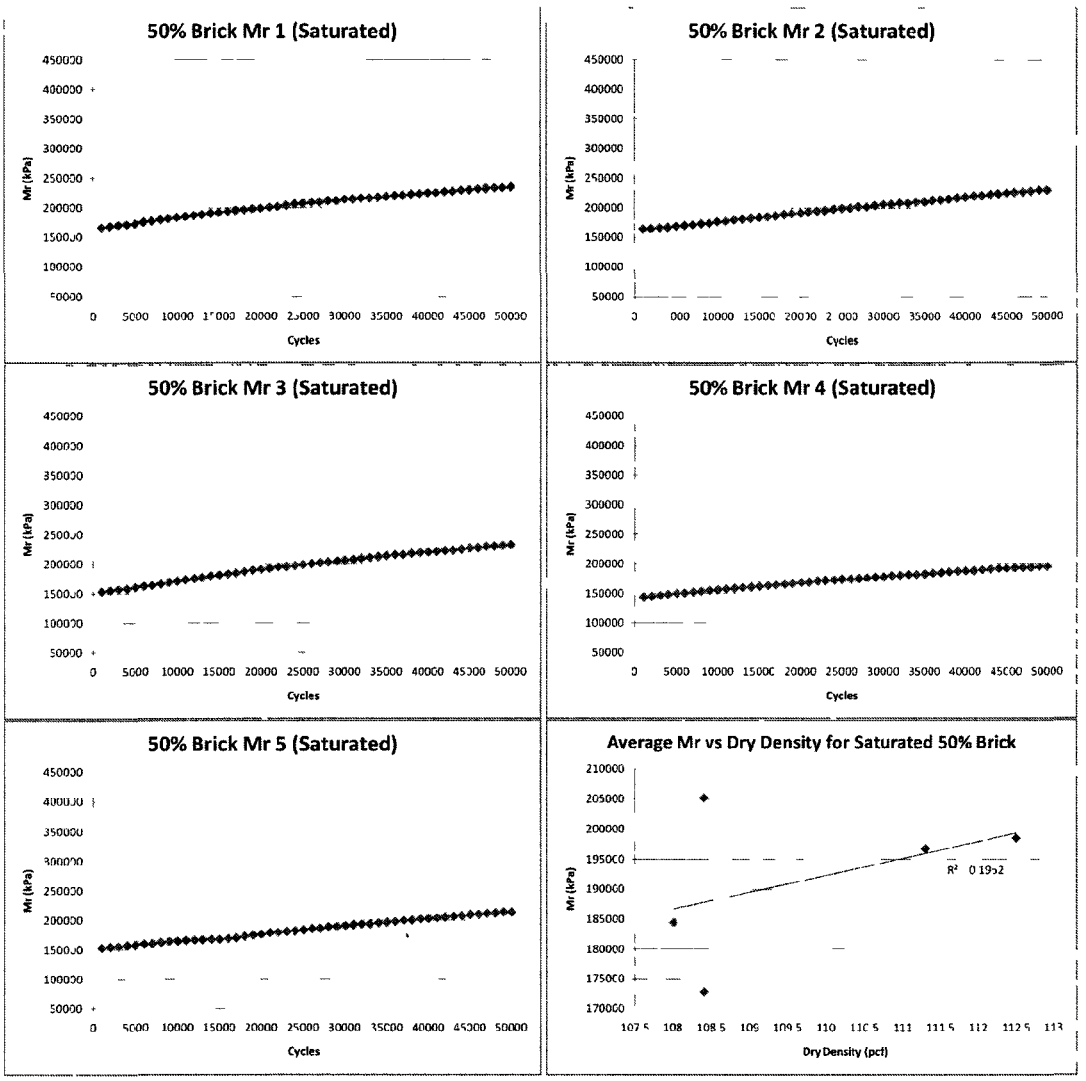

	Specimen #	Linear Fit (kPa)	SRM_I (kPa)	SRM_I (psi)
50% Brick	1	y = 1.3759x + 170141	170,141	24,677
	2	y = 1.374x + 163491	163,491	23,712
	3	y = 1.6219x + 155361	155,361	22,533
	4	y = 1.0566x + 145895	145,895	21,160
	5	y = 1.2743x + 151940	151,940	22,037

70% Brick SRM (Unsaturated)

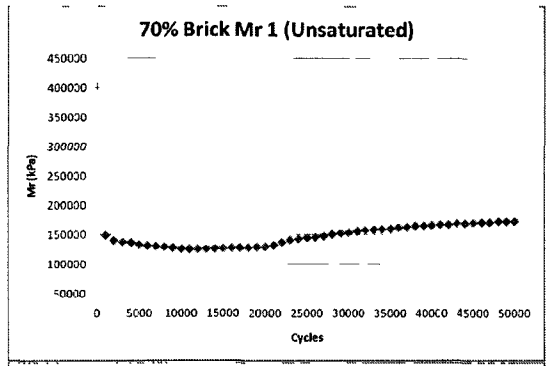

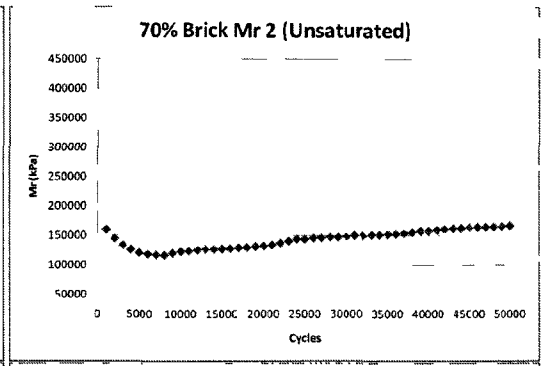

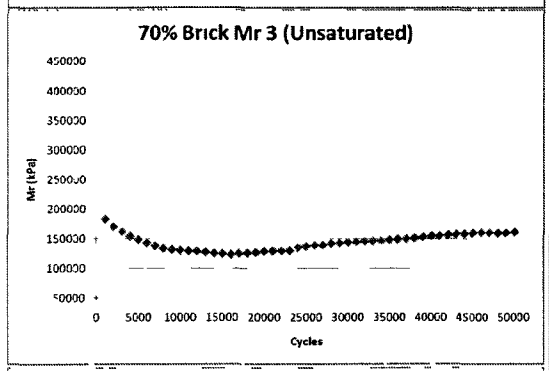

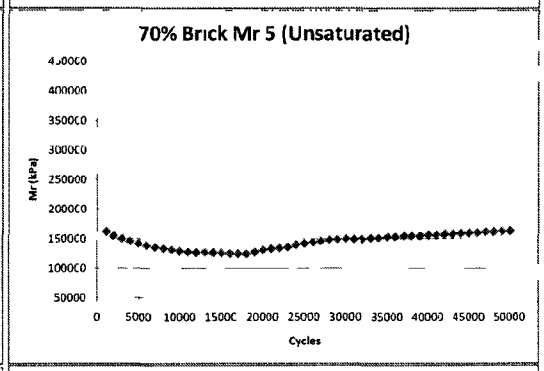

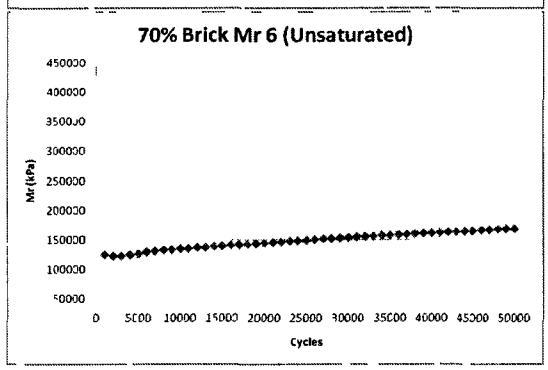

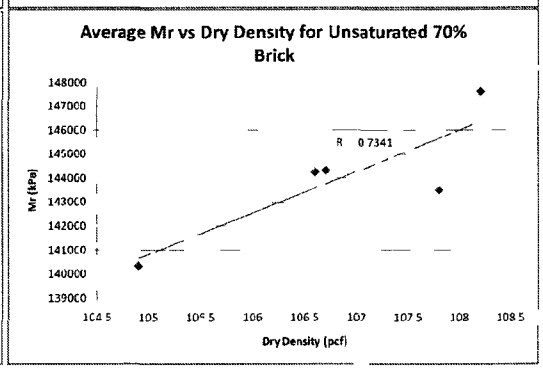

**NOTE: Specimen 4 excluded due to power failure

	Specimen #	Linear Fit (kPa)	SRM_I (kPa)	SRM_I (psi)
70% Brick	1	y = 1 0483x + 120873	120,873	17,531
	2	y = 0 9157x + 120137	120,137	17,424
	3	y = 0 3741x + 134705	134,705	19,537
	5	y = 0 5963x + 129112	129,112	18,726
	6	y = 0 9134x + 124860	124,860	18,109

100% Brick SRM (Unsaturated)

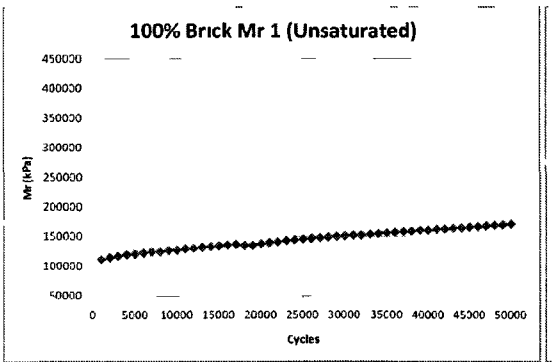

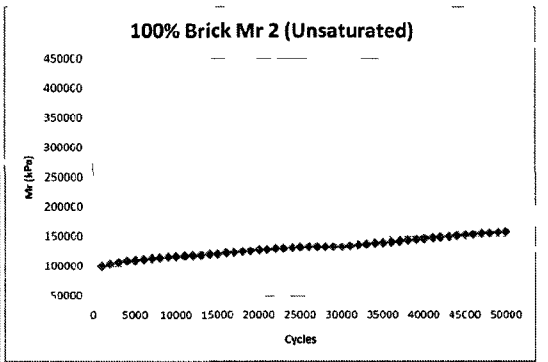

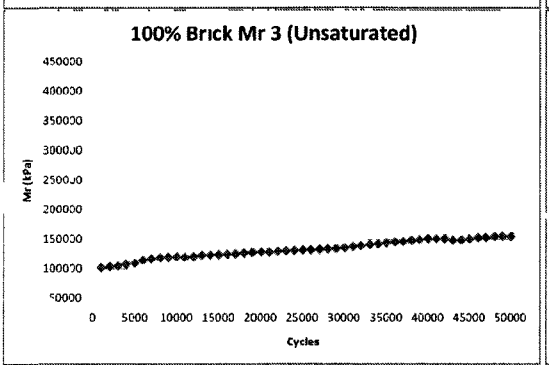

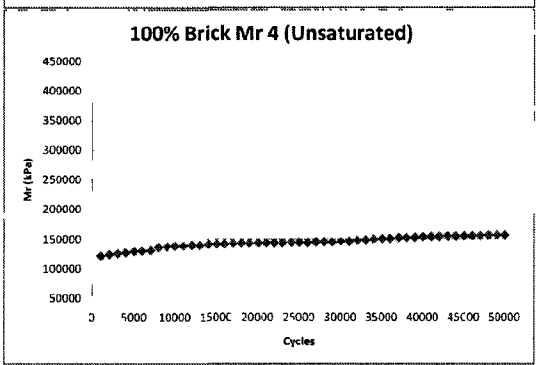

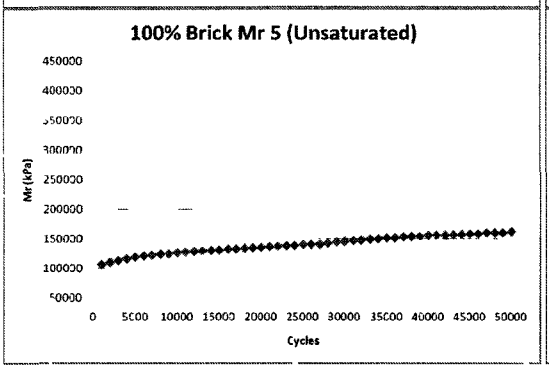

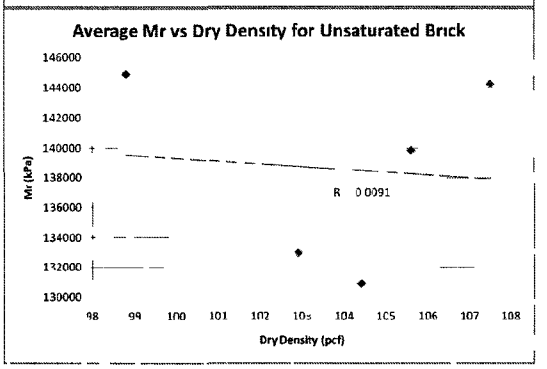

	Specimen #	Linear Fit (kPa)	SRM_I (kPa)	SRM_I (psi)
100% Brick	1	y = 1 1421x + 115784	115784	16,793
	2	y = 1 0409x + 104371	104371	15,138
	3	y = 1 0099x + 107242	107242	15,554
	4	y = 0 5942x + 129089	129089	18,723
	5	y = 0 9993x + 114355	114355	16,586

100% Brick SRM (Saturated)

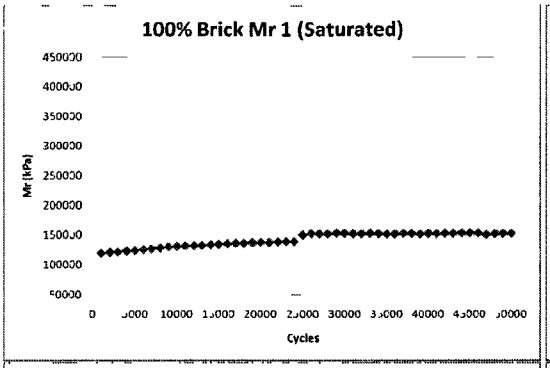

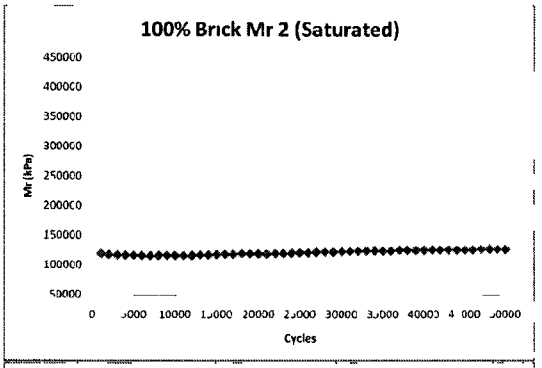

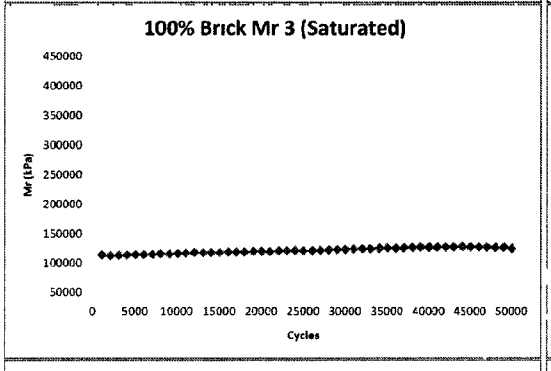

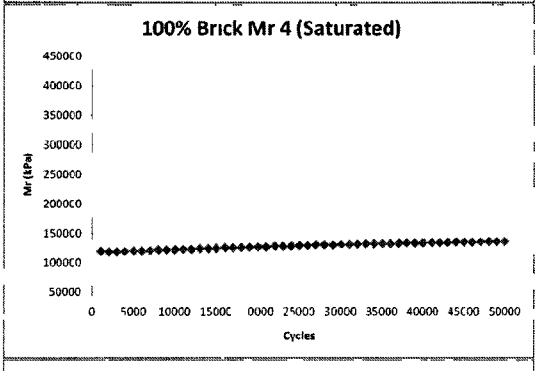

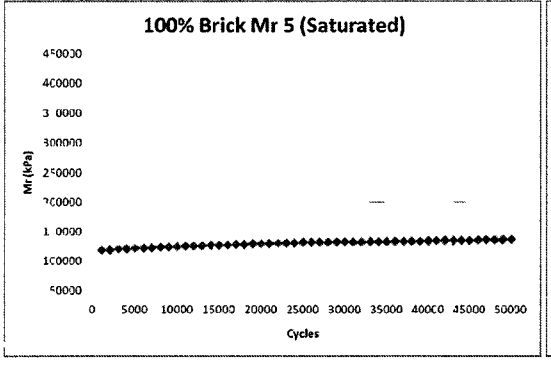

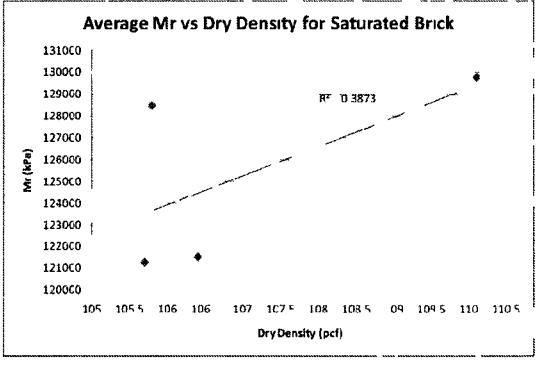

	Specimen #	Linear Fit (kPa)	SRM_I (kPa)	SRM_I (psi)
100% Brick	1	y = 0 7308x + 123640	123640	17,932
	2	y = 0 2437x + 115060	115060	16,688
	3	y = 0 3077x + 113683	113683	16,488
	4	y = 0 3708x + 119034	119034	17,264
	5	y = 0 3408x + 121082	121082	17,561

Crushed Stone SRM (Unsaturated)

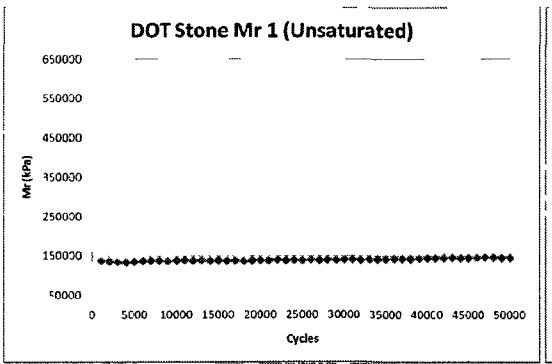

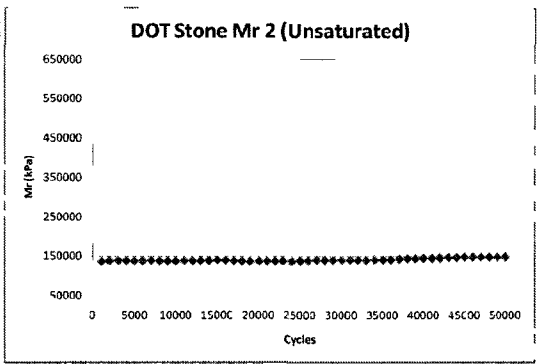

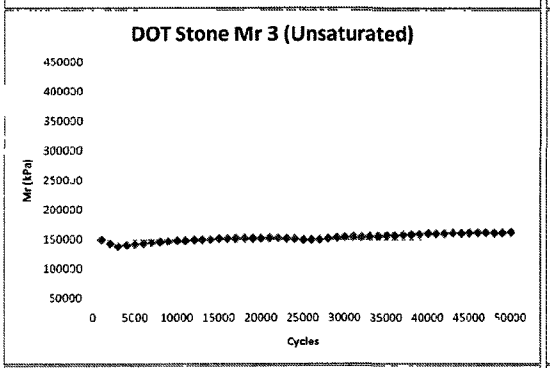

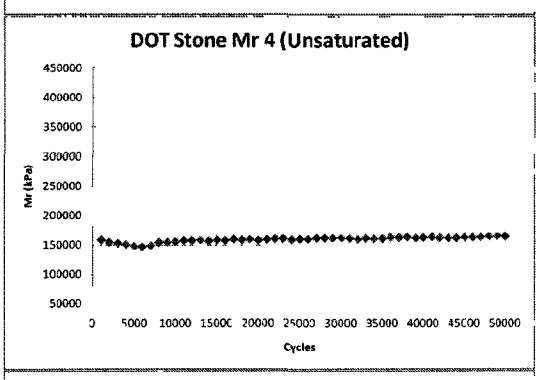

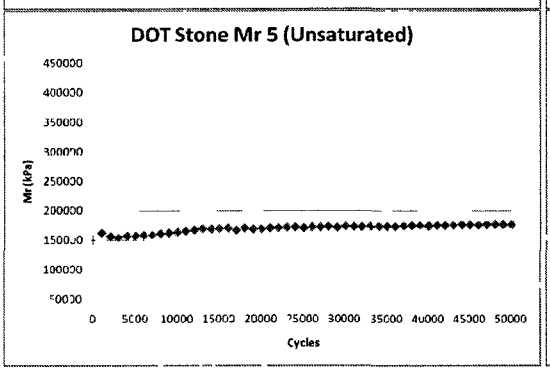

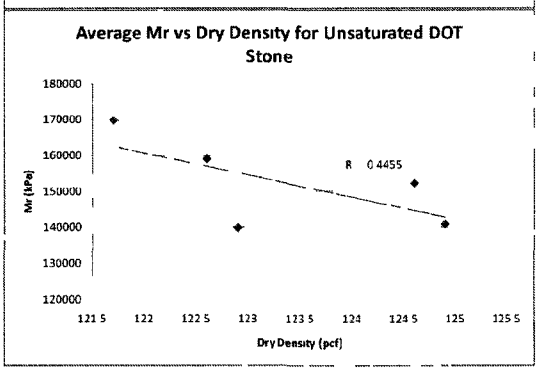

	Specimen #	Linear Fit (kPa)	SRM_I (kPa)	SRM_I (psi)
DOT Stone	1	y = 0 2234x + 134144	134,144	19,456
	2	y = 0 2213x + 135260	135,260	19,618
	3	y = 0 3959x + 142256	142,256	20,632
	4	y = 0 2518x + 152855	152,855	22,170
	5	y = 0 3537x + 151713	151,713	22,004

APPENDIX D

MICRO-DEVAL RESULTS

100% RCA - Dry			
Sample	Wgt. Before (g)	Wgt. After (g)	Percent Loss
1	1504.7	1222	18.8%
2	1499.2	1236.9	17.5%
3	1499.5	1222.7	18.5%
4	1500.6	1240.7	17.3%
5	1501.2	1236.3	17.6%
		Average	**17.9%**

100% RCA - Saturated			
Sample	Wgt. Before (g)	Wgt. After (g)	Percent Loss
1	1503.1	1151.6	23.4%
2	1501.2	1140.5	24.0%
3	1500.7	1132	24.6%
4	1502.1	1134.7	24.5%
5	1502.1	1146.1	23.7%
		Average	**24.0%**

100% Brick - Dry			
Sample	Wgt. Before (g)	Wgt. After (g)	Percent Loss
1	1500.2	1018.7	32.1%
2	1498.4	1022.3	31.8%
3	1500.5	1046.9	30.2%
4	1501.3	1031.9	31.3%
5	1501.5	1031.8	31.3%
		Average	**31.3%**

100% Brick - Saturated			
Sample	Wgt. Before (g)	Wgt. After (g)	Percent Loss
1	1503.4	863.1	42.6%
2	1501.6	904.8	39.7%
3	1502.2	912.9	39.2%
4	1501	887.1	40.9%
5	1499.9	913.8	39.1%
		Average	**40.3%**

10% Brick - Saturated			
Sample	Wgt. Before (g)	Wgt. After (g)	Percent Loss
1	1499.6	1119.8	25.3%
2	1499.8	1124.3	25.0%
3	1537.5	1154.7	24.9%
4	1537.6	1156.8	24.8%
5	1537.9	1156.7	24.8%
		Average	**25.0%**

APPENDIX E

FREEZE-THAW RESULTS

100% RCA			
Sample	Wgt. Before (g)	Wgt. After (g)	Percent Loss
1	1511.8	1145.3	24.2%
2	1506.8	1239.8	17.7%
3	1518	1219.4	19.7%
4	1505.9	1179.9	21.6%
5	1503.9	1096.1	27.1%
		Average	**22.1%**

100% Brick			
Sample	Wgt. Before (g)	Wgt. After (g)	Percent Loss
1	1535.5	1486.8	3.2%
2	1505.3	1481.6	1.6%
3	1509.8	1462.3	3.1%
4	1540.4	1399.6	9.1%
5	1518.1	1453.7	4.2%
		Average	**4.3%**

APPENDIX F

GCTS CATS CONFIGURATION FILE

```
Software: GCTS C.A.T.S. Advanced                Version: 1.82
Controller ID: MR Demo
Test: Triaxial
Date: 04/01/07
Time: 15:51

********************************************************************************
~~~~~ Software Information ~~~~~~~~~~~~~~~~~~~~~~~~~~~~~~~~~~~~~~~~~~~~~~~~~~~~

Serial #: 2031-876
Analog Inputs: 28
Counter Input(s): 1
User Defined Function Inputs: 5
User Defined Correction Inputs: 5
Analog Outputs: 6
Temperature Outputs: 2
Digital Inputs/Outputs: 48
Volume Change Devices (VCDs): 2
Pressure Volume Controllers (PVCs): 3
Flushing Tools: 0
Max Stabilization Points: 50
Included Test:
        Triaxial - Stages:
                Saturation
                Consolidation
                Dynamic Loading
                Resilient Modulus
                Universal
                Static Loading
Configuration File: UNH_SYSTEM.cfg

********************************************************************************
~~~~~ Controller Connection ~~~~~~~~~~~~~~~~~~~~~~~~~~~~~~~~~~~~~~~~~~~~~~~~~~~

Controller Connection: Local
Communication Type: RS232
        COMM Port: 1
Status Refresh Rate: 0.25 (sec)

********************************************************************************
~~~~~ System ~~~~~~~~~~~~~~~~~~~~~~~~~~~~~~~~~~~~~~~~~~~~~~~~~~~~~~~~~~~~~~~~~~~

Controller Type: SCON 1000
Testing System: Other
Bytes to Read from Board Memory: 1000
Hydraulic
Specimen Type: Soil
Maximum Air Supply Pressure: 0.000 MPa
Scan & Servo Loop Rate: 1024 (Hz)

********************************************************************************
~~~~~ Boards ~~~~~~~~~~~~~~~~~~~~~~~~~~~~~~~~~~~~~~~~~~~~~~~~~~~~~~~~~~~~~~~~~~~

===== Main A/D board(s) ========================================================

 Type: GCTS A/D Board, rev A & B
 Address: 0x800
 Analog Inputs: 8
```

```
===== Auxiliary D/A board(s) ==================================================

 Type: GCTS D/A Board
 Address: 0x880
 Analog Outputs: 4

===== Auxiliary Digital board(s) ==============================================

 Type: DIO24: CIO-
 Address: 0x898
 Digital Inputs: 12
 Digital Outputs: 12
 Port Configurations:
 Chip [1]:
  A1: Output
  B1: Input
  CL1: Output
  CU1: Input

===== External Data Acquisition System ========================================

 Type: DI-194RS
 COM Port: 2

===== Auxiliary Counter Board =================================================

(none)

*******************************************************************************
~~~~~ Analog Inputs ~~~~~~~~~~~~~~~~~~~~~~~~~~~~~~~~~~~~~~~~~~~~~~~~~~~~~~~~~~~

===============================================================================
#  Name                          Sensor                 Expected Values
===============================================================================
1  Axial Load Cell               22.24 kN Load Cell     Max: 22237 (N)
                                                        Min: -22237 (N)
Gain: 12.138
Offset: -0.0102 (Volts)
Digital Filter: 100 (Hz)
Warning Interlock:
        Max: NS
        Min: NS
        Actions: (none)
Abort Interlock:
        Max: NS
        Min: NS
Software Offset: 281 (N)

----- Sensor ID: 22.24 kN Load Cell ------------------------------------------

Sensor Type: SG
Model #: SW10-5K
Serial #: 101487
Parameter: Force/Load
Range (N):      Max: 22237      Min: -22237
Calibration:    Date: 06/30/06
        Type: Linear - Two point
Point     Engineering Value (N)         Output (mV/Volt)
First     0                             -0.051
Second    17825                         -3.353
Equation: Output (N) = -5398.24*(mV/Volt) + -275.31
SG Sensor Resistance Information:
        Output Bridge Resistance, Rb (Ohms): 0
```

```
        Default Calibration Resistance, Rcal (Ohms): 0
        Output for Rcal (mV/V): 0

----- GCTS DSB Board ID: DSB-111, revA&B Serial #: 01 -------------------------

DC Excitation -  Max (VDC): 5.000000
                 Min (VDC): -5.000000
AC Excitation (VAC rms): 5.000000
Gain Correction Factor: 1.000000
SG Pre-Gain: 20.000000
Residual Offset Voltage (Volts): 0.000000

================================================================================
2  Frame LVDT                   Frame LVDT            Max: 50 (mm)
                                                      Min: -50 (mm)
Gain: 1.97822
Offset: 0 (Volts)
Digital Filter: 100 (Hz)
Warning Interlock:
        Max: NS
        Min: NS
        Actions: (none)
Abort Interlock:
        Max: NS
        Min: NS
Software Offset: -11.5 (mm)

----- Sensor ID: Frame LVDT ---------------------------------------------------

Sensor Type: AC
Model #: PR-750-2000
Serial #: 35343
Parameter: Displacement/Length
Range (mm):     Max: 50 Min: -50
Calibration:    Date: 06/30/06
        Type: Linear - One point
Full Scale Output: -0.715 (Volts/Volt)
Offset: 0 (Volts/Volt)
Negative Output Correction Factor: NS
Equation: Output (mm) = -69.9301*(Volts/Volt) + 0

----- GCTS DSB Board ID: DSB-111, revA&B Serial #: 02 -------------------------

DC Excitation -  Max (VDC): 5.000000
                 Min (VDC): -5.000000
AC Excitation (VAC rms): 5.000000
Gain Correction Factor: 1.000000
SG Pre-Gain: 20.000000
Residual Offset Voltage (Volts): 0.000000

================================================================================
3  Cell Press_AIR               Cell Press_AIR        Max: 345 (kPa)
                                                      Min: -345 (kPa)
Gain: 15.873
Offset: 0 (Volts)
Digital Filter: 80 (Hz)
Warning Interlock:
        Max: NS
        Min: NS
        Actions: (none)
Abort Interlock:
        Max: NS
        Min: NS
```

```
Software Offset: -0.1 (kPa)

----- Sensor ID: Cell Press_AIR ----------------------------------------------

Sensor Type: SG
Model #: Omega
Serial #: 300
Parameter: Pressure/Stress
Range (kPa):    Max: 345        Min: -345
Calibration:    Date: 03/31/2007
        Type: Linear - One point
Full Scale Output: 3.15 (mV/Volt)
Offset: 0 (mV/Volt)
Negative Output Correction Factor: NS
Equation: Output (kPa) = 109.524*(mV/Volt) + 0
SG Sensor Resistance Information:
        Output Bridge Resistance, Rb (Ohms): 0
        Default Calibration Resistance, Rcal (Ohms): 0
        Output for Rcal (mV/V): 0

----- GCTS DSB Board ID: DSB-111, revA&B Serial #: 03 -------------------------

DC Excitation -  Max (VDC): 5.000000
                 Min (VDC): -5.000000
AC Excitation (VAC rms): 5.000000
Gain Correction Factor: 1.000000
SG Pre-Gain: 20.000000
Residual Offset Voltage (Volts): 0.000000

================================================================================
4  CBR Axial Load Cell          CBR Axial Load Cell     Max: 44485 (N)
                                                        Min: -44485 (N)
Gain: 12.0465
Offset: 2.00272e-005 (Volts)
Digital Filter: 100 (Hz)
Warning Interlock:
        Max: NS
        Min: NS
        Actions: (none)
Abort Interlock:
        Max: NS
        Min: NS
Software Offset: 1362 (N)

----- Sensor ID: CBR Axial Load Cell ------------------------------------------

Sensor Type: SG
Model #: SW10-10K-B000
Serial #: 105212
Parameter: Force/Load
Range (N):      Max: 44485      Min: -44485
Calibration:    Date: 03/29/07
        Type: Linear - One point
Full Scale Output: -4.1505 (mV/Volt)
Offset: 0.0001 (mV/Volt)
Negative Output Correction Factor: NS
Equation: Output (N) = -10717.7*(mV/Volt) + 1.07177
SG Sensor Resistance Information:
        Output Bridge Resistance, Rb (Ohms): 0
        Default Calibration Resistance, Rcal (Ohms): 0
        Output for Rcal (mV/V): 0

----- GCTS DSB Board ID: DSB-111, revA&B Serial #: 04 -------------------------
```

```
DC Excitation -  Max (VDC): 5.000000
                 Min (VDC): -5.000000
AC Excitation (VAC rms): 5.000000
Gain Correction Factor: 1.000000
SG Pre-Gain: 20.000000
Residual Offset Voltage (Volts): 0.000000

================================================================================
5  axial LVDT2                  Displ 0.25 #4          Max: 6.35 (mm)
                                                       Min: -6.35 (mm)
Gain: 2.8167
Offset: -0.8484 (Volts)
Digital Filter: NS
Warning Interlock:
        Max: NS
        Min: NS
        Actions: (none)
Abort Interlock:
        Max: NS
        Min: NS
Software Offset: 1.13 (mm)

------ Sensor ID: Displ 0.25 #4 ------------------------------------------------

Sensor Type: AC
Model #: CD375 -250
Serial #: NA #4
Parameter: Displacement/Length
Range (mm):     Max: 6.35       Min: -6.35
Calibration:    Date: 07/21/06
        Type: Linear - Two point
Point     Engineering Value (mm)        Output (Volts/Volt)
First     0                             -0.12
Second    5                             -0.5154
Equation: Output (mm) = -12.6454*(Volts/Volt) + -1.51745

------ GCTS DSB Board ID: DSB-111, revA&B Serial #: 05 -------------------------

DC Excitation -  Max (VDC): 5.000000
                 Min (VDC): -5.000000
AC Excitation (VAC rms): 5.000000
Gain Correction Factor: 1.000000
SG Pre-Gain: 20.000000
Residual Offset Voltage (Volts): 0.000000

================================================================================
6  Pore Volume                  pore pressure LVDT     Max: 150 (cm³)
                                                       Min: -150 (cm³)
Gain: 2.05003
Offset: -0.00707006 (Volts)
Digital Filter: 100 (Hz)
Warning Interlock:
        Max: NS
        Min: NS
        Actions: (none)
Abort Interlock:
        Max: NS
        Min: NS
Software Offset: 41.9 (cm³)

------ Sensor ID: pore pressure LVDT -------------------------------------------
```

```
Sensor Type: AC
Model #: PR750-2000
Serial #: 35342
Parameter: Volume
Range (cmł):    Max: 150        Min: -150
Calibration:    Date: 06/30/06
        Type: Linear - Two point
Point     Engineering Value (cmł)       Output (Volts/Volt)
First     -40.22                        -0.186
Second    0                             -0.001
Equation: Output (cmł) = 217.405*(Volts/Volt) + 0.217405

----- GCTS DSB Board ID: DSB-111, revA&B Serial #: 06 -------------------------

DC Excitation -  Max (VDC): 5.000000
                 Min (VDC): -5.000000
AC Excitation (VAC rms): 5.000000
Gain Correction Factor: 1.000000
SG Pre-Gain: 20.000000
Residual Offset Voltage (Volts): 0.000000

================================================================================
7  LVDT_1                       Displ 0.25 #3          Max: 6.35 (mm)
                                                       Min: -6.35 (mm)
Gain: 2.8167
Offset: -0.8484 (Volts)
Digital Filter: 100 (Hz)
Warning Interlock:
        Max: NS
        Min: NS
        Actions: (none)
Abort Interlock:
        Max: NS
        Min: NS
Software Offset: 0.00 (mm)

----- Sensor ID: Displ 0.25 #3 -----------------------------------------------

Sensor Type: AC
Model #: CD375 -250
Serial #: NA #3
Parameter: Displacement/Length
Range (mm):     Max: 6.35       Min: -6.35
Calibration:    Date: 07/26/06
        Type: Linear - Two point
Point     Engineering Value (mm)        Output (Volts/Volt)
First     0                             -0.12
Second    5                             -0.5154
Equation: Output (mm) = -12.6454*(Volts/Volt) + -1.51745

----- GCTS DSB Board ID: DSB-111, revA&B Serial #: 07 -------------------------

DC Excitation -  Max (VDC): 5.000000
                 Min (VDC): -5.000000
AC Excitation (VAC rms): 5.000000
Gain Correction Factor: 1.000000
SG Pre-Gain: 20.000000
Residual Offset Voltage (Volts): 0.000000

================================================================================
8  pore pressure                Pore Pressure          Max: 1000 (kPa)
                                                       Min: -1000 (kPa)
Gain: 22.482
```

```
Offset: -0.00300002 (Volts)
Digital Filter: NS
Warning Interlock:
        Max: NS
        Min: NS
        Actions: (none)
Abort Interlock:
        Max: NS
        Min: NS
Software Offset: -5 (kPa)

----- Sensor ID: Pore Pressure ----------------------------------------------

Sensor Type: SG
Model #: Omega PX300-200GV
Serial #: 0
Parameter: Pressure/Stress
Range (kPa):    Max: 1000       Min: -1000
Calibration:    Date: 06/30/06
        Type: Linear - Two point
Point     Engineering Value (kPa)       Output (mV/Volt)
First     500                           1.097
Second    0                             -0.015
Equation: Output (kPa) = 449.64*(mV/Volt) + 6.74461
SG Sensor Resistance Information:
        Output Bridge Resistance, Rb (Ohms): 0
        Default Calibration Resistance, Rcal (Ohms): 0
        Output for Rcal (mV/V): 0

----- GCTS DSB Board ID: DSB-111, revA&B Serial #: 08 -------------------------

DC Excitation -  Max (VDC): 5.000000
                 Min (VDC): -5.000000
AC Excitation (VAC rms): 5.000000
Gain Correction Factor: 1.000000
SG Pre-Gain: 20.000000
Residual Offset Voltage (Volts): 0.000000

================================================================================
9  Not defined
================================================================================
================================================================================
10 Pump Oil Level               Pump Oil Level          Max: 400 (mm)
                                                        Min: 0 (mm)
DC External Excitation:
        Max: 1 (VDC)
        Min: 0 (VDC)
Digital Filter: NS
Warning Interlock:
        Max: NS
        Min: 150 (mm)
        Actions: (none)
Abort Interlock:
        Max: NS
        Min: 100 (mm)
Software Offset: 0.0000 (mm)

----- Sensor ID: Pump Oil Level ----------------------------------------------

Sensor Type: DC
Model #: MPX5010GP
Serial #: 0
DC Sensor Output: Absolute
```

```
Parameter: Displacement/Length
Range (mm):     Max: 1000       Min: 0
Calibration:    Date: 07/01/03
        Type: Linear - Two point
Point     Engineering Value (mm)        Output (Volts)
First     0                             0.229
Second    230                           1.07
Equation: Output (mm) = 273.484*(Volts) + -62.6278

------ GCTS DSB Board ID:  Serial #: 08 ----------------------------------------

================================================================================
11 Not defined
================================================================================
================================================================================
12 Not defined
================================================================================
================================================================================

********************************************************************************
~~~~~ User Defined Function Inputs ~~~~~~~~~~~~~~~~~~~~~~~~~~~~~~~~~~~~~~~~~~~~

--------------------------------------------------------------------------------
#  Name                          Expected Values
--------------------------------------------------------------------------------
1  AVE LVDT1_2                   Max: 2.54 (mm)
                                 Min: -2.54 (mm)
        Inputs Function:
                0.5 *AI-7: LVDT_1+0.5 *AI-5: axial LVDT2
                Multiplication Coefficient: 1
Software Offset: 0.00 mm
--------------------------------------------------------------------------------
2  Not defined
--------------------------------------------------------------------------------
3  Not defined
--------------------------------------------------------------------------------
4  Not defined
--------------------------------------------------------------------------------
5  Not defined
--------------------------------------------------------------------------------

********************************************************************************
~~~~~ User Defined Correction Inputs ~~~~~~~~~~~~~~~~~~~~~~~~~~~~~~~~~~~~~~~~~~

--------------------------------------------------------------------------------
#  Name                          Expected Values
--------------------------------------------------------------------------------
1  Not defined
--------------------------------------------------------------------------------
2  Not defined
--------------------------------------------------------------------------------
3  Not defined
--------------------------------------------------------------------------------
4  Not defined
--------------------------------------------------------------------------------
5  Not defined
--------------------------------------------------------------------------------

********************************************************************************
~~~~~ Analog Outputs ~~~~~~~~~~~~~~~~~~~~~~~~~~~~~~~~~~~~~~~~~~~~~~~~~~~~~~~~~~

--------------------------------------------------------------------------------
#  Name
```

---

1 Load Frame
Valve: Servo
Static Attributes:
Max Control Error: 6 (pfs)
Max Control Rate: 5 (pfs/sec)
Dynamic Attributes:
Max Control Error: 30 (pfs)
Peak & Valley Compensation:
Sensitivity: 0.5 (pfs)
Convergence Rate: [illegible] (%) 30%
Dither:
Amplitude: 0.25 (Volts)
Frequency: 150 (Hz)
Digital Output Control: DO-1: Load Frame Solenoid
Primary Feedbacks:
Force/Pressure: AI-1: Axial Load Cell
Displacement/Volume: AI-2: Frame LVDT

---

2 Cell Pressure_water
Valve: Servo
Static Attributes:
Max Control Error: 50 (pfs)
Max Control Rate: 5 (pfs/sec)
Dynamic Attributes:
Max Control Error: 50 (pfs)
Peak & Valley Compensation:
Sensitivity: 0.05 (pfs)
Convergence Rate: 0.5 (%)
Dither: NS
Digital Output Control: DO-2: Cell Pressure Solenoid
Control Type: AO:On=>DO:On, AO:Off=>DO:Off *
Primary Feedbacks:
Force/Pressure: AI-3: Cell Press_AIR
Displacement/Volume: AI-4: CBR Axial Load Cell

---

3 Pore Pressure
Valve: Servo
Static Attributes:
Max Control Error: 6 (pfs)
Max Control Rate: 5 (pfs/sec)
Dynamic Attributes:
Max Control Error: 30 (pfs)
Peak & Valley Compensation:
Sensitivity: 3 (pfs)
Convergence Rate: 25 (%)
Dither: NS
Digital Output Control: DO-3: Pore Pressure Solenoid
Control Type: AO:On=>DO:On, AO:Off=>DO:Off *
Primary Feedbacks:
Force/Pressure: AI-8: pore pressure
Displacement/Volume: AI-6: Pore Volume

---

4 Cell Pressure_air
Valve: Proportional
Static Attributes:
Max Control Error: 25 (pfs)
Max Control Rate: 5 (pfs/sec)
Dynamic Attributes:
Max Control Error: 30 (pfs)

```
                Peak & Valley Compensation:
                        Sensitivity: 3 (pfs)
                        Convergence Rate: 25 (%)
        Dither:
                Amplitude: 1.15 (Volts)
                Frequency: 78.46 (Hz)
        Digital Output Control: (none)
        Primary Feedbacks:
                Force/Pressure: UFI-2:
                Displacement/Volume: NS

--------------------------------------------------------------------------------

********************************************************************************
~~~~~ Temperature Outputs ~~~~~~~~~~~~~~~~~~~~~~~~~~~~~~~~~~~~~~~~~~~~~~~~~~~~~~

===== Temperature Output 1:  (Not Defined) =====================================

===== Temperature Output 2:  (Not Defined) =====================================


********************************************************************************
~~~~~ Digital Input ~~~~~~~~~~~~~~~~~~~~~~~~~~~~~~~~~~~~~~~~~~~~~~~~~~~~~~~~~~~~

--------------------------------------------------------------------------------
#  Name
--------------------------------------------------------------------------------
1  Digital Input 1
2  Digital Input 2
3  Digital Input 3
4  Digital Input 4
5  Digital Input 5
6  Digital Input 6
7  Digital Input 7
8  Digital Input 8
9  Emergency Button Input
10 Digital Input 10
11 Digital Input 11
12 Digital Input 12
--------------------------------------------------------------------------------

********************************************************************************
~~~~~ Digital Output ~~~~~~~~~~~~~~~~~~~~~~~~~~~~~~~~~~~~~~~~~~~~~~~~~~~~~~~~~~~

--------------------------------------------------------------------------------
#  Name                            System Controlled
--------------------------------------------------------------------------------
1  Load Frame Solenoid
2  Cell Pressure Solenoid
3  Pore Pressure Solenoid
4  Digital Output 4
5  Digital Output 5
6  Digital Output 6
7  Digital Output 7
8  Digital Output 8
9  Digital Output 9
10 Digital Output 10
11 Digital Output 11
12 Digital Output 12
--------------------------------------------------------------------------------

********************************************************************************
~~~~~ Hardware Interlocks ~~~~~~~~~~~~~~~~~~~~~~~~~~~~~~~~~~~~~~~~~~~~~~~~~~~~~~
```

```
System Abort:
        Emergency Button: DI-9: Emergency Button Input
                Error on: Low
        Software Abort: (none)
Watchdog Timer: NS

System Abort Actions:
        Turn off hydraulic pump
User Abort Actions:
        (none)

********************************************************************************
~~~~~ Hydraulics ~~~~~~~~~~~~~~~~~~~~~~~~~~~~~~~~~~~~~~~~~~~~~~~~~~~~~~~~~~~~~~~

Low Pump Pressure Digital Control: DO-9: Digital Output 9
High Pump Pressure Digital Control: DO-9: Digital Output 9

M - Motor On Digital Input: (none)
P - Power (L1/L2/L3) Digital Input: (none)
S - Filter Service Digital Input: (none)

Oil Pressure Input: (none)
Oil Temperature Input: (none)
Oil Level Input: AI-10: Pump Oil Level

Warning Level for Pump Run Time: 500 (hrs)

********************************************************************************
~~~~~ Volume Change Devices (VCDs): 2 ~~~~~~~~~~~~~~~~~~~~~~~~~~~~~~~~~~~~~~~~

===== Volume Change Device1: (Not Defined) ===================================

===== Volume Change Device2: (Not Defined) ===================================


********************************************************************************
~~~~~ Pressure Volume Controllers (PVCs): 3 ~~~~~~~~~~~~~~~~~~~~~~~~~~~~~~~~~~~

===== Pressure Volume Controller 1: (Not Defined) ============================

===== Pressure Volume Controller 2: (Not Defined) ============================

===== Pressure Volume Controller 3: (Not Defined) ============================


********************************************************************************
~~~~~ User Units  ~~~~~~~~~~~~~~~~~~~~~~~~~~~~~~~~~~~~~~~~~~~~~~~~~~~~~~~~~~~~~

Parameter       Unit Name           Slope     Offset    Standard Unit
--------------------------------------------------------------------------------
Displacement/Length
Area
Volume
Velocity (Linear)
Acceleration (Linear)
Mass
Force/Load
Moment/Torque
Pressure/Stress
Work
Power
Angle
```

```
Velocity (Angular)
Acceleration (Angular)
Temperature
Voltage
Current
Resistance
Strain
--------------------------------------------------------------------------------
Note: the slope and the offset are given from the standard
          unit in each parameter
--------------------------------------------------------------------------------

********************************************************************************
~~~~~ PID Tuning Control Parameters ~~~~~~~~~~~~~~~~~~~~~~~~~~~~~~~~~~~~~~~~~~~~

===== AO-1: Load Frame =========================================================

--------------------------------------------------------------------------------
Feedback Input               P          I          D          Polarity
--------------------------------------------------------------------------------
AI-1: Axial Load Cel         45         0.75       0.0005     Inverse
        Forward Gain: 0.5
        Forward Loop Filter: 500 (Hz)
        Stabilization: NS
--------------------------------------------------------------------------------
AI-2: Frame LVDT             42.5       0.8        0.0005     Inverse
        Forward Gain: 0.5
        Forward Loop Filter: 500 (Hz)
        Stabilization: NS
--------------------------------------------------------------------------------
UFI-1: AVE LVDT1_2           10         1          0.0005     Inverse
        Forward Gain: 0
        Forward Loop Filter: 200 (Hz)
        Stabilization: NS
--------------------------------------------------------------------------------
Ea - Axial Strain            50         0.8        0.0005     Inverse
        Forward Gain: 0.5
        Forward Loop Filter: 500 (Hz)
        Stabilization: NS
--------------------------------------------------------------------------------
Er - Radial Strain           42.5       0.8        0.0005     Normal
        Forward Gain: 0.5
        Forward Loop Filter: 500 (Hz)
        Stabilization: NS
--------------------------------------------------------------------------------
Eoct - Octahedral St         42.5       0.8        0.0005     Inverse
        Forward Gain: 0.5
        Forward Loop Filter: 500 (Hz)
        Stabilization: NS
--------------------------------------------------------------------------------
Shear Strain                 42.5       0.8        0.0005     Inverse
        Forward Gain: 0.5
        Forward Loop Filter: 500 (Hz)
        Stabilization: NS
--------------------------------------------------------------------------------
Sd - Deviator Stress         14.5       0.4        0.0005     Inverse
        Forward Gain: 0
        Forward Loop Filter: 500 (Hz)
        Stabilization: NS
--------------------------------------------------------------------------------
Sa - Axial Stress            45         0.75       0.0005     Inverse
        Forward Gain: 0.5
        Forward Loop Filter: 500 (Hz)
```

```
        Stabilization: NS
-------------------------------------------------------------------------------
Sa' - Axial Effectiv        45        0.75      0.0005    Inverse
        Forward Gain: 0.5
        Forward Loop Filter: 500 (Hz)
        Stabilization: NS
-------------------------------------------------------------------------------
p Cambridge Mohr Par        45        0.75      0.0005    Inverse
        Forward Gain: 0.5
        Forward Loop Filter: 500 (Hz)
        Stabilization: NS
-------------------------------------------------------------------------------
p' Cambridge Mohr Pa        45        0.75      0.0005    Inverse
        Forward Gain: 0.5
        Forward Loop Filter: 500 (Hz)
        Stabilization: NS
-------------------------------------------------------------------------------
p MIT Mohr Parameter        45        0.75      0.0005    Inverse
        Forward Gain: 0.5
        Forward Loop Filter: 500 (Hz)
        Stabilization: NS
-------------------------------------------------------------------------------
p' MIT Mohr Paramete        45        0.75      0.0005    Inverse
        Forward Gain: 0.5
        Forward Loop Filter: 500 (Hz)
        Stabilization: NS
-------------------------------------------------------------------------------
q Mohr Parameter Str        45        0.75      0.0005    Inverse
        Forward Gain: 0.5
        Forward Loop Filter: 500 (Hz)
        Stabilization: NS
-------------------------------------------------------------------------------
Toct - Octahedral Sh        45        0.75      0.0005    Inverse
        Forward Gain: 0.5
        Forward Loop Filter: 500 (Hz)
        Stabilization: NS
-------------------------------------------------------------------------------

===== AO-2: Cell Pressure_water ==========================================

-------------------------------------------------------------------------------
Feedback Input              P         I         D         Polarity
-------------------------------------------------------------------------------
Sc' - Cell Effective        1         0.1       0.0005    Inverse
        Forward Gain: 0
        Forward Loop Filter: 500 (Hz)
        Stabilization: NS
-------------------------------------------------------------------------------
p Cambridge Mohr Par        1         0.1       0.0005    Inverse
        Forward Gain: 0
        Forward Loop Filter: 500 (Hz)
        Stabilization: NS
-------------------------------------------------------------------------------
p' Cambridge Mohr Pa        1         0.1       0.0005    Inverse
        Forward Gain: 0
        Forward Loop Filter: 500 (Hz)
        Stabilization: NS
-------------------------------------------------------------------------------
p MIT Mohr Parameter        1         0.1       0.0005    Inverse
        Forward Gain: 0
        Forward Loop Filter: 500 (Hz)
        Stabilization: NS
-------------------------------------------------------------------------------
```

```
p' MIT Mohr Paramete        1         0.1       0.0005    Inverse
        Forward Gain: 0
        Forward Loop Filter: 500 (Hz)
        Stabilization: NS
-------------------------------------------------------------------------------

===== AO-3: Pore Pressure ==============================================

-------------------------------------------------------------------------------
Feedback Input              P         I         D         Polarity
-------------------------------------------------------------------------------
AI-6: Pore Volume           10.2      1.2       0         Normal
        Forward Gain: 0
        Forward Loop Filter: 200 (Hz)
        Stabilization: NS
-------------------------------------------------------------------------------
AI-8: pore pressure         0.499999  0.2       0         Inverse
        Forward Gain: 0
        Forward Loop Filter: 500 (Hz)
        Stabilization: NS
-------------------------------------------------------------------------------
Sa' - Axial Effectiv        1.2       0.2       0.0005    Inverse
        Forward Gain: 0
        Forward Loop Filter: 100 (Hz)
        Stabilization: NS
-------------------------------------------------------------------------------
Sc' - Cell Effective        1.2       0.2       0.0005    Inverse
        Forward Gain: 0
        Forward Loop Filter: 100 (Hz)
        Stabilization: NS
-------------------------------------------------------------------------------
p' Cambridge Mohr Pa        1.2       0.2       0.0005    Inverse
        Forward Gain: 0
        Forward Loop Filter: 100 (Hz)
        Stabilization: NS
-------------------------------------------------------------------------------
p' MIT Mohr Paramete        1.2       0.2       0.0005    Inverse
        Forward Gain: 0
        Forward Loop Filter: 100 (Hz)
        Stabilization: NS
-------------------------------------------------------------------------------

===== AO-4: Cell Pressure_air ==========================================

-------------------------------------------------------------------------------
Feedback Input              P         I         D         Polarity
-------------------------------------------------------------------------------
AI-1: Axial Load Cel        0         0         0         Normal
        Forward Gain: 0
        Forward Loop Filter: 0 (Hz)
        Stabilization: NS
-------------------------------------------------------------------------------
AI-3: Cell Press_AIR        0         1         0         Normal
        Forward Gain: 0
        Forward Loop Filter: 500 (Hz)
        Stabilization: NS
-------------------------------------------------------------------------------

===== TO-1: (Not Defined) ==============================================

===== TO-2: (Not Defined) ==============================================
```

```
**********************************************************************
~~~~~ Triaxial Test Configuration ~~~~~~~~~~~~~~~~~~~~~~~~~~~~~~~~~~~~~~~~

===== Control ==================================================================

Axial Actuator: AO-1: Load Frame
Cell Pressure: AO-4: Cell Pressure_air
Back Pressure: AO-3: Pore Pressure

===== Hardware =================================================================

Loading Piston Diameter: 1.25 inch
Lateral Deformation Measurement:  None
Seating/Contact Stress:  5.000 (kPa)
Pore Pressure Drain Valve Control:
        Pressure/Volume Controller

===== Triaxial Inputs ==========================================================

Axial Load: AI-1: Axial Load Cell
Frame Axial Deformation: AI-2: Frame LVDT
Gauge Axial Deformation: (none)
CP - Cell Pressure: AI-3: Cell Press_AIR
U - Pore Pressure: AI-8: pore pressure
Lateral Deformation: (none)
External (Cell) Volume: (none)
Pore Volume: AI-6: Pore Volume

===== Specimen ================================================================

Height: 200.000 (mm)
Diameter: 100.000 (mm)
Axial Gauge Length: NS
Type: Sand
Height of Platen(s):  0.000 (mm)
Diametral Membrane Thickness:  0.000 (mm)
Mass of Initial Moist Apparatus:  0.000 (gr)
Mass of Final Moist Apparatus:  0.000 (gr)
Mass of Final Dry Apparatus:  0.000 (gr)
Calculation of Radial Strain - Er:  Er = (Ev - Ea)/2
Calculation of Volumetric Strain - Ev:  Ev = internal dv/V
Strain Handling Threshold: 0.500 (%)

===== Resilient Modulus ========================================================

Inputs:
        Gauge Axial Deformation 1: AI-7: LVDT_1
        Gauge Axial Deformation 2: AI-5: axial LVDT2
Time to Apply and Stabilize Cell Pressure: 15 sec
```